

**Investigating the Chirality Transfer Feedback Model in
Ferroelectric Liquid Crystals Using Deuterium NMR
Spectroscopy**

by

Christa Margaret Huntley

A thesis submitted to the Department of Chemistry
in conformity with the requirements
for the degree of Master of Science

Queen's University
Kingston, Ontario, Canada

July, 2008

Copyright © Christa Huntley, 2008

For my parents, Terry and Gail

Abstract

Ferroelectric liquid crystals (FLCs) are being investigated as alternatives to nematic liquid crystals in display applications due to their low power requirements and fast switching times. Commercial FLCs consist of a chiral dopant in an achiral smectic C (SmC) liquid crystal host. A bulk property that arises from the chiral nature of this mixture is a spontaneous polarization (P_S), which depends on the polarization power of the chiral dopant (δ_p). The magnitude of δ_p reflects the ability of a dopant to induce a polarization in an achiral host. It has been proposed that the magnitude of δ_p can be enhanced by matching dopant and host structures, which may enhance the propagation of chiral perturbations from the dopant to the host. This is known as the chirality transfer feedback (CTF) model. Previous studies in the Lemieux lab featured ^2H NMR to detect chiral perturbations exerted by a dopant on the liquid crystal host based on the observation of pairs of quadrupolar doublets in the ^2H NMR spectra.

In the work described herein, the contribution of chirality transfer feedback to the difference in quadrupolar splitting between pairs of quadrupolar doublets ($\Delta\Delta\nu_Q$) was assessed by ^2H NMR spectroscopy. These experiments confirmed the results reported by Finden and Yuh by demonstrating the presence of chiral perturbations exerted by a diester substituted 6,6'-spirobiindandione dopant ((*RS*)-**2.6**-*d*₄) on the achiral SmC host **NCB76**, and the absence of those perturbations using the diester substituted 5,5'-spirobiindandione analogue ((*RS*)-**2.3**-*d*₄).

Subsequent studies explored the effect of modifying the chiral topography of the 2,2'-spirobiindan-1,1'-dione core on the magnitude of δ_p . Both the 5,5'- and 6,6'-

disubstituted cores were reduced to give the corresponding mono-carbonyl derivatives ((*R*)-**3.4-*d*₄** and (*R*)-**3.8-*d*₄**), substituted with ether side-chains. Finally, ester side-chains were added to the 6,6'- mono-carbonyl derivative ((*R*)-**3.9-*d*₄**) for comparison with previous experiments. The ferroelectric induction properties of these dopants were investigated in **NCB76** at mole fractions ranging from $x_d = 0.03 - 0.10$. The mono-carbonyl 5,5'- and 6,6'-diether dopants gave absolute polarization powers of 120 nC/cm² and 123 nC/cm² respectively, which are not significantly different. This suggests that a reduction in the chiral topography of the spirobiindandione core greatly affects the polarization power of the dopant and may reduce the contribution from chirality transfer to δ_p . This was confirmed by a measurement of the polarization power of the 6,6'-diester mono-carbonyl dopant (*R*)-**3.9-*d*₄** in **NCB76**, which gave a δ_p value of 117 nC/cm².

Acknowledgements

I would like to thank my supervisor, Dr. R. P. Lemieux for all of his support and guidance throughout this journey.

I feel very lucky to have worked with many amazing people over the years in the Lemieux group. Many thanks go to: Camilla Andersson, Carl-Johan Carling, Qian “Rebecca” Cui, Linli Fang, Jeremy Finden, Scott Hartley, Naohiko Ikuma, Li Li, Mark Moran, Markus Ohlin, Jeffrey Roberts, Qingxiang Song, Matthew Thompson, Eaganie “Eggy” Yuh and Peng Zhang, for entertainment, assistance and everlasting encouragement.

I would like to thank all of the people in the chemistry department who have helped me along the way. Special thanks go to Dr. Françoise Sauriol and Ruiyao Wang for their help in the NMR facility, and Dr. Bernd Keller, Jie “Jessie” Sui and Yi-Min She in the mass spectrometry lab. I would also like to thank the ladies of the main office, specifically Annette Keyes, Barb Armstrong, and Pam Bandy-Dafoe; Ed Maracle and Robin Roberts in the electronics shop; Susan Thomson-Lafosse and Robert Dumont in chemical stores; and Dan O’Grady for glassblowing. Special thanks also goes to Dr. Henryka Tilk for being an excellent teaching assistant supervisor, and undergraduate laboratory technicians Ted Ison and Lyndsay Hull.

Finally, I would like to thank all of my friends, inside the department and out, for their moral support and friendly smiles, and my parents and sister for being infinitely supportive of chemistry they don’t understand and words they can’t pronounce. I could not have done this without you.

Table of Contents

Abstract.....	ii
Acknowledgements.....	iv
Table of Contents.....	v
List of Tables.....	viii
List of Figures.....	ix
Abbreviations.....	xiii
Chapter 1. Introduction.....	1
1.1. Classification of Liquid Crystals.....	2
1.2. Calamitic Liquid Crystal Phases.....	3
1.3. Origins of Molecular Tilt.....	5
1.4. Chirality in Liquid Crystals.....	6
1.4.1. <i>Ferroelectric Liquid Crystals</i>	6
1.4.2. <i>Molecular Origins of P_S</i>	9
1.4.3. <i>Type I Dopants</i>	12
1.4.4. <i>Type II Dopants</i>	12
1.5. Chirality Transfer Feedback Model.....	14
1.5.1. <i>Indirect Evidence of Chirality Transfer</i>	16
1.5.2. <i>Direct Evidence of Chirality Transfer</i>	18
1.6. ² H NMR Spectroscopy.....	20
1.6.1. <i>Detection of Chirality using ²H NMR</i>	21
1.7. Spirobiindandione Dopants.....	23

1.7.1. <i>Conformational Analysis</i>	27
1.8. Project Outline.....	30
1.9. References.....	31
Chapter 2. ^2H NMR Spectroscopy: Detection of Chirality Transfer Feedback on 2,2'-Spirobiindan-1,1'-dione Dopants.....	34
2.1. Synthesis and Resolution.....	35
2.2. Results.....	38
2.2.1. <i>^2H NMR Spectroscopy: Dopants with Ester Side-Chains</i>	38
2.2.2. <i>^2H NMR Spectroscopy: Dopants with Ether Side-Chains</i>	42
2.3. References.....	44
Chapter 3. Effect of 2,2'-Spirobiindan-1,1'-dione Core Modification on Polarization Power.....	45
3.1. Synthesis and Resolution.....	45
3.2. Results.....	48
3.2.1. <i>Dopant-host Compatibility</i>	48
3.2.2. <i>Polarization Power Measurements</i>	50
3.3. References.....	54
Chapter 4. Conclusions and Future Work.....	56
Chapter 5. Experimental.....	59
5.1. Synthesis and Characterization.....	59
5.1.1. <i>General</i>	59
5.1.2. <i>Materials</i>	59
5.1.3. <i>Synthetic Procedures</i>	60

5.2. ^2H NMR Spectroscopy.....	69
5.3. Determination of Transition Temperatures by Polarized Microscopy.....	70
5.4. Ferroelectric Polarization Measurements.....	70
5.4.1. <i>Sample Preparation</i>	70
5.4.2. <i>Polarization Measurements</i>	71
5.5. References.....	71
Appendix 1. ^1H NMR Spectra of Novel Compounds.....	72
Appendix 2. Polarization Power Data.....	79

List of Tables

Table 1-1.	Polarization power of 1.7a-g in the achiral SmC hosts PhB , DFT , NCB76 and PhP1 at $T-T_C = -5$ K.....	15
Table 1-2.	Polarization power of 1.15a-b , 1.16a-d , and 1.17 in the achiral SmC hosts PhB , DFT , NCB76 and PhP1 at $T-T_C = -10$ K.....	26
Table 3-1.	Polarization power for dopants <i>(R)</i> - 3.4-d₄ , <i>(R)</i> - 1.15a , <i>(R)</i> - 3.8-d₄ , <i>(R)</i> - 1.16a , <i>(R)</i> - 3.9-d₄ and <i>(R)</i> - 1.16c in NCB76 at $T-T_C = -10$ K.....	52

List of Figures

Figure 1-1.	Examples of amphiphilic, calamitic, discotic and polycatenar liquid crystals.....	3
Figure 1-2.	Schematic representation of isotropic, nematic, smectic A, smectic C and crystalline phases of calamitic liquid crystals.....	4
Figure 1-3.	Schematic representation of the coupling of outboard dipoles in accordance with McMillan's model.....	5
Figure 1-4.	Schematic representation of steric effects associated with molecular packing in accordance with Wulf's model.....	6
Figure 1-5.	Symmetry elements of the achiral SmC and the chiral SmC* phases.....	7
Figure 1-6.	(a) Helical structure of the SmC* phase in the absence of external constraints and (b) ferroelectric liquid crystals in the surface stabilized state.....	8
Figure 1-7.	Molecular switching between $+\theta$ and $-\theta$ orientations induced by changing the applied field in a SSFLC.....	8
Figure 1-8.	An example of the bent-cylinder binding site with a guest molecule in the SmC* phase, according to the Boulder model.....	10
Figure 1-9.	Conformational analysis of the dopant MDW 222	11
Figure 1-10.	Orientation of transverse dipoles of Type II dopants described using the tilt plane and polar axis of the molecules.....	14
Figure 1-11.	Illustration of core-core interactions between the dinitro biphenyl core of 1.7 and cores of hosts (a) PhB and (b) PhP1	16

Figure 1-12.	Polarization power δ_p and SmC* helical pitch p as a function of increasing alkoxy chain lengths n for dopants 1.7a-g in host PhP1 . Also included are data points for $n = 1, 18$	17
Figure 1-13.	Reduced polarization P_o vs. mole fraction of probe molecule, x_{probe} , at $T - T_C = -5$ K in the presence of (+)- 1.7d and (-)- 1.7d at a constant mole fraction of $x_{1.7d} = 0.04$ for (a) MDW950 in PhP1 and (b) 1.9 in PhB	19
Figure 1-14.	^2H NMR spectra of (a) benzyl alcohol- d_7 and (b) ethanol- d_6 in the chiral nematic host PBLG	22
Figure 1-15.	^2H NMR spectra of 10 mol % mixtures of 1.13-d_3 in host PhB from 59°C to 53°C.....	23
Figure 1-16.	^2H NMR spectra in the SmC* phase of mixtures of (a) 10 mol % mixtures of (<i>RS</i>)- 1.15a-d_4 in the four liquid crystal hosts, (b) mixtures of 1.16a-d_4 in the four hosts at the following concentrations: 2.6 mol % (PhP1), 3 mol % (PhB), 3 mol % (DFT) and 5 mol % (NCB76) and (c) 10 mol % mixtures of (<i>RS</i>)- 1.17-d_4 in the four liquid crystal hosts, at $T - T_C = -10$ K.....	25
Figure 1-17.	Bar graphs showing a comparison of polarization powers (δ_p) of diether and diester alkyl chains on (a) 5,5'-disubstituted-2,2'-spirobiindan-1,1'-dione (1.15) and (b) 6,6'-disubstituted-2,2'-spirobiindan-1,1'-dione (1.16), in all four LC hosts.....	27
Figure 1-18.	Space-filling model showing minimized zig-zag conformations of dopants (a) (<i>R</i>)- 1.15a and (b) (<i>R</i>)- 1.16a as end-on views of the spirobiindandione core.....	29

Figure 1-19.	Space-filling models of the conformations P (left) and C₂ (right) for (<i>R</i>)- 1.15a in relation to the 3-cylinder zig-zag binding site according to the Boulder model.....	30
Figure 2-1.	² H NMR spectra in the SmC* phase of dopant (<i>RS</i>)- 2.3-d₄ in (a) PhP1 (8 mol %), (b) PhB (8 mol %), (c) DFT (3 mol %) and (d) NCB76 (5 mol %) at $T-T_C = -10$ K.....	39
Figure 2-2.	² H NMR spectra in the SmC* phase of dopant (<i>RS</i>)- 2.6-d₄ in (a) PhP1 (3 mol %), (b) PhB (5 mol %), (c) DFT (3 mol %) and (d) NCB76 (5 mol %) at $T-T_C = -10$ K.....	39
Figure 2-3.	² H NMR spectra in the SmC* phase of dopants (i) (<i>RS</i>)- 2.3-d₄ and (ii) (<i>RS</i>)- 2.6-d₄ in hosts (a) DFT (3 mol %) and (b) NCB76 (5 mol %) at $T-T_C = -10$ K.....	41
Figure 2-4.	Partial phase diagrams for mixtures of (a) (<i>R</i>)- 1.15a , (b) (<i>R</i>)- 1.16a , (c) (<i>R</i>)- 1.15b and (d) (<i>R</i>)- 1.16c in NCB76	42
Figure 2-5.	² H NMR spectra in the SmC* phase of dopants (a) (<i>RS</i>)- 1.16a-d₄ and (b) (<i>RS</i>)- 2.7-d₄ in NCB76 (5 mol %) at $T-T_C = -10$ K.....	43
Figure 3-1.	Partial phase diagrams for mixtures of (a) (<i>R</i>)- 3.4-d₄ , (b) (<i>R</i>)- 3.8-d₄ , (c) (<i>R</i>)- 1.15a and (d) (<i>R</i>)- 1.16a in NCB76	49
Figure 3-2.	Partial phase diagrams for mixtures of (a) (<i>R</i>)- 3.9-d₄ and (b) (<i>R</i>)- 1.16c in NCB76	49
Figure 3-3.	Absolute reduced polarization, $ P_o $, versus mole fraction, x_d , of (a) (<i>R</i>)- 3.4-d₄ , (b) (<i>R</i>)- 3.8-d₄ and (c) (<i>R</i>)- 3.9-d₄ in the SmC host NCB76 at $T-T_C = -10$ K.....	50

Figure 3-4. Comparison of polarization power values for dopants (R) -**1.15a**- d_4 and (R) -**3.4**- d_4 , (R) -**1.16a**- d_4 and (R) -**3.8**- d_4 , (R) -**1.16c**- d_4 and (R) -**3.9**- d_451

Abbreviations

*	Chiral centre
$\Delta\nu_Q$	Quadrupolar splitting
$\Delta\Delta\nu_Q$	Difference in quadrupolar splitting values for two different ^2H atoms
δ	Chemical shift
δ_p	Polarization power (Equation (1-2))
η	Orientalional viscosity
θ	Tilt angle
θ_{CD}	Angle between C-D bond and magnetic field
μ_{\perp}	Transverse dipole moment
τ_r	Electro-optical rise time
Ac	Acetyl
AC	Alternating current
AIBN	2,2'-Azobisisobutyronitrile
aq.	Aqueous
C_2	C_2 conformer
calc'd	Calculated
CD	Circular dichroism
conc.	Concentrated
Cr	Crystalline
CTF	Chirality transfer feedback

DCC	1,3-Dicyclohexylcarbodiimide
dec.	Decomposed
DFT	2',3'-Difluoro-4''-heptyl-4-nonyl-[1,1',4',1'']terphenyl
DIAD	Diisopropyl azodicarboxylate
DMAP	<i>N,N</i> -Dimethylaminopyridine
DMF	<i>N,N</i> -Dimethylformamide
DMSO	Dimethylsulfoxide
<i>E</i>	Electric field
EI	Electron impact ionization
Et	Ethyl
Et ₂ O	Diethyl ether
EtOAc	Ethyl acetate
EtOH	Ethanol
FID	Free induction decay
FLC	Ferroelectric liquid crystal
h	Hours
HPLC	High performance liquid chromatography
HRMS	High resolution mass spectrometry
I	Isotropic
<i>I</i>	Spin quantum number
ITO	Indium-tin oxide
<i>J</i>	Coupling constant
LC	Liquid crystal

LCD	Liquid crystal display
MDW 222	4-(Decyloxy)phenyl 4-((<i>S</i>)-2-octyloxy)benzoate
MDW 950	5-(2 <i>S</i> ,3 <i>S</i> -Difluorooctyloxy)-2-(4-octyloxyphenyl)pyridine
min	Minutes
mp	Melting point
MS	Mass spectrometry
N	Nematic
<i>N</i>	Number density (Equation (1-5))
N*	Chiral nematic
n	Director
<i>n</i>	Side-chain length (number of carbon atoms)
NBS	<i>N</i> -Bromosuccinimide
NCB76	4-(4'-Heptyl[1,1'-biphenyl]-4-yl)-1-hexylcyclohexanecarbonitrile
NMR	Nuclear magnetic resonance
<i>p</i>	Helical pitch
P	P conformer
<i>P_o</i>	Reduced polarization (Equation (1-4))
<i>P_s</i>	Spontaneous polarization
PBLG	Poly- γ -benzyl-L-glutamate
PhB	4-[(\pm)-(4-Methylhexyl)oxy]phenyl 4-decyloxybenzoate
PhP1	2-(4-Butyloxyphenyl)-5-(octyloxy)pyrimidine
ppm	Parts per million

PTFE	Polytetrafluoroethylene
Q_D	Deuterium quadrupole moment
rt	Room temperature
S	Order parameter (Equation (1-1))
sat.	Saturated
SmA	Smectic A
SmA*	Chiral smectic A
SmC	Smectic C
SmC*	Chiral smectic C
SSFLC	Surface-stabilized ferroelectric liquid crystal
T	Temperature
T_C	Curie point
THF	Tetrahydrofuran
TOF-MS	Time of flight mass spectrometry
V_{CD}	Electric field gradient along the C-D bond
x_d	Mole fraction of dopant
\mathbf{z}	Layer normal

Chapter 1. Introduction

Liquid crystals (LCs) were discovered in 1888 by Friedrich Reinitzer,¹ who noticed two distinct melting points during an investigation of cholesteryl benzoate. Although the unique behaviour of this compound observed by polarized microscopy had been previously noted by others, Reinitzer was the first to report this phenomenon in the literature. Otto Lehmann later associated this behaviour to a new state of matter, a “liquid crystal”.²

Liquid crystals are ordered fluids that possess characteristics of both highly ordered crystalline phases and disordered liquid phases. These materials have macroscopic properties that allow for their commercial use in many applications, including flat-panel displays and thermometers. Nematic liquid crystals are most commonly used in display applications; however, ferroelectric smectic C liquid crystals offer a substantial improvement in electro-optical switching times, and are being investigated as alternatives.

Previous work in the Lemieux lab has led to the development of new materials that have unique chiral induction properties in smectic liquid crystal mixtures. ²H NMR studies relating to the chirality transfer feedback model have been conducted (*vide infra*). This thesis describes an attempt to further our understanding of structure-property relationships in ferroelectric liquid crystals through the synthesis and characterization of new dopants, as well as the continuation of ²H NMR studies to provide further insight into the chirality transfer feedback model.

1.1. Classification of Liquid Crystals

Molecules that form liquid crystalline phases are called mesogens, and can be categorized as either lyotropic or thermotropic. The formation of lyotropic liquid crystal phases depends on temperature and the mesogen concentration in a solvent; soaps and cell membranes formed by phospholipids are examples of such materials. Molecules that form lyotropic phases are amphiphilic and contain two incompatible segments that may be hydrophobic and hydrophilic, for example, as shown in structure **1.1**. Lyotropic LCs will not be discussed further in this thesis.

The formation of thermotropic liquid crystal phases depends on temperature. Based on their structural differences, thermotropic LCs can be classified into three main types: calamitic, discotic and polycatenar. Calamitic mesogens are rod-shaped and composed of a rigid aromatic core and flexible side-chains (*e.g.* **1.2**). Discotic mesogens have a disc-like rigid aromatic centre with several flexible side-chains (*e.g.* **1.3**). Polycatenar mesogens have a rigid core, much like that of calamitic mesogens, however they have multiple side-chains which can adopt conformations varying from highly splayed to linear (*e.g.* **1.4**).

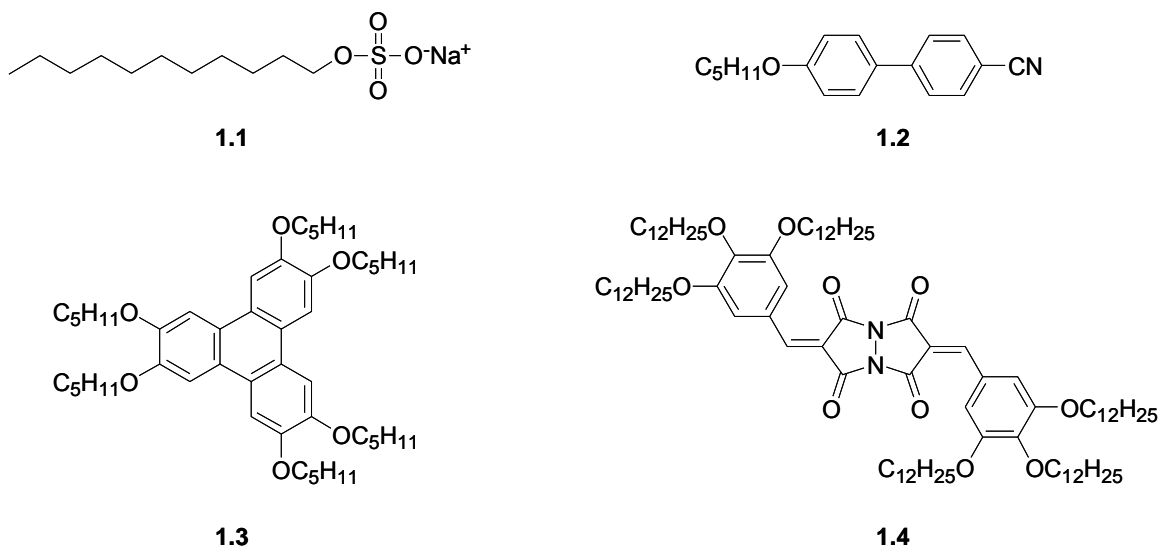


Figure 1-1. Representative examples of amphiphilic (**1.1**), calamitic (**1.2**), discotic (**1.3**) and polycatenar (**1.4**) liquid crystals.

Liquid crystal mesogens are anisometric, in the sense that one molecular dimension is of much longer or shorter length than the other two. Anisometric molecular shape results in anisotropic properties such as birefringence, which is critical for the use of liquid crystals in display applications.

1.2. Calamitic Liquid Crystal Phases

Calamitic mesogens generally have a rod-shaped structure formed by a rigid aromatic core and one or two alkyl side-chains. Calamitic mesogens can form two common types of LC phases, nematic and smectic. Although it is difficult to predict which liquid crystal phase a sample will form at any particular temperature, the phase sequence as a function of temperature is well established. A schematic representation of the phase sequence for calamitic mesogens is shown in Figure 1-2. Upon cooling from a completely disordered isotropic liquid, the nematic phase (N) forms, and exhibits orientational ordering of the molecular long axis along a director (**n**). The nematic phase

is the most disordered liquid crystal phase. The order parameter, S , describes the orientational order in a liquid crystal phase according to Equation (1-1):

$$S = \frac{1}{2} \langle 3 \cos^2 \theta - 1 \rangle \quad (1-1)$$

where θ is the angle between \mathbf{n} and the molecular long axis of the molecules. In a disordered liquid phase, $S \approx 0$. In a highly ordered crystalline phase, S values approach 1. In the nematic phase, S values are typically between 0.4 and 0.7.³

The smectic A phase (SmA) forms at temperatures below that of the nematic, and exhibits orientational order similar to N, as well as short range positional order in the form of distinct layers. The long axes of calamitic mesogens in the SmA phase are oriented parallel to the smectic layer normal (\mathbf{z}), where $\mathbf{n} \parallel \mathbf{z}$. The smectic C phase (SmC) forms at temperatures below that of the SmA phase. Mesogens in the SmC phase maintain the orientational order and lamellar structure of the SmA phase, but the director \mathbf{n} is uniformly tilted at an angle θ with respect to \mathbf{z} . Smectic phases typically have an order parameter of 0.8.⁴

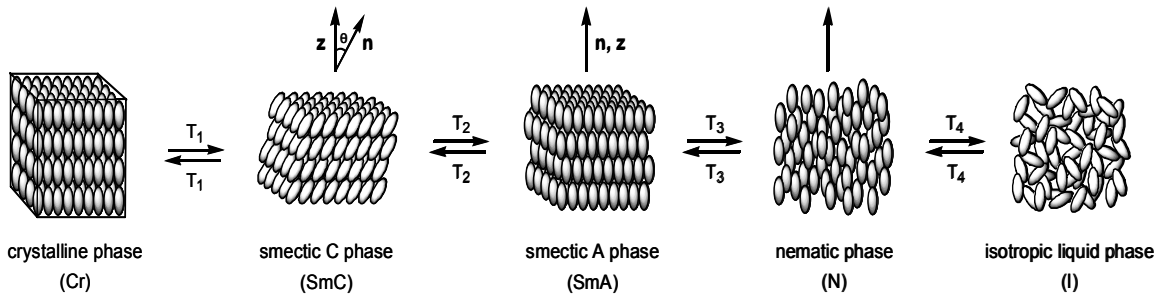


Figure 1-2. Schematic representation of crystalline (Cr), smectic C (SmC), smectic A (SmA), nematic (N) and isotropic (I) phases of calamitic liquid crystals.

1.3. Origins of Molecular Tilt

Upon cooling from the SmA phase to the SmC phase, mesogens tilt at an angle θ from the layer normal. There are two important models for the origin of such tilt, proposed by McMillan⁵ and Wulf.⁶ In 1973, McMillan suggested that tilt in the SmC phase arises from a coupling of outboard dipoles (dipoles normally associated with side chain ether linkages) between neighbouring mesogens. Dipoles within a constituent mesogen are pointed in opposite directions perpendicular to the molecular long axis, and dipoles of adjacent mesogens are parallel to one another (see Figure 1-3(a)). Upon cooling into the SmC phase, rotation about the molecular long axis of the molecule is restricted (“frozen out”), and the coupling of outboard dipoles imposes a torque on the system, causing it to tilt (Figure 1-3(b)). At the time, all liquid crystals forming SmC phases contained polar end groups, and such was the basis of McMillan’s model.

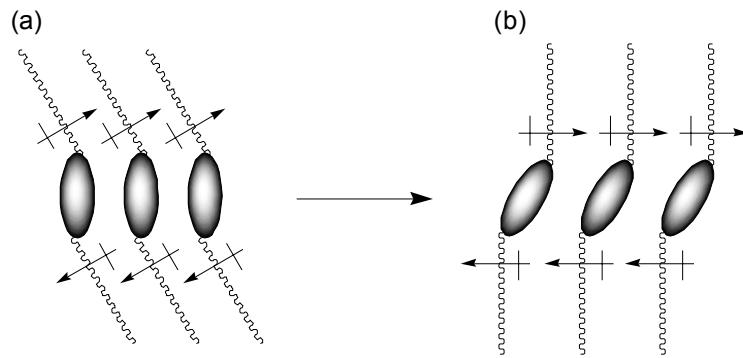


Figure 1-3. Schematic representation of the coupling of outboard dipoles in accordance with McMillan’s model (a) before cooling and (b) after cooling.

Wulf’s model uses steric factors to account for the origin of tilt. Wulf documented in 1975 that symmetrical mesogens in the SmA phase behave like cylinders and can freely rotate around their molecular long axes (Figure 1-4(a)). Upon cooling

however, rotation is more restricted and free volume in the packing of molecules with a zig-zag shape is minimized in the tilted layer structure (Figure 1-4(b)).

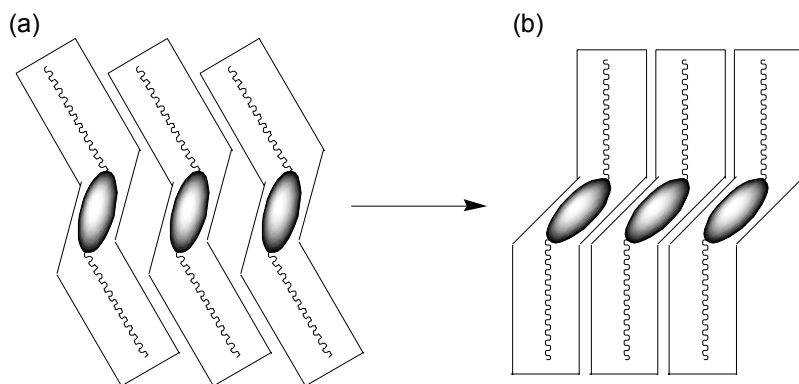


Figure 1-4. Schematic representation of steric effects associated with molecular packing in accordance with Wulf's model (a) before cooling and (b) after cooling.

In 1978, Durand *et al.* determined that mesogenic cores are more tilted than side-chains using X-ray and optical techniques.⁷ Initially, discrepancies were found between X-ray and optical tilt angle measurements in SmC materials, which were inconsistent with mesogens modeled as rigid rods. Thus, a zig-zag structure was a more accurate model for these systems. Secondly, layer spacing measurements generally gave tilt angles that were less than those measured by polarized microscopy, which is consistent with a layer structure of zig-zag molecules in which the cores are more tilted than the side-chains. This result was later confirmed by Clark *et al.* in 2001.⁸

1.4. Chirality in Liquid Crystals

1.4.1. Ferroelectric Liquid Crystals

The achiral SmC phase has three symmetry elements; a C_2 axis of rotation perpendicular to the layer normal, a reflection σ plane congruent with the tilt plane, and an inversion centre. However, Meyer and co-workers predicted that in the chiral SmC phase (SmC*), the elimination of the σ reflection plane would result in a macroscopic

electric polarization parallel to the C_2 axis, which is the sum of contributions of transverse dipole moments of the constituent mesogens along the C_2 axis (Figure 1-5). This permanent electric polarization is known as the spontaneous polarization, (P_S), and such SmC* phases are ferroelectric.⁹

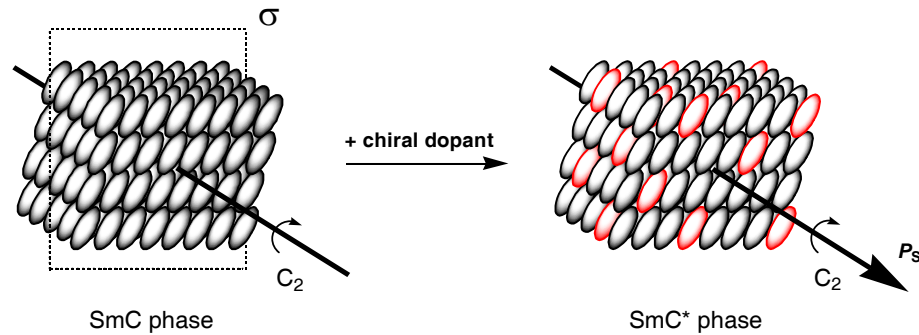


Figure 1-5. Symmetry elements of the achiral SmC and the chiral SmC (SmC*) phases, and the resulting P_S .

In the absence of external constraints, the SmC* phase forms a helical structure (Figure 1-6(a)), in which the P_S vector rotates from one layer to the next resulting in a net P_S of zero. However, in 1980, Clark and Lagerwall demonstrated that the SmC* helix spontaneously unwinds when the material is aligned between rubbed polyimide-coated glass slides, with a spacing on the order of the helical pitch, p (Figure 1-6(b)).¹⁰ In this aligned state, the SmC* phase is termed a surface-stabilized ferroelectric liquid crystal (SSFLC).

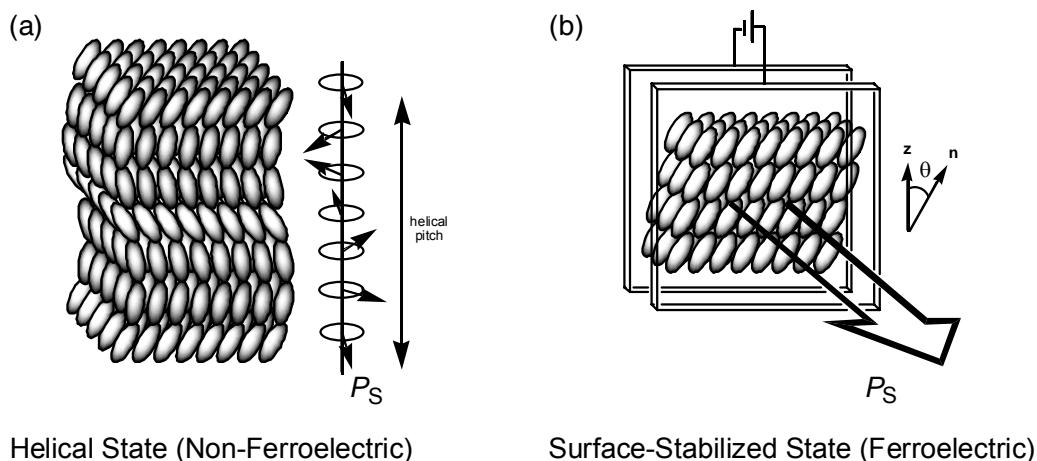


Figure 1-6. (a) Helical structure of the SmC* phase in the absence of external constraints, (b) the SmC* phase in the ferroelectric surface-stabilized state.

When an external field is applied parallel to the C_2 axis, the tilted mesogens of a SSFLC can be switched from one tilt orientation to another by precession of \mathbf{n} about \mathbf{z} . Mesogens go from $+\theta$ tilt orientation to $-\theta$ as the electric field is reversed, thus resulting in an ON/OFF light shutter when the SSFLC film is placed between crossed polarizers (Figure 1-7).

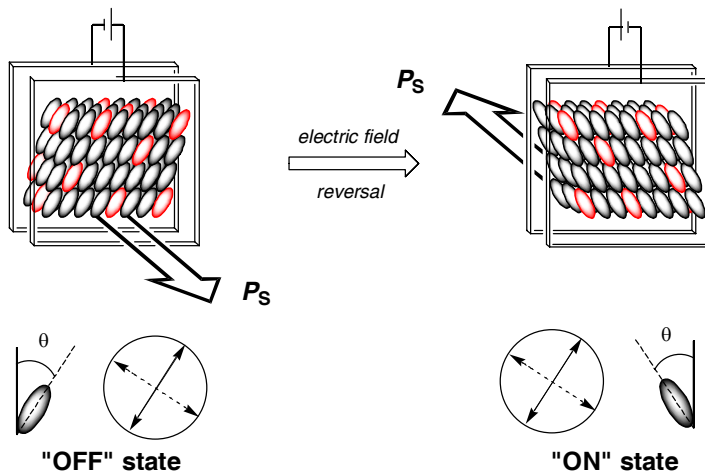


Figure 1-7. Switching ($+\theta$ and $-\theta$ orientations) between opposite applied fields in a SSFLC.

An ideal SmC* material for display applications is one that has a short switching time between $+\theta$ and $-\theta$ tilt orientations under an applied field. The switching time

(electro-optical rise time), τ_r , is dependant on the magnitude of P_S , the applied field (E) and the orientational viscosity (η), as described by Equation (1-2).¹¹

$$\tau_r \propto \frac{\eta}{|P_S|E} \quad (1-2)$$

Smectic C* liquid crystals consisting solely of chiral mesogens are not suitable for use as ON/OFF light shutters due to their highly viscous nature, which results in slower switching times. However, Kuczyński and Stegemeyer found that P_S can be induced in an achiral SmC phase after the addition of a chiral polar molecule (or “dopant”) that may or may not be mesogenic.¹² Stegemeyer and coworkers extended this work by determining the direct relationship between P_S and the mole fraction of dopant.¹³ Commercial devices featuring an ON/OFF light shutter typically consist of a chiral dopant with high polarization power (δ_p) doped into a low viscosity SmC host mixture with a wide temperature range. The ability of a dopant to induce a P_S in an otherwise achiral SmC host mixture is described as its polarization power (Equation (1-3)), where x_d is the mole fraction of the dopant and P_o is the reduced polarization, which is normalized for variations in tilt angle θ according to Equation (1-4).¹⁴

$$\delta_p = \left(\frac{dP_o(x_d)}{dx_d} \right)_{x_d \rightarrow 0} \quad (1-3)$$

$$P_o = \frac{P_S}{\sin \theta} \quad (1-4)$$

1.4.2. Molecular Origins of P_S

Developed by Walba and Clark in 1986,¹⁵ the Boulder model provides a rationale for spontaneous polar ordering at the molecular level. Recall the zig-zag conformation of the SmC phase determined through optical and X-ray experiments by Durand *et al.*

described in Section 1.3. This ordering is described by the Boulder model as a bent-cylinder (binding site) which has a zig-zag shape and is C_2 symmetric, as shown in Figure 1-8. As mesogens adopt this zig-zag shape, with rigid cores more tilted than side chains in an all *anti*- conformation, steric coupling between any polar functional group and the chiral centre results in an orientational bias of the corresponding molecular dipole along the C_2 axis that contributes to P_S .

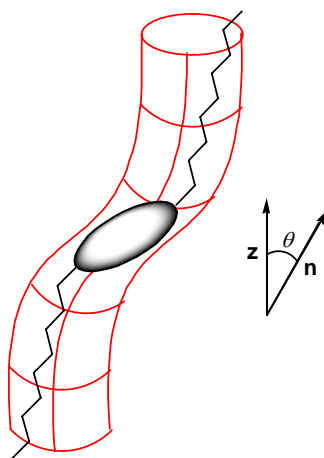
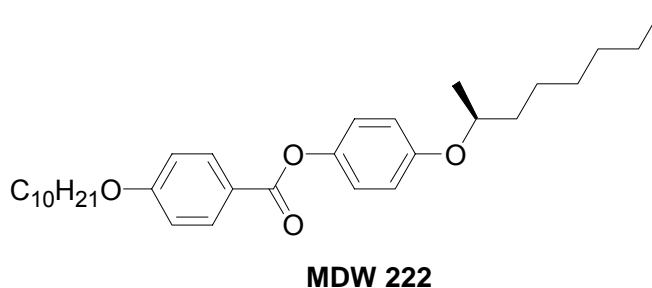


Figure 1-8. The bent-cylinder binding site with a guest molecule in the SmC^* phase, according to the Boulder model.

Wand *et al.* used compound **MDW 222** to illustrate the concept of the Boulder model.¹⁶ This compound consists of many polar functional groups, however, the only group contributing to P_S is that of the chiral ether side-chain. Other functional groups are too far away from the chiral centre to contribute to P_S .



Although there are three possible conformers for the so-called “stereo-polar unit” of **MDW 222**, one conformer (**A**) can be disregarded because the alkoxy dipole is oriented in the tilt plane of the SmC* phase and cannot contribute to P_S . All three conformations are shown in Figure 1-9 as Newman projections about the C₂-C₃ bond of the octyloxy side chain. The magnitude of P_S is a function of the difference in energy between the two conformers, **B** and **C**, each of which corresponds to P_S of opposite signs. By examining the Newman projections, conformer **B** is energetically more favoured due to less steric repulsion between the alkyl chain and the methyl group. The physics convention describes dipoles from negative to positive, and in the case of **B**, P_S points from left to right. This corresponds to a $-P_S$, which was confirmed by Wand *et al.* experimentally in 1991.

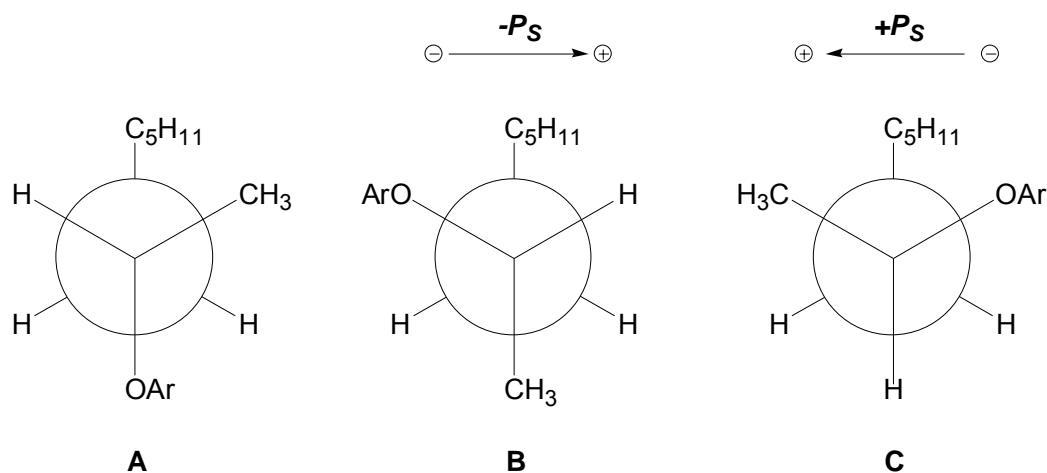
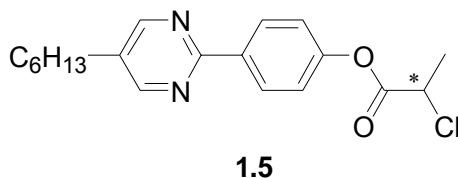


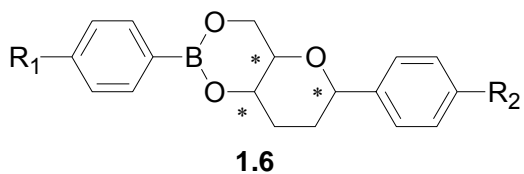
Figure 1-9. Newman projections along the C₂-C₃ bond of the three conformers of **MDW 222**, according to the Boulder model. Dipole moments are shown according to the physics convention. A $-P_S$ is predicted for the more favoured conformer **B**, which was confirmed experimentally.

1.4.3. Type I Dopants



The majority of chiral dopants are Type I dopants, such as **1.5**, in which the stereo-polar unit is located in the side-chain. Polarization powers for these dopants are normally independent of the structure of the SmC host. This observation can be rationalized by considering the amount of disorder associated with the alkyl side-chains that precludes any molecular recognition. Due to a lack of molecular recognition between the dopant and the host, Type I dopants act as *passive* guests, and conform to the zig-zag binding site imposed by the Boulder model, which is assumed to be invariant of the structure of the host. The Boulder model breaks down with regards to Type II dopants, where factors other than the imposition of an achiral zig-zag binding site come into play.

1.4.4. Type II Dopants



Type II dopants (such as **1.6**) contain a stereo-polar unit in the core of the molecule. The polarization power of such dopants tends to be dependant on the nature of the host because core-core correlation in SmC* phase allows for molecular recognition between dopant and host structures.¹⁷ Stegemeyer and coworkers explained the dependence of δ_p on host structure for Type II dopants based on a mathematical description of P_S (Equation (1-5)). The description contains two terms: (i) a polar

ordering term that is a function of the conformational asymmetry of the stereopolar unit, and (ii) a rotational distribution term that describes the orientation of the transverse dipole resulting from the stereopolar unit:

$$P_s = N\mu_{\perp} \cos\psi_o \langle \cos\psi \rangle \quad (1-5)$$

where N is the number density, μ_{\perp} is the magnitude of the molecular transverse dipole moment, $\langle \cos\psi \rangle$ is the polar order parameter (if $\langle \cos\psi \rangle = 1$, the molecules are perfectly ordered with respect to the polar axis), and ψ_o is the angle between μ_{\perp} and the molecular reference axis. According to Stegemeyer, Type II dopant-host dependence is due to variations of the rotational distribution of the transverse dipole caused by core-core interactions with host molecules. Thus, a dopant with a high polar ordering may yet induce a low P_s in a given host if the transverse dipole is oriented close to the tilt plane (Figure 1-10). The observed host dependence of Type II dopants suggests that these dopants are no longer *passive* guests in the SmC* phase, but rather *active* guests that can modify the shape of the bent cylinder binding site. Stegemeyer also suggested that chirality transfer from dopant to host might take place, resulting in a polar ordering of host molecules. In such cases, variations in δ_p would be a function of the transverse dipole of the host molecules.

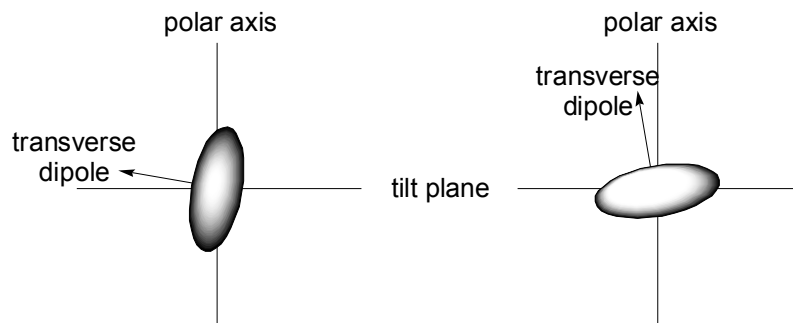
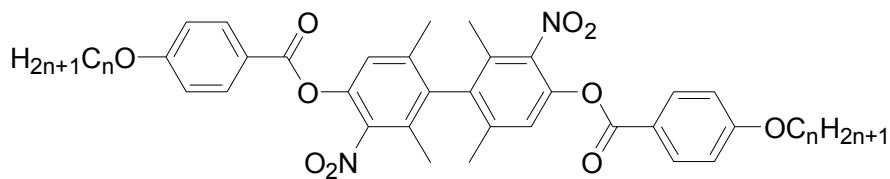


Figure 1-10. Examples of transverse dipoles of Type II dopants dependent on the orientation of the mesogens. Dipoles oriented close to the tilt plane induce a smaller P_S compared to those oriented close to the polar axis.

1.5. Chirality Transfer Feedback Model

Previous work in the Lemieux group featured a series of dopants with axially chiral biphenyl cores. The polarization power of dopants **1.7a-g** exhibited pronounced Type II behaviour, with the highest δ_p values recorded in hosts with complementary core structures, and δ_p values below the detection limit in other hosts.¹⁸ The four achiral hosts used by the Lemieux group are **PhB**, **DFT**, **NCB76** and **PhP1**. Compounds **1.7c** and **1.7d** showed large polarization powers in the host **PhP1**, and almost negligible polarization powers in the host **PhB** (see Table 1-1). Compound **1.7c** in **PhP1** is particularly noteworthy, as it has the highest δ_p reported in the literature thus far. The Type II behaviour can be explained in part by Stegemeyer's model, *i.e.*, a shift in rotational distribution bringing the transverse dipole closer to the polar axis. However, it was postulated that such a shift could not fully account for the pronounced Type II behaviour of these dopants and for the remarkably large magnitude of δ_p in **PhP1**.



a, n=4; **b**, n=6; **c**, n = 8; **d**, n = 9;
e, n = 12; **f**, n = 14; **g**, n = 16

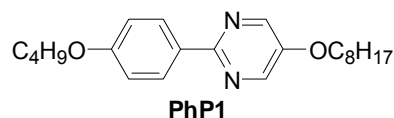
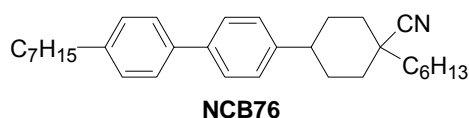
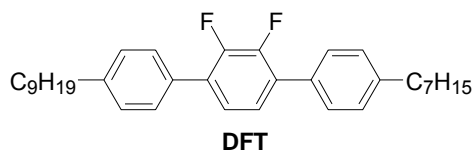
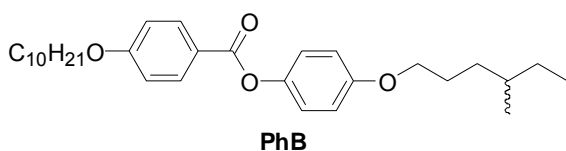


Table 1-1. Polarization powers of **1.7a-g** in the four achiral SmC hosts **PhB**, **DFT**, **NCB76** and **PhP1**. Polarization power values measured at $T-T_C = -5$ K. Taken from reference 18.

Dopant	δ_p (nC/cm ²) ^{a,b}			
	PhB	DFT	NCB76	PhP1
(+) 1.7a	<30 (-) ^c	<30 (+) ^c	183 ± 6 (+)	505 ± 51 (+)
(-) 1.7b	171 ± 11 (+)	98 (-) ^d	274 ± 12 (-)	1199 ± 81 (-)
(+) 1.7c	<30 (-) ^c	124 (+) ^d	373 ± 54 (+)	1738 ± 95 (+)
(-) 1.7d	<34 (-) ^c	312 ± 32 (-)	514 ± 38 (-)	1555 ± 119 (-)
(+) 1.7e	250 ± 11 (+)	602 ± 37 (+)	768 ± 23 (+)	1423 ± 149 (+)
(-) 1.7f	496 ± 43 (-)	817 ± 54 (-)	856 ± 73 (-)	1392 ± 140 (-)
(+) 1.7g	499 ± 42 (+)	550 ± 44 (+)	940 ± 71 (+)	1329 ± 60 (+)

^a Sign of polarization in parentheses. ^b Uncertainty is ± standard error of least-squares fit. ^c Estimated upper limit based on a detection limit of 0.3 nC/cm² at the highest dopant mole fraction. ^d Values extrapolated from a single P_o measurement at $x_d = 0.03 - 0.04$.

Lemieux *et al.* proposed the *chirality transfer feedback* (CTF) model to account for the large host dependence displayed by **1.7a-g**. The CTF model suggests that a chiral dopant may desymmetrize the bent-cylinder binding site through a *transfer of chirality* (perturbation) via core-core interactions in the SmC* phase. This effect, in turn, causes a shift in the conformational equilibrium of the dopant molecule (favouring one orientation of the transverse dipole along the C₂ axis) as a *feedback* effect (Figure 1-11). This model

highlights the importance of dopant-host core-core structural interactions on δ_p , which was first proposed by Gottarelli and coworkers for nematic liquid crystals.¹⁹

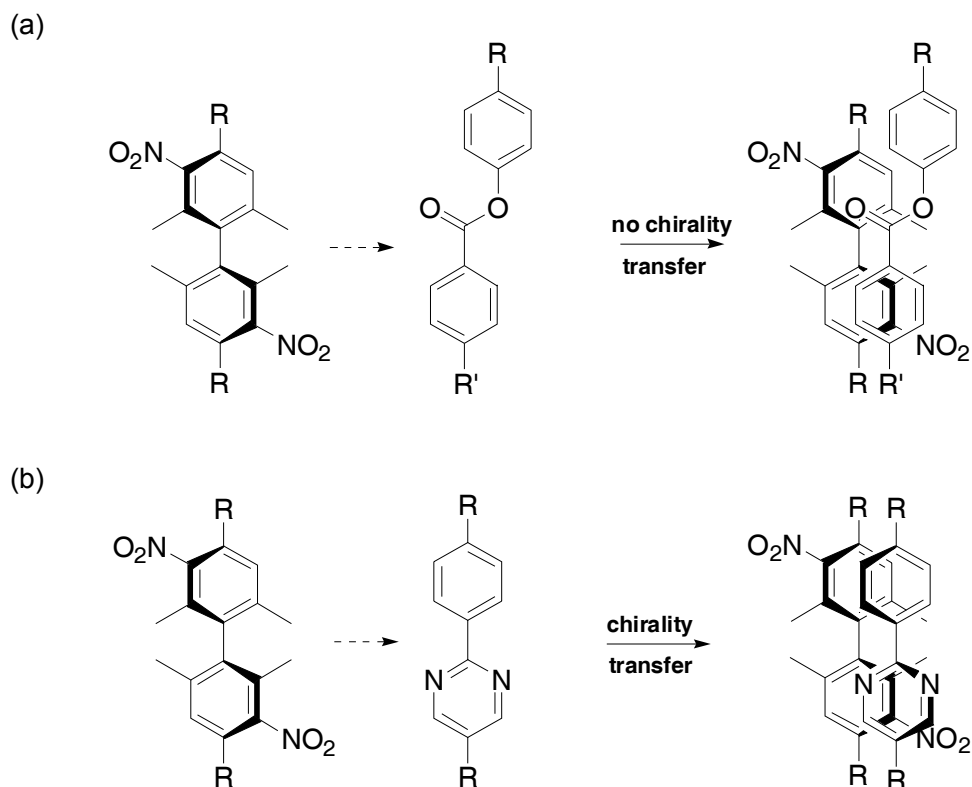
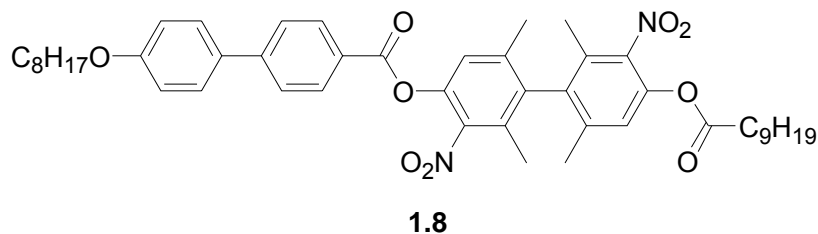


Figure 1-11. Illustration of core-core interactions between the dinitro biphenyl core and host cores of (a) **PhB** and (b) **PhP1**. A better structural match with host **PhP1** can be seen.

1.5.1. Indirect Evidence of Chirality Transfer



In order to test the CTF model, a number of studies were performed. Firstly, compound **1.8** was synthesized and doped into **PhP1**. Compounds **1.7c** and **1.8** have approximately the same molecular length, however the position of the core of **1.8** should be offset from the host molecular core, and thus have a lower δ_p . As expected, it was

found that **1.8** has a smaller δ_p of (-) 1101 nC/cm², compared to that of **1.7c** ((+) 1738 nC/cm²).

Secondly, the effect of varying chain lengths on the polarization power of **1.7** was also determined. As shown in Table 1-1, the polarization power of **1.7** increases in each host as the alkoxy chain length increases, until a certain value $n(\text{max})$ is reached. This observation was attributed to an increase in positional order of mesogens within layers, therefore increasing chirality transfer via core-core interactions.

Lastly, helical pitch measurements were carried out in mixtures formed by dopants **1.7a-g** (2 mol %) in **PhP1**, and a trend of decreasing pitch with increasing chain length was observed, with the exception of very long chain lengths (Figure 1-12). That is, the smaller the pitch (which is inversely proportional to chirality transfer) the greater the polarization power.

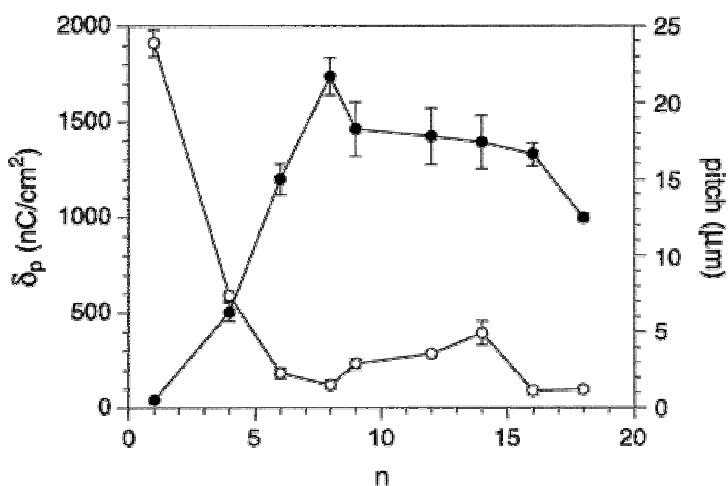
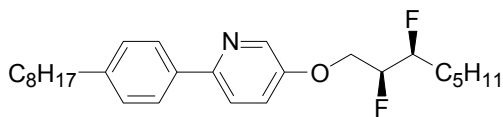
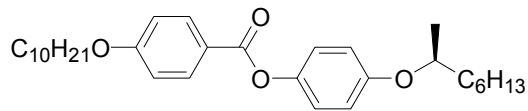


Figure 1-12. Polarization power δ_p (\bullet) and SmC* helical pitch p (\circ) as a function of increasing alkoxy chain lengths n for dopants **1.7a-g** in host **PhP1**. Also included are data points for $n = 1, 18$. Taken from reference 18.

1.5.2. Direct Evidence of Chirality Transfer



MDW950



1.9

Although the experiments described in the previous section supported the notion that CTF was contributing to δ_p in these systems, additional proof was sought. Probe experiments involving dopant **1.7d** and another dopant, either **MDW950** or **1.9**, were performed in hosts **PhP1** and **PhB**, respectively. The dopants **MDW950** (provided by Displaytech) and **1.9** mimic host molecules and are considered *probes* in the system. Studies were undertaken to measure any perturbation of **1.7d** on the probes and its effect on the polarization power of the probes in **PhP1** and **PhB**, assuming that the effect of **1.7d** on the polarization of the system would scale with the extent of the perturbation. Initially, the polarization power values of **MDW950** and **1.9** in **PhP1** and **PhB**, respectively, were measured in the absence of **1.7d** to provide a standard for reference. These measurements were then repeated after the addition of 4 mol % (+)-**1.7d** and (-)-**1.7d**, and the results were compared. Figure 1-13 shows the plots of reduced polarization P_o versus mole fraction of the probe in the presence of either (+)-**1.7d** or (-)-**1.7d**. Both enantiomers were used to determine whether the perturbation is chiral in nature. If the perturbation is achiral in nature, both enantiomers will have the same effect on the polarization power of the probe. However, if the perturbation is chiral in nature, each enantiomer will impart a different effect.

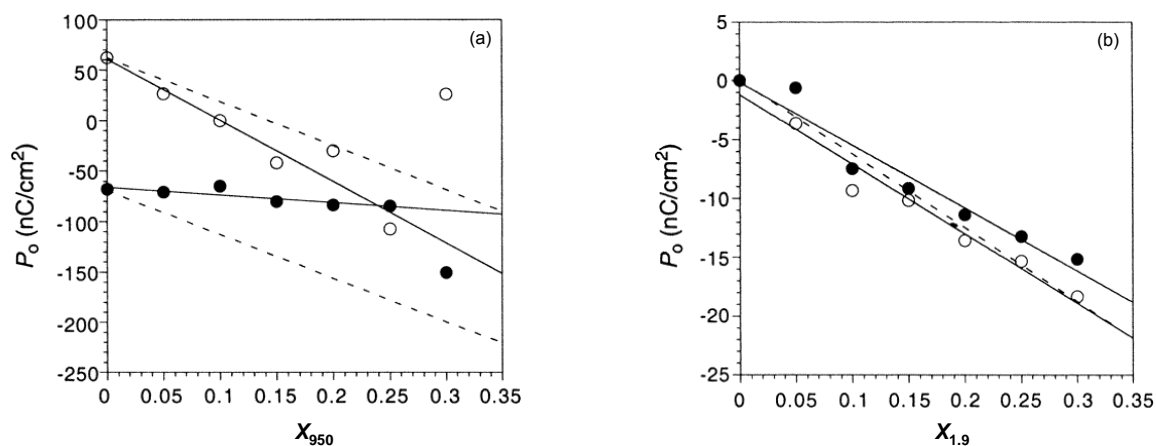


Figure 1-13. Reduced polarization P_o vs. mole fraction of probe molecule, x_{probe} , at $T - T_C = -5$ K in the presence of (+)-**1.7d** (\circ) and (-)-**1.7d** (\bullet) at a constant mole fraction of $x_{1.7d} = 0.04$ for (a) **MDW950** in **PhP1** and (b) **1.9** in **PhB**. The dashed lines correspond to the polarization power of the probe in the host in the absence of **1.7d**. Solid lines in (a) exclude data points at $x_{950} = 0.30$. Taken from reference 20.

In the case of **MDW950** in the achiral SmC host **PhP1**, the plots of P_o vs. x_d were linear up to $x_{950} = 0.25$, but deviated from linearity at higher mole fractions, possibly due to a cooperative effect between probe molecules. However, these results are significantly different from those predicted by the reference plot (dashed lines in Figure 1-13(a)). Hence, the polarization powers of the probe (excluding the data point at $x_{950} = 0.30$) were $\delta_{950} = -605 \pm 88$ nC/cm² in the presence of (+)-**1.7d** and $\delta_{950} = -78 \pm 23$ nC/cm² in the presence of (-)-**1.7d**, higher and lower than the predicted value of -435 ± 11 nC/cm². These polarization power results suggest that the dopant **1.7d** is not a *passive* guest in the system of **MDW950** and **PhP1**; rather, it is an *active* guest exerting a chiral perturbation on the system.²⁰ On the other hand, the plots of P_o vs. $x_{1,9}$ for the phenylbenzoate probe **1.9** in **PhB** in the presence of either enantiomer of **1.7d** are roughly superimposable and do not deviate from the predicted result (Figure 1-13(b)). Polarization powers in this system were $\delta_{1,9} = -59 \pm 5$ nC/cm² in the presence of (+)-**1.7d** and $\delta_{1,9} = -53 \pm 6$ nC/cm² in the presence of (-)-**1.7d**, which are not significantly different according to a student's t-

test at the 95% confidence level. This result is consistent with the structural dissimilarity between dopant **1.7d** and the host **PhB**, indicating a *passive* guest with no significant chiral perturbation being exerted on the system.

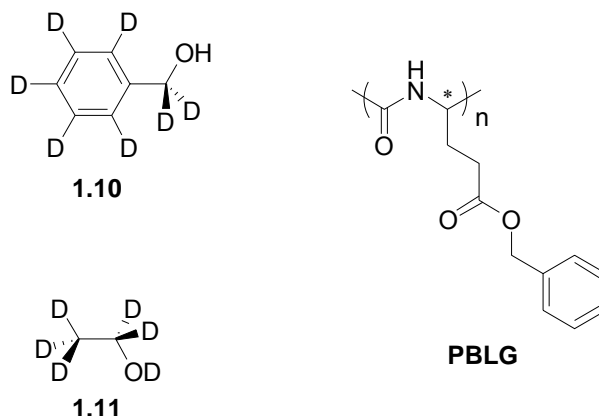
1.6. ^2H NMR spectroscopy

^2H NMR has been used by many research groups to assess dopant solubility in liquid crystal hosts. In an isotropic environment, signals arising from the interaction of ^2H quadrupole nuclei ($I = 1$) and the electric field gradient average to produce a singlet. However, in an anisotropic liquid crystalline environment, these interactions produce a quadrupolar doublet with quadrupolar splitting $\Delta\nu_Q$. The magnitude of $\Delta\nu_Q$ is directly proportional to the orientational order of the C-D bond, according to Equation (1-6):

$$\Delta\nu_Q = \frac{3}{2} \frac{Q_D V_{CD}}{h} \left(\frac{1}{2} \langle 3 \cos^2 \theta_{CD}^z - 1 \rangle \right) \quad (1-6)$$

where Q_D is the deuterium quadrupole moment, V_{CD} is the electric field gradient along the C-D bond, and θ_{CD}^z is the angle between the electric field gradient and the external magnetic field.

1.6.1. Detection of Chirality Using ^2H NMR



^2H NMR spectroscopy of achiral dopants in the chiral nematic liquid crystal host poly- γ -benzyl-L-glutamate (**PBLG**) was originally reported in 1981 by Czarniecka and Samulski, and subsequently by others in the 1990's.^{22, 23} In the case of benzyl alcohol- d_7 (**1.10**), the two benzylic deuterons gave different quadrupolar splitting $\Delta\nu_Q$, which was consistent with non-equivalent diastereotopic deuterons. In this case, it was postulated that interactions between **1.10** and **PBLG** caused enantiotopic deuterons to become diastereotopic in the local chiral environment of the host.²¹ Courtieu and coworkers showed that the relative intensities of the two diastereotopic signals in ^2H NMR for **1.10** could be used as a measure of enantiomeric excess.²² The ^2H NMR spectra of both benzyl alcohol- d_7 (Figure 1-14(a)) and ethanol- d_6 (**1.11**, Figure 1-14(b)) in **PBLG** show the non-equivalence of enantiotopic deuterons in a chiral liquid crystal host.^{22, 23}

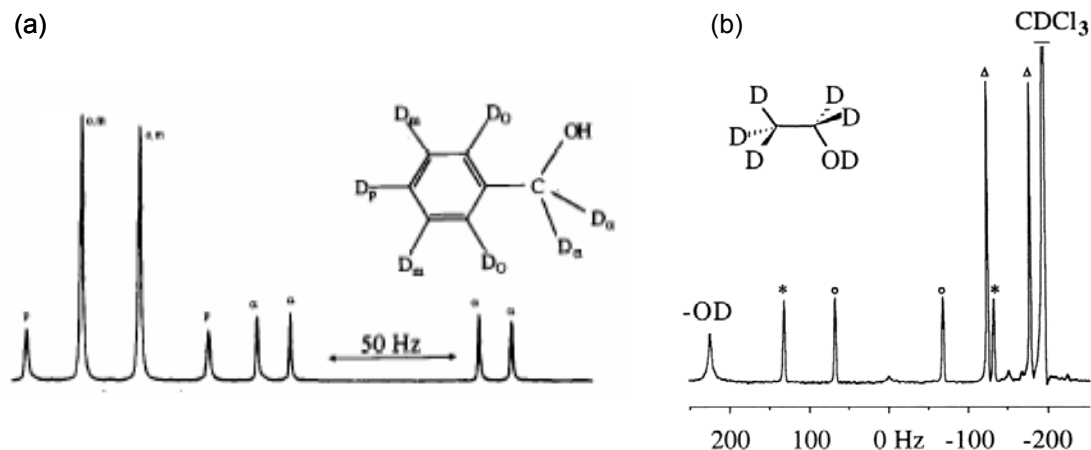
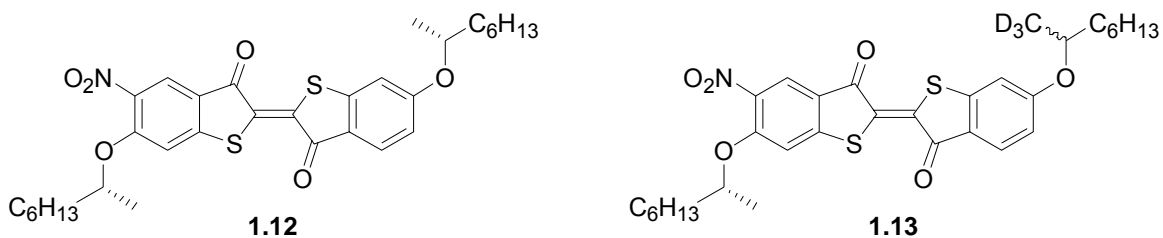


Figure 1-14. ^2H NMR spectra of (a) benzyl alcohol- d_7 and (b) ethanol- d_6 in the chiral nematic host poly- γ -benzyl-L-glutamate. Enantiotopic deuterons become diastereotopic in a chiral environment and each contributes to a separate quadrupolar doublet in the ^2H NMR spectra. Taken from references 22 and 23 respectively.

In the Lemieux group, variable temperature ^2H NMR studies were first conducted for compound **1.13**. The purpose of these studies was to determine the compatibility of these dopants in the four achiral liquid crystals hosts. Mixtures of compound **1.12** in **PhB** had showed homogeneous textures by polarized microscopy at 10 mol %. However, examination of the same mixture with the deuterated analogue **1.13** by ^2H NMR showed that the dopant was partitioned between liquid crystalline and isotropic microdomains (*i.e.*, microphase separation), over a temperature range of 7 K (Figure 1-15).²⁴ This was determined by the appearance of an isotropic singlet together with a quadrupolar doublet in the spectra.



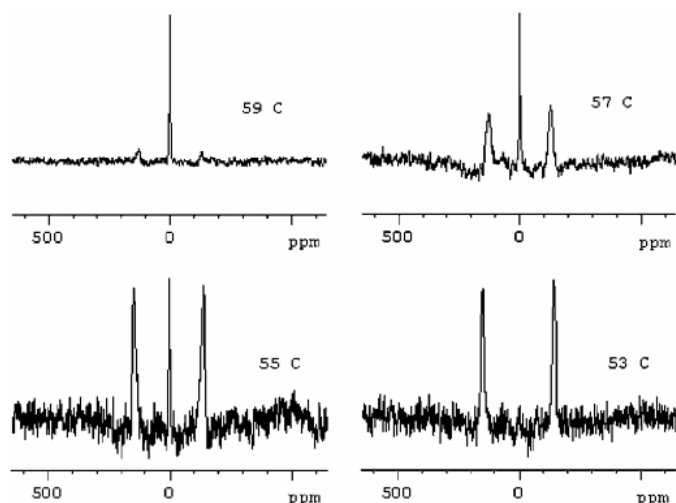
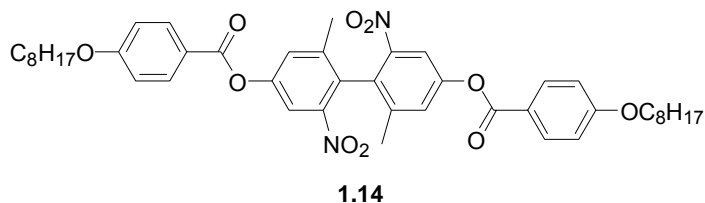
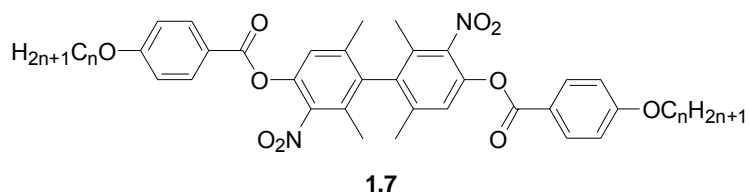


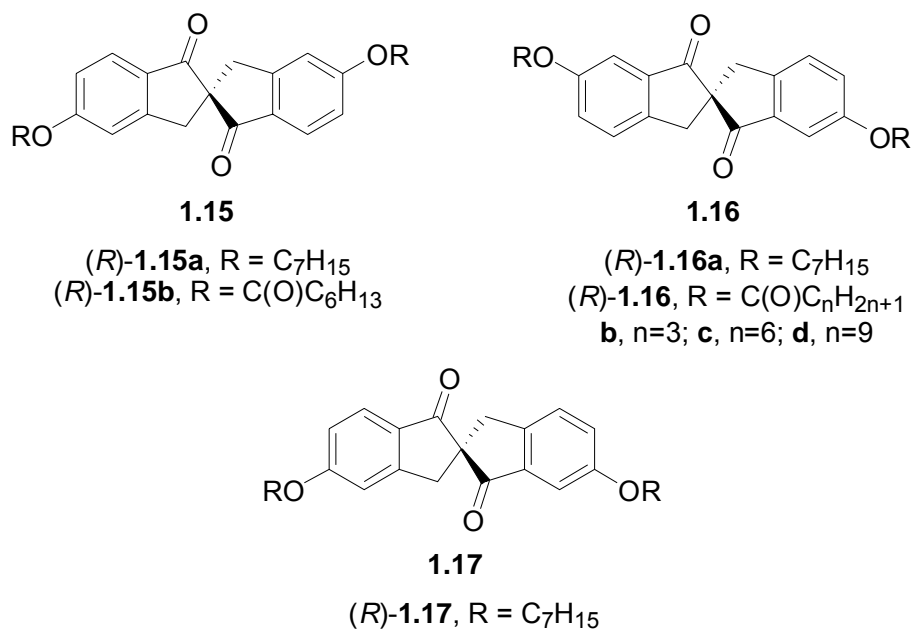
Figure 1-15. ^2H NMR spectra of **1.13** in host **PhB** at temperature ranges throughout phases I-SmC. Notice microphase separation at temperatures 57 °C and 55 °C. Taken from reference 24.

1.7. Spirobiindandione Dopants



Many factors must be taken into consideration when designing new dopants with large polarization powers. In the case of **1.7**, increased steric interaction between the ortho-nitro substituent and the ester group increased the conformational energy bias to ca. 1.2 kcal/mol between conformers of opposite polarity in a SmC host, which is 0.8 kcal/mol higher than that estimated for the first generation of dinitrobiphenyl dopant, **1.14**. The increase in conformational bias resulted in an increase in polarization power for these dopants from $+161 \pm 11 \text{ nC/cm}^2$ (**1.14**) to $+1738 \pm 95 \text{ nC/cm}^2$ (**1.7**) in the host

PhP1. Based on these results, the Lemieux group sought to further increase polarization powers of Type II dopants by synthesizing spirobiindandione compounds, where the core should be conformationally more rigid with respect to the side-chains within the constraints of the binding site. Three dopants that met this requirement were 2,2'-spirobiindan-1,1'-dione molecules substituted in the 5,5'-(**1.15**), 6,6'-(**1.16**), and 5,6'-(**1.17**) positions.



Initial studies featured the syntheses of **1.15a**, **1.16a** and **1.17**, and the evaluation of their polarization powers in the four achiral LC hosts. Deuterated versions (side-chains = -OCD₂C₆H₁₃) were used in ²H NMR studies to determine dopant-host compatibility. Dopant (*RS*)-**1.15a-d₄** showed good solubility at 10 mol % in all LC hosts, according to the observation of at least one quadrupolar doublet and no isotropic singlet in the ²H NMR spectra (Figure 1-16). Despite being structurally similar, the ²H NMR spectra of dopants (*RS*)-**1.16a-d₄** and (*RS*)-**1.17-d₄** featured an isotropic singlet together with a weak quadrupolar doublet in the LC host **PhP1**, at mole fractions well below the solubility limit.

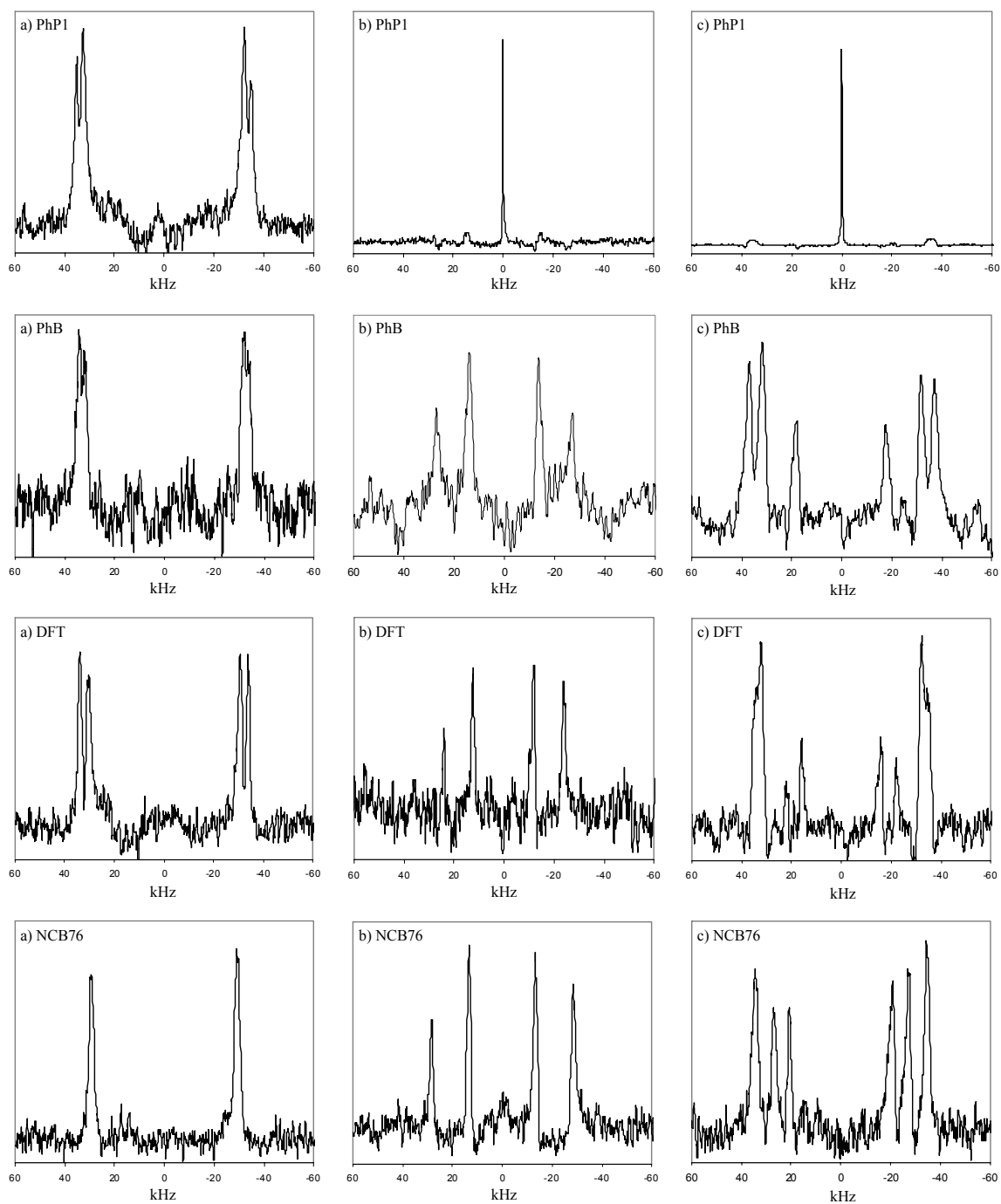


Figure 1-16. ^2H NMR spectra in the SmC^* phase of (a) 10 mol % mixtures of $(RS)\text{-1.15a-}d_4$ in the four liquid crystal hosts, (b) mixtures of $(RS)\text{-1.16a-}d_4$ in the four liquid crystal hosts at the following concentrations: 2.6 mol % (**PhP1**), 3 mol % (**PhB**), 3 mol % (**DFT**), and 5 mol % (**NCB76**) and (c) 10 mol % mixtures of $(RS)\text{-1.17-}d_4$ in the four liquid crystal hosts. Spectra recorded at $T - T_C = -10$ K. Taken from reference 25.

The observation of pairs of quadrupolar doublets ($\Delta\Delta\nu_Q$ ranging from 0 kHz for *(RS)*-**1.15a**-*d*₄ in **NCB76** to 30 kHz for *(RS)*-**1.16a**-*d*₄ in **NCB76**) suggests a non-equivalence of the methylene deuterons in the SmC* phase, due to a chiral perturbation of the local environment.²⁵ Based on the expectation that the magnitude of chiral perturbations in the system should correlate with the difference in quadrupolar splitting $\Delta\Delta\nu_Q$, dopant *(RS)*-**1.16a**-*d*₄ has the largest perturbation of all of the dopants in **NCB76**. The ²H NMR spectra of dopant *(RS)*-**1.17**-*d*₄ in all four hosts exhibited characteristics of both *(RS)*-**1.15a**-*d*₄ and *(RS)*-**1.16a**-*d*₄, and will not be discussed further.

Polarization power measurements were conducted for these dopants, and the results are reported in Table 1-2. Polarization powers of dopant *(R)*-**1.15a** are uniformly positive, and the highest polarization power of $+749 \pm 35$ was recorded in the host **PhP1**. Conversely, dopant *(R)*-**1.16a** has polarization powers that are uniformly negative, with the highest polarization power of -1037 ± 100 recorded in **NCB76**. Dopant *(R)*-**1.17** gave polarization powers that had inconsistent signs throughout the hosts, further showing that it is a hybrid of *(R)*-**1.15a** and *(R)*-**1.16a**.

Table 1-2. Polarization powers of *(R)*-**1.15a-b**, *(R)*-**1.16a-d**, and *(R)*-**1.17** in the four achiral SmC hosts. Values measured at $T-T_C = -10$ K. Taken from references 25 and 27.

Dopant	δ_p (nC/cm ²) ^{a,b}			
	PhB	DFT	NCB76	PhP1
<i>(R)</i> - 1.15a	460 ± 13 (+)	21 ± 3 (+)	363 ± 30 (+)	749 ± 35 (+)
<i>(R)</i> - 1.16a	79 ± 9(-)	285 ± 26 (-)	1037 ± 100 (-)	> 160 (-)
<i>(R)</i> - 1.17	130 ± 7 (-)	220 ± 5 (-)	144 ± 7 (-)	> 11 (+)
<i>(R)</i> - 1.15b	242 ± 24 (+)	<30 (+/-) ^c	474 ± 44 (+)	315 ± 26 (+)
<i>(R)</i> - 1.16b	> 120 (-)	(-) ^d	1389 ± 51 (-)	< 30 (-)
<i>(R)</i> - 1.16c	> 97 (-)	(-) ^d	1449 ± 36 (-)	< 39 (-)
<i>(R)</i> - 1.16d	> 150 (-)	> 240 (-)	1213 ± 68 (-)	< 27 (-)

^a Sign of polarization in parentheses. ^b Uncertainty is ± standard error of least-squares fit. ^c Inversion of polarization with temperature. ^d Dopants crystallized above the Curie point.

In order to investigate further the behaviour of chiral dopants with spirobiindandione cores, the diester dopants (*R*)-**1.15b** and (*R*)-**1.16b-d** were synthesized and their polarization powers were measured. Polarization powers for the diester dopants follow the same trends as the diether dopants, with the highest polarization power of $-1449 \pm 36 \text{ nC/cm}^2$ occurring from dopant (*R*)-**1.16c** in host **NCB76**.^{26, 27} A comparison of polarization powers of (*R*)-**1.15** and (*R*)-**1.16** is shown in Figure 1-17.

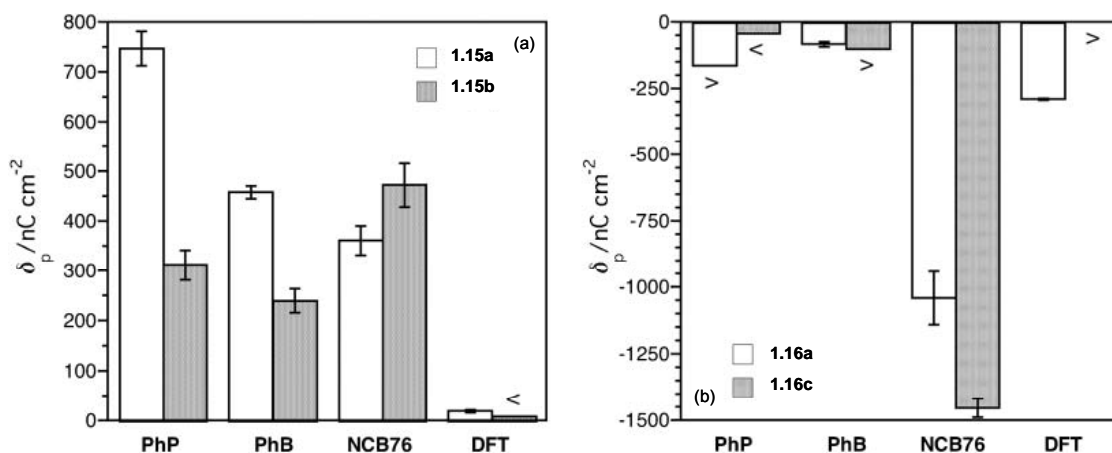


Figure 1-17. Bar graphs showing a comparison of polarization powers (δ_p) of diether and diester alkyl chains on (a) 5,5'-disubstituted-2,2'-spirobiindan-1,1'-dione ((*R*)-**1.15**) and (b) 6,6'-disubstituted-2,2'-spirobiindan-1,1'-dione ((*R*)-**1.16**), in all four LC hosts. Note the uniformly positive δ_p for dopant (*R*)-**1.15** and uniformly negative δ_p for dopant (*R*)-**1.16**. Taken from reference 27.

1.7.1. Conformational Analysis

In order to understand the relative signs of polarization and host dependence of dopants (*R*)-**1.15a** and (*R*)-**1.16a**, conformational analyses were conducted at the AM1 level. These calculations included constraints imposed by the Boulder model as a bent-cylinder zig-zag binding site, with the core more tilted than the side-chains fully extended in an all-*anti* conformation, and treated the dopant as a *passive* guest in the system. The calculations identified a total of 8 conformers, but 5 of these conformers could be disregarded: two with transverse dipoles that lie within the tilt plane and do not contribute

to polarization, and three with molecular shapes that do not conform to the bent cylinder binding site. Of the remaining three conformers, two of them are degenerate, **P** and **P'**. The calculations suggest that each dopant may be in equilibrium between two different conformations: the **P/P'** conformations and the **C₂** conformation. The **P/P'** conformers have one indanone ring congruent with the tilt plane defined by **n** and **z**, whereas the **C₂** conformer has the **C₂** axis of the core coincident with the polar axis. More importantly, the calculations indicate that the **P/P'** and **C₂** conformers have transverse dipole moments μ_{\perp} oriented in opposite directions along the polar axis. Thus, this model suggests that the overall spontaneous polarization resulting from these dopants may depend on the position of the equilibrium between the **P/P'** and **C₂** conformations. The space-filling models showing the **P/P'** and **C₂** conformers for (*R*)-**1.15a** and (*R*)-**1.16a** are shown in Figure 1-18 as side-on views of the spirobiindandione core. Although essentially the same conformational distribution is shown for (*R*)-**1.15a** and (*R*)-**1.16a**, the calculations predict polarization values of opposite signs, which is consistent with the δ_p results obtained experimentally.

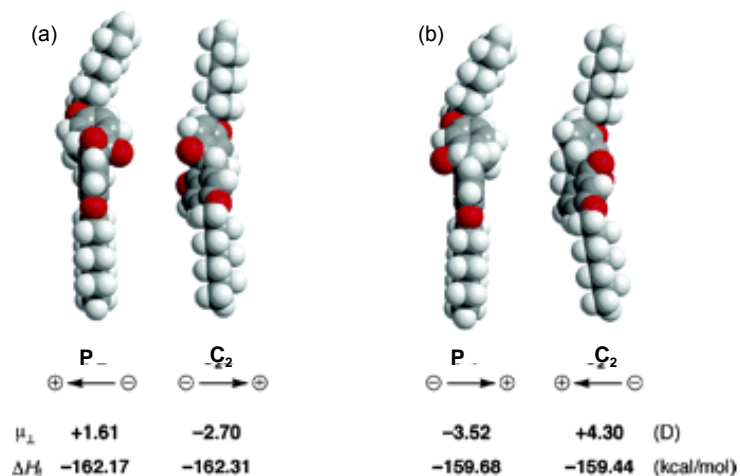


Figure 1-18. Space-filling model showing minimized zig zag conformations of dopant (a) (*R*)-**1.15a** and (b) (*R*)-**1.16a** as side-on views of the spirobiindandione cores. The tilt plane is vertical and normal to the plane of the page, and the polar axis is horizontal and in the plan of the page. The μ_{\perp} vectors point from negative to positive according to the physics convention. Taken from reference 25.

An initial hypothesis to explain the host dependence of δ_p (excluding any contributions from CTF) was that steric demands of the spirobiindandione core controls the **P/C₂** equilibrium. If the bent cylinder binding site is simplified to 3-cylindrical sections forming a zig-zag shape, it can be seen from Figure 1-19 that the core section for the **P** conformation is ca. 1.5 Å shorter than that of the **C₂** conformer. This suggest that the equilibrium between the conformers would shift towards the **P** conformer (positive μ_{\perp}) as the host core length becomes shorter, and towards the **C₂** conformer (negative μ_{\perp}) for hosts with longer core lengths. This hypothesis is consistent with results for dopant (*R*)-**1.15a**, where δ_p increases towards more positive values with decreasing host core length (+21 nC/cm² in **DFT**, core length = 14.4 Å vs. +749 nC/cm² in **PhP1**, core length = 9.7 Å). However, this hypothesis breaks down for dopant (*R*)-**1.16a**, where other factors such as chirality transfer may come in to play, especially with respect to the unusually high δ_p values recorded for (*R*)-**1.16a** in **NCB76**. The

contribution of a chirality transfer feedback effect with the 6,6'-disubstituted system would be consistent with the observation of pairs of quadrupolar doublets in the ^2H NMR spectra and the large $\Delta\Delta\nu_Q$ values observed in **NCB76**.

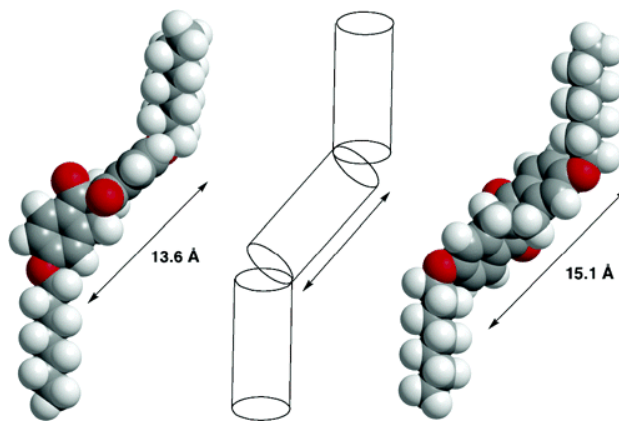


Figure 1-19. Space-filling models of the conformations **P** (left) and **C₂** (right) for *(R)*-**1.15a** in relation to the 3-cylinder zig-zag binding site according to the Boulder model.

1.8. Project Outline

The aim of this project is twofold: first, to extend the work of Finden and Yuh by using ^2H NMR spectroscopy to investigate the contribution of CTF to the polarization power of the 5,5'- and 6,6'-disubstituted-2,2'-spirobiindan-1,1'-dione dopants with different linking groups. Secondly, to examine the effect of removing one of the carbonyl groups on the spirobiindandione core on the polarization power of the dopants.

In the first section of this thesis, ^2H NMR studies are used to determine the magnitude of chiral perturbation of 5,5'-bis-(octanoyloxy-2,2- d_2)-2,2'-spirobiindan-1,1'-dione (*(RS)*-**2.3- d_4**) and the 6,6'- analogue (*(RS)*-**2.6- d_4**) on four achiral LC hosts. These results were correlated to δ_p measurements obtained by Finden *et al.* for the non-deuterated dopants *(R)*-**1.15b** and *(R)*-**1.16c**. Furthermore, a deuterated version of dopant **1.15a** in which the CD_2 group is one carbon removed from the oxygen was synthesized to

compare the effect of increasing the distance between the CD₂ group and the chiral core on $\Delta\Delta v_Q$.

Next, reduced versions of the spirobiindandione cores were synthesized, and the polarization powers of these compounds were measured in **NCB76**. Half reduced molecules were synthesized for both the 5,5'- and 6,6'- systems, and 1,1-*d*₂-heptyloxy side chains were added to both versions. 2,2-*d*₂-Octanoyloxy side chains were added to the 6,6'-system, based on encouraging results from the first part of this thesis.

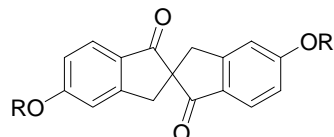
1.9. References

- (1) Reinitzer, F. *Monatsh. Chem.* **1888**, 9, 421.
- (2) Lehmann, O. *Z. Phys. Chem.* **1889**, 4, 462.
- (3) Goodby, J. W. In *Handbook of Liquid Crystals*; Demus, D.; Goodby, J.; Gray, G. W.; Spiess, H.-W.; Vill, V. Eds.; Wiley-VCH: Weinheim, 1998; Vol. 2A.
- (4) Gray, G. W.; Goodby, J. W. G. *Smectic Liquid Crystals: Textures and Structures*; Leonard Hill: Glasgow, 1984.
- (5) McMillan, W. L. *Phys. Rev. A.* **1973**, 8, 1921.
- (6) Wulf, A. *Phys. Rev. A.* **1975**, 11, 365.
- (7) Bartolino, R.; Doucet, J.; Durand, G. *Ann. Phys.* **1978**, 3, 389.
- (8) Jang, W.G.; Glaser, M.A.; Park, C.S.; Kim, K.H.; Lansac, Y.; Clark, N.A. *Phys. Rev. E.* **2001**, 64, 050712.
- (9) Meyer, R. B.; Liébert, L.; Strzelecki, L.; Keller, P. *J. Phys. (Paris) Lett.* **1975**, 36, L69.
- (10) Clark, N. A.; Lagerwall, S. T. *Appl. Phys. Lett.* **1980**, 36, 899.
- (11) Handschy, M. A.; Clark, N. A. *Appl. Phys. Lett.* **1982**, 41, 39.

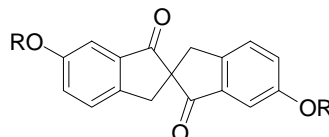
- (12) Kuczyński, W.; Stegemeyer, H. *Chem. Phys. Lett.* **1980**, *70*, 123.
- (13) Stegemeyer, H.; Meister, R.; Hoffmann, U.; Sprick, A.; Becker, A. *J. Mater. Chem.* **1995**, *5*, 2183.
- (14) Siemensmeyer, K.; Stegemeyer, H. *Chem. Phys. Lett.* **1988**, *148*, 409.
- (15) Walba, D. M.; Slater, S. C.; Thurmes, W. N.; Clark, N. A.; Handschy, M. A.; Supon, F. *J. Am. Chem. Soc.* **1986**, *108*, 5210.
- (16) Wand, M. D.; Vohra, R.; Walba, D. M.; Clark, N. A.; Shao, R. *Mol. Cryst. Liq. Cryst.* **1991**, *202*, 183.
- (17) Lemieux, R. P. *Acc. Chem. Res.* **2001**, *34*, 845.
- (18) Vizitiu, D.; Lazar, C.; Halden, B. J.; Lemieux, R. P. *J. Am. Chem. Soc.* **1999**, *121*, 8229.
- (19) Gottarelli, G.; Hibert, M.; Samori, B.; Solladié, G.; Spada, G. P.; Zimmermann, R. *J. Am. Chem. Soc.* **1983**, *105*, 7318.
- (20) Hartley, C.S.; Lazar, C.; Wand, M.D.; Lemieux, R.P. *J. Am. Chem. Soc.* **2002**, *124*, 13513.
- (21) Czarniecka, K.; Samulski, E. T. *Mol. Cryst. Liq. Cryst.* **1981**, *63*, 205.
- (22) Meddour, A.; Canet, I.; Loewenstein, A.; Péchiné, J. M.; Courtieu, J. *J. Am. Chem. Soc.* **1994**, *116*, 9652.
- (23) Merlet, D.; Loewenstein, A.; Smadja, W.; Courtieu, J.; Lesot, P. *J. Am. Chem. Soc.* **1998**, *120*, 963.
- (24) Vlahakis, J. Z.; Lemieux, R.P. *J. Mater. Chem.* **2004**, *14*, 1486.
- (25) Boulton, C. J.; Finden, J. G.; Yuh, E.; Sutherland, J. J.; Wand, M. D.; Wu, G.; Lemieux, R. P. *J. Am. Chem. Soc.* **2005**, *127*, 13656.

- (26) Finden, J. G. Ph.D. thesis, Queen's University, 2006.
- (27) Finden, J. G.; Yuh, E.; Huntley, C.; Lemieux, R. P. *Liq. Cryst.* **2007**, *34*, 1095.

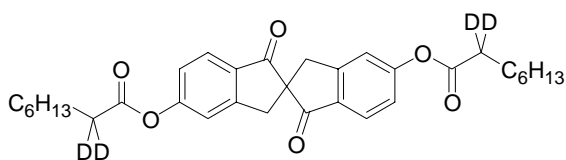
Chapter 2. ^2H NMR Spectroscopy: Detection of Chirality Transfer Feedback on 2,2'-Spirobiindan-1,1'-dione Dopants



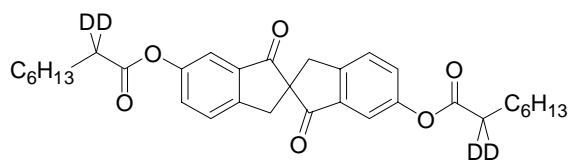
(*R*)-**1.15a**, R = C₇H₁₅
 (*R*)-**1.15b**, R = C(O)C₆H₁₃
 (*RS*)-**1.15a-d₄**, R = CD₂C₆H₁₃



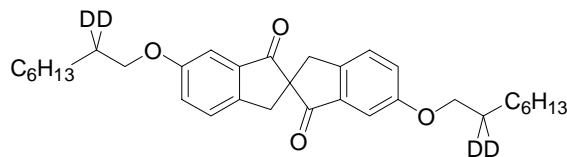
(*R*)-**1.16a**, R = C₇H₁₅
 (*R*)-**1.16b**, R = C(O)C_nH_{2n+1}
b, n=3; **c**, n=6; **d**, n=9
 (*RS*)-**1.16a-d₄**, R = CD₂C₆H₁₃



(*RS*)-**2.3-d₄**



(*RS*)-**2.6-d₄**



(*RS*)-**2.9-d₄**

As discussed in the introduction, recent studies have shown that the host dependence of the polarization power of atropisomeric dinitrophenyl dopants is due in part to chirality transfer feedback (CTF).¹ The spirobiindandione dopants (*R*)-**1.15a-b** and (*R*)-**1.16a-d** exhibit polarization powers that also vary greatly with the structure of the achiral host. Furthermore, the 6,6'-disubstituted dopants (*R*)-**1.16a** and (*R*)-**1.16c** exhibit polarization powers almost 300 % greater than those of the 5,5'-analogues (*R*)-**1.15a** and (*R*)-**1.15b** in the same host, **NCB76**.² ^2H NMR studies completed by Lemieux *et al.* found that the appearance of pairs of quadrupolar doublets in the SmC* phase for

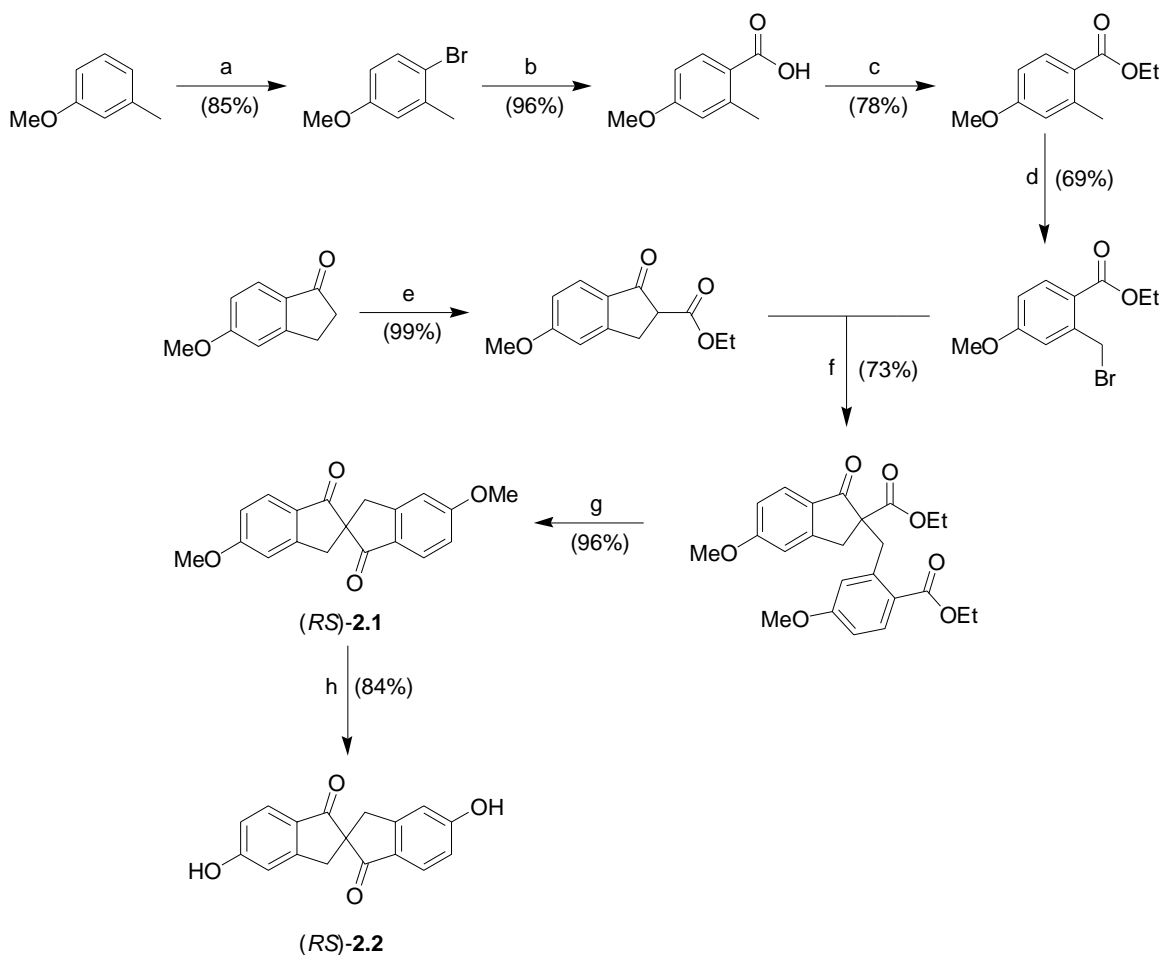
the diether systems ((*RS*)-**1.15a-d₄** and (*RS*)-**1.16a-d₄**) is consistent with a chiral perturbation of the dopant on its local environment, where the magnitude of the difference in quadrupolar splitting between doublets ($\Delta\Delta\nu_Q$) reflects the extent of chiral perturbation exerted by the dopant on the host. We sought to investigate the effect of CTF on δ_p in the deuterated diester systems of both the 5,5'- and 6,6'-spirobiindandione systems ((*RS*)-**2.3-d₄** and (*RS*)-**2.6-d₄**) by detecting chiral perturbations using ²H NMR spectroscopy. As described herein, these results are consistent with our original interpretation of the ²H NMR spectra for (*R*)-**1.15a-d₄** and (*R*)-**1.16a-d₄** in **NCB76**; *i.e.*, that the appearance of pairs of quadrupolar doublets is due to a local chiral perturbation causing the CD₂ deuterons to become diastereotopic.

2.1. Synthesis and Resolution

The dopant 5,5'-bis-(octanoyloxy-2,2-*d*₂)-2,2'-spirobiindan-1,1'-dione, (*RS*)-**2.3-d₄**, was synthesized following an approach first developed by C. J. Boulton, and optimized by E. Yuh, and is shown in Scheme 2-1.^{2, 3, 4} The 6,6'-bis-(octanoyloxy-2,2-*d*₂)-2,2'-spirobiindan-1,1'-dione, (*RS*)-**2.6-d₄**, was synthesized according to an approach developed by J. Finden, and is shown in Scheme 2-2. The cores of compounds (*RS*)-**2.3-d₄**, (*RS*)-**2.6-d₄** and (*RS*)-**2.9-d₄** were obtained using synthetic routes adapted from Nieman and Keay for a 2,2'-spirobiindan-1,1'-dione.⁵ As shown in Scheme 2-3, the dopant (*RS*)-**2.3-d₄** was synthesized from the diol (*RS*)-**2.2** using DCC/DMAP and 2,2-*d*₂-octanoic acid (C/D/N Isotopes Inc.) in methylene chloride, with a yield of 52 %. The dopant (*RS*)-**2.6-d₄** was synthesized in a similar manner using diol (*RS*)-**2.5**, with a yield of 70 % (Scheme 2-4). Deuterated octanoic acid was used instead of heptanoic acid as a side chain because of its commercial availability. Reduction of 2,2-*d*₂-octanoic acid (**2.7**)

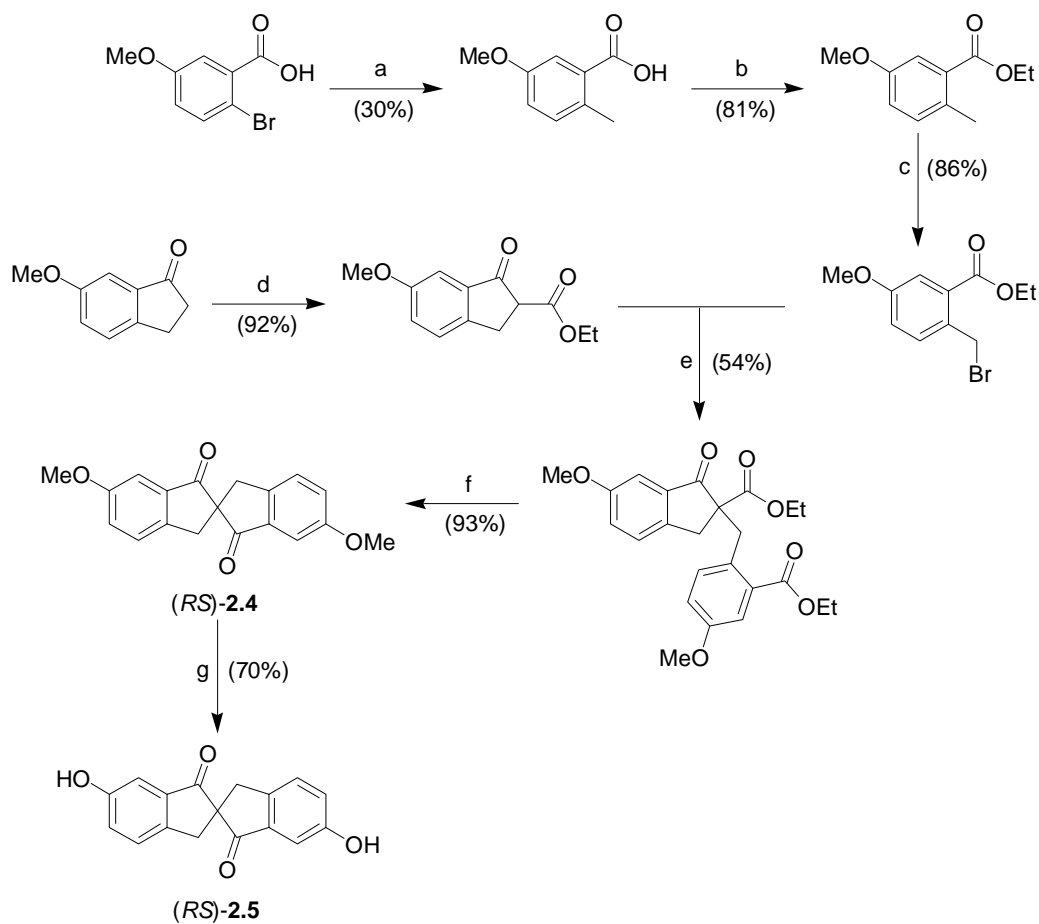
with LiAlH_4 gave 2,2- d_2 -octanol, **2.8**, in a 60 % yield. Dopant (*RS*)-**2.9- d_4** was then synthesized in a 66 % yield via a Mitsunobu reaction using **2.8** as the side-chain (Scheme 2-5). Prior to doping into the liquid crystal hosts, all dopants were recrystallized from hexanes after filtration through a 0.45 μm PTFE membrane.

Scheme 2-1.



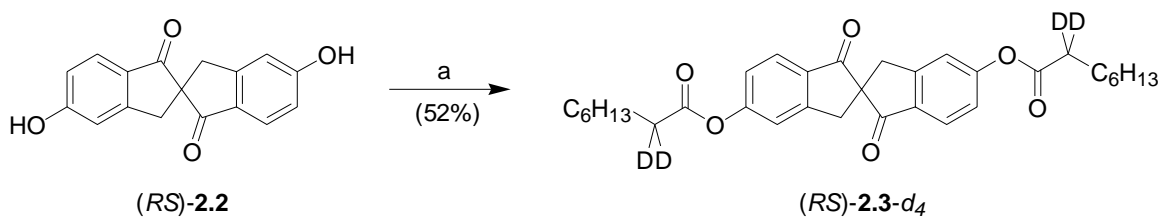
Reagents and conditions: (a) NBS, acetonitrile, rt; (b)(i) $^n\text{BuLi}$, THF, -78°C , (ii) CO_2 ; (c) H_2SO_4 , EtOH, reflux; (d) NBS, AIBN, cyclohexane, reflux; (e) diethyl carbonate, NaH, toluene, reflux; (f) NaH, DMF, 60°C ; (g) H_2SO_4 , EtOH, H_2O reflux; (h) AlCl_3 , toluene, reflux.

Scheme 2-2.



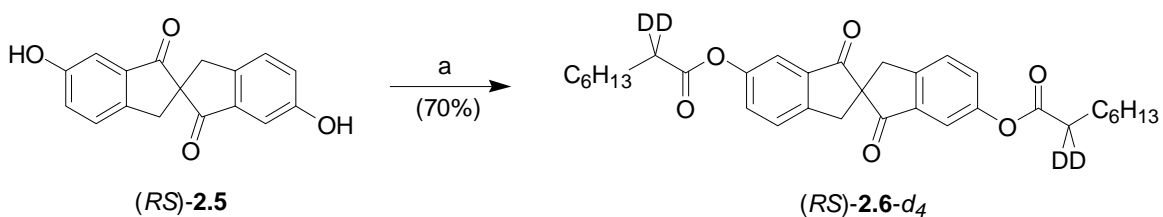
Reagents and conditions: (a)(i) ${}^n\text{BuLi}$, THF, -78°C , (ii) CH_3I ; (b) H_2SO_4 , EtOH, reflux; (c) NBS, cyclohexane, reflux; (d) diethyl carbonate, NaH, toluene, reflux; (e) NaH, DMF, 60°C ; (f) H_2SO_4 , EtOH, H_2O , reflux; (g) AlCl_3 , toluene, reflux.

Scheme 2-3.



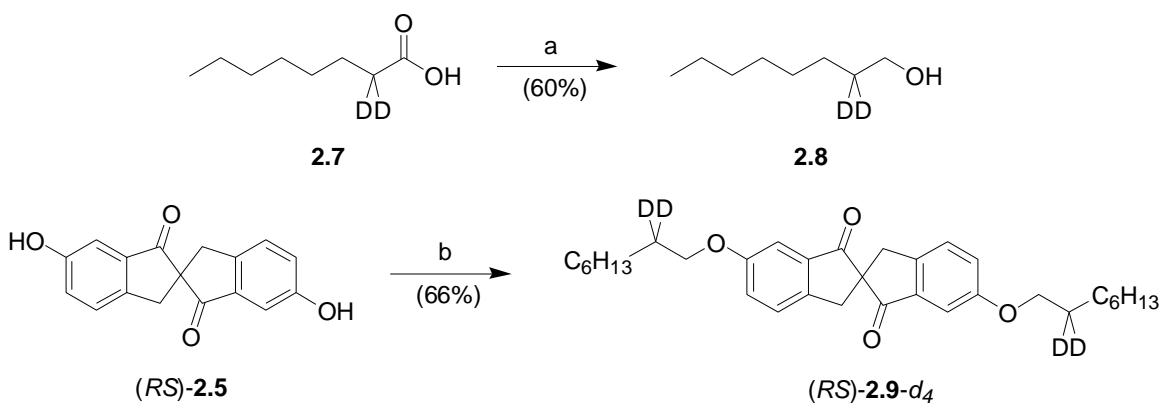
Reagents and Conditions: (a) 2,2- d_2 -octanoic acid, DCC, DMAP, CH_2Cl_2 , rt.

Scheme 2-4.



Reagents and Conditions: (a) 2,2- d_2 -octanoic acid, DCC, DMAP, CH_2Cl_2 , rt.

Scheme 2-5.



Reagents and Conditions: (a) LiAlH_4 , Et_2O , reflux; (b) 2.8, PPh_3 , DIAD, THF, rt.

2.2. Results

2.2.1. ^2H NMR Spectroscopy: Dopants with Ester Side Chains

The dopants (*RS*)-2.3- d_4 and (*RS*)-2.6- d_4 were doped into the four commercially available hosts **PhP1**, **PhB**, **DFT**, and **NCB76** at mole fractions corresponding to ca. half their solubility limits, to ensure that no phase separation occurred. The ^2H NMR spectra of these mixtures were recorded in the SmC^* phase at 10 K below the $\text{SmA}^* - \text{SmC}^*$ phase transition ($T - T_C = -10$ K) and are shown in Figures 2-1 and 2-2 for dopants (*RS*)-2.3- d_4 and (*RS*)-2.6- d_4 respectively.

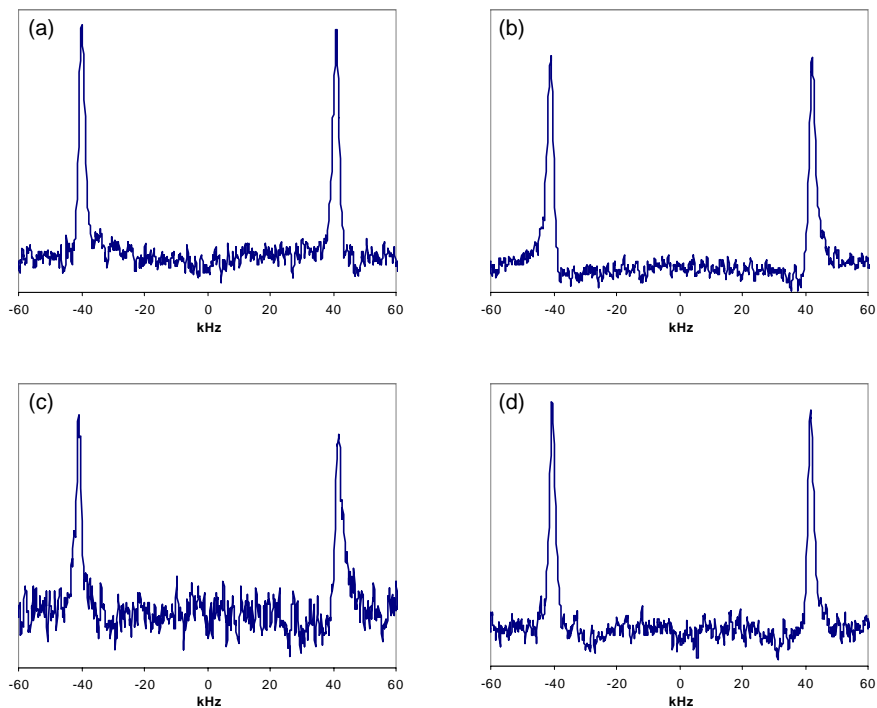


Figure 2-1. ^2H NMR spectra (92 MHz) of dopant (*RS*)-2.3- d_4 in (a) **PhP1** (8 mol %), (b) **PhB** (8 mol %), (c) **DFT** (3 mol %), and (d) **NCB76** (5 mol %). Spectra were recorded in the SmC^* phase at $T-T_C = -10$ K.

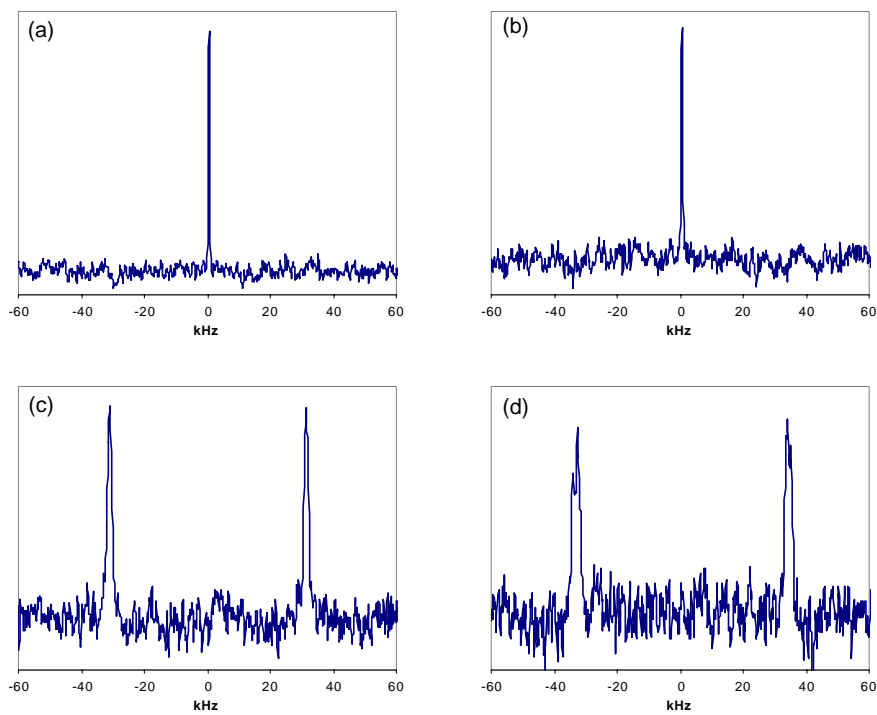


Figure 2-2. ^2H NMR spectra (92 MHz) of dopant (*RS*)-2.6- d_4 in (a) **PhP1** (3 mol %), (b) **PhB** (5 mol %), (c) **DFT** (3 mol %), and (d) **NCB76** (5 mol %). Spectra were recorded in the SmC^* phase at $T-T_C = -10$ K.

The appearance of only one quadrupolar doublet in all four hosts for dopant (*RS*)-**2.3-*d*₄** indicates that all dopant molecules reside in a SmC* environment, and further suggests the absence of any chiral perturbation in this system. ²H NMR spectra for the dopant (*RS*)-**2.6-*d*₄** in liquid crystal hosts **PhB** and **PhP1** each show an isotropic singlet, which indicates that the dopant molecules reside in an isotropic environment, and is consistent with phase diagrams showing poorer compatibility with the SmC hosts.⁶ However, (*RS*)-**2.6-*d*₄** in **NCB76** shows two quadrupolar doublets, with a very small difference in quadrupolar splitting, $\Delta\Delta\nu_Q = 2$ kHz. This value is much smaller than that observed with the 6,6'-diether, (*RS*)-**1.16a-*d*₄** ($\Delta\Delta\nu_Q = 30$ kHz).⁷ Based on our assumption that the magnitude of chiral perturbations exerted by a dopant on its local environment should be proportional to $\Delta\Delta\nu_Q$, everything else being equal (see Section 1.6), there are two possible explanations for the reduced value of $\Delta\Delta\nu_Q$: (i) the splitting observed is an artifact of the noise in the ²H NMR spectrum, or (ii) the splitting is real, and the reduced $\Delta\Delta\nu_Q$ value is due to the fact that the CD₂ group in the diester system is farther away from the stereogenic center than in the diether system, due to the C=O group. Comparison with noise artifacts in other spectra (normally less than 1 kHz) suggests that the observed $\Delta\Delta\nu_Q$ is real. Unfortunately, improving the signal/noise ratio by increasing the power level of the spectrometer was not an option because it would have compromised the probe integrity.

Interestingly, quadrupolar splitting $\Delta\nu_Q$ values varied significantly between dopants $(RS)\text{-2.3-}d_4$ and $(RS)\text{-2.6-}d_4$ in the hosts **NCB76** and **DFT**. As shown in Figure 2-3, the quadrupolar splitting ($\Delta\nu_Q$) is 82 kHz for the 5,5'-diester ($(RS)\text{-2.3-}d_4$), compared to 68 kHz for the 6,6'-diester ($(RS)\text{-2.6-}d_4$) under the same conditions. According to Equation 1-6, $\Delta\nu_Q$ is proportional to the orientational order of the C-D bond. Hence, a reduction in $\Delta\nu_Q$ can be attributed to a reduction in the orientational order of the C-D bond, which may result from a stronger perturbation exerted by the dopant $(RS)\text{-2.6-}d_4$ on the liquid crystals host. These results are consistent with phase diagrams showing the 6,6'-disubstituted dopants causing a greater destabilization of the liquid crystal hosts than the 5,5'-disubstituted dopants (Figure 2-4). They also suggest that the perturbation exerted by the 6,6'-diester in **NCB76** is chiral in nature, which might explain the unusually large δ_p measured for this dopant/host combination.

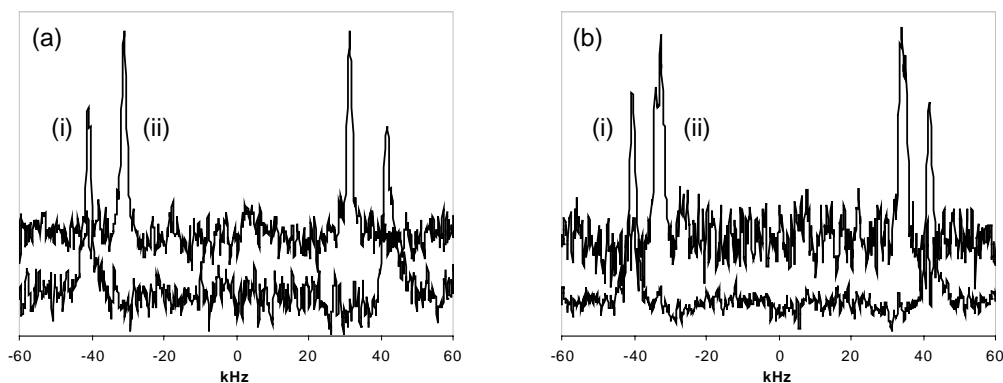


Figure 2-3. ^2H NMR spectra (92 MHz) of dopants (i) $(RS)\text{-2.3-}d_4$ and (ii) $(RS)\text{-2.6-}d_4$, in hosts (a) **DFT** (3 mol %) and (b) **NCB76** (5 mol %). Spectra were recorded in the SmC^* phase at $T - T_C = -10$ K.

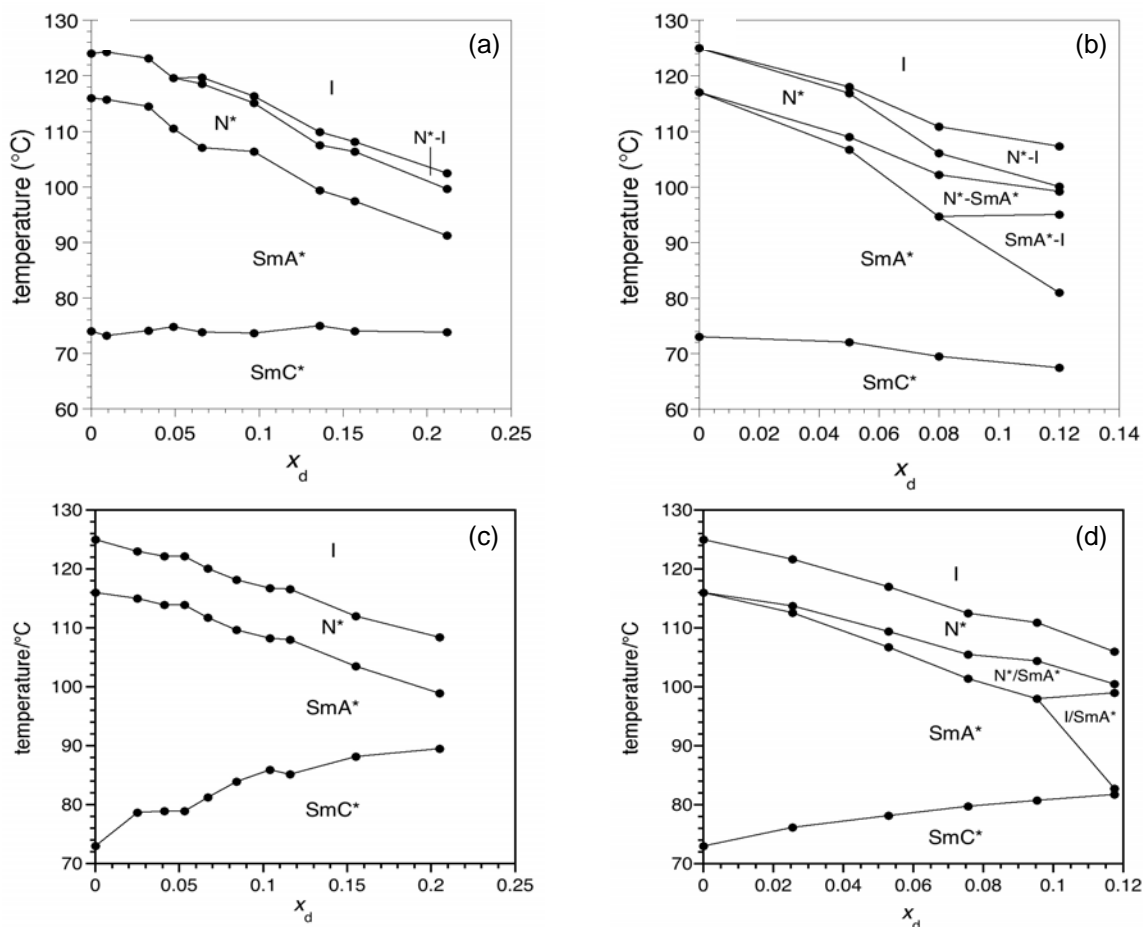


Figure 2-4. Partial phase diagrams for mixtures of (a) *(R)*-**1.15a**, (b) *(R)*-**1.16a**, (c) *(R)*-**1.15b** and (d) *(R)*-**1.16c** in **NCB76**. The phase transition temperatures were measured by polarized microscopy on cooling: x_d is the dopant mole fraction.

2.2.2. ^2H NMR Spectroscopy: Dopants with Ether Side-Chains

In order to test the hypothesis that the appearance of pairs of quadrupolar doublets in the ^2H NMR spectra of *(R)*-**1.16a-d**₄ is due to the feedback effect of a chiral perturbation exerted by the dopant on its local environment, we designed the dopant *(RS)*-**2.9-d**₄, in which the CD_2 group is one carbon removed from the stereogenic spiro centre of the molecule. Such disposition, which is similar to that found in the diester dopant *(R)*-**2.6-d**₄, is expected to reduce $\Delta\Delta\nu_Q$ by reducing the exposure of the CD_2 group to the chiral perturbation produced by the chiral core.

Compound (*RS*)-**2.9-*d*₄** was doped into **NCB76** at a mole fraction of 5 mol % to ensure consistency with previous experiments. A comparison of the ²H NMR spectra for compounds (*RS*)-**1.16a-*d*₄** (CD₂ at C₁) and (*RS*)-**2.9-*d*₄** (CD₂ at C₂) is shown in Figure 2-5. From the spectra, it can be seen that the difference in quadrupolar splitting between doublets ($\Delta\Delta\nu_Q$) is much smaller in the case of (*RS*)-**2.9-*d*₄** (ca. 2 kHz) than in the case of (*RS*)-**1.16a-*d*₄** (30 kHz). Interestingly, these results seem to parallel those obtained for the 6,6'-diester, (*RS*)-**2.6-*d*₄**, and are entirely consistent with our hypothesis that the difference in quadrupolar splitting $\Delta\Delta\nu_Q$ observed with (*RS*)-**1.16a-*d*₄** is due to a local chiral perturbation exerted by the dopant, which causes the CD₂ deuterons to become diastereotopic. The results also suggest that this effect is highly sensitive to the location of the CD₂ group relative to the perturbing stereogenic centre. Indeed, shifting the CD₂ group away from the core by only 1.5 Å removes almost entirely its diastereotopic character. This makes it difficult, if not impossible, to detect any chiral perturbations existing in the diester series.

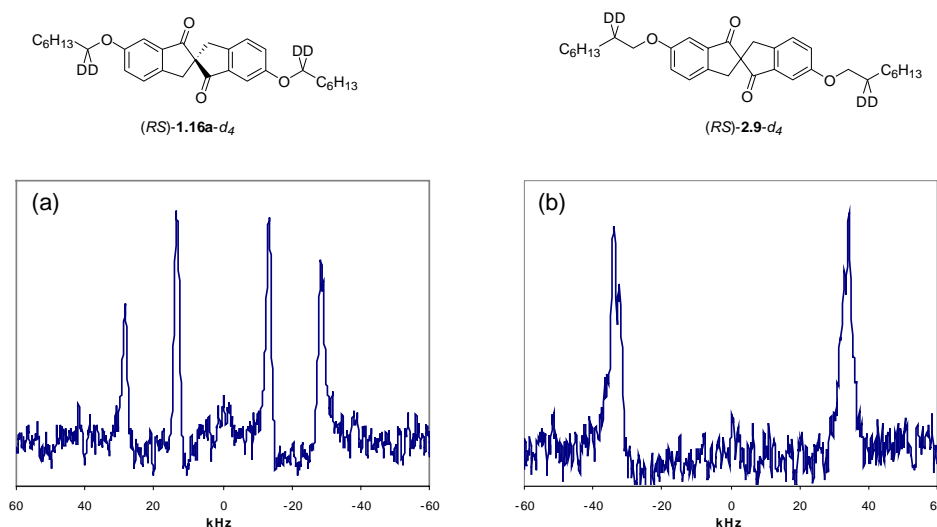


Figure 2-5. ²H NMR spectra (92 MHz) of dopants (a) (*RS*)-**1.16a-*d*₄** and (b) (*RS*)-**2.9-*d*₄** in **NCB76** at 5 mol %. Spectra were recorded in the SmC* phase at $T - T_C = -10$ K.

2.3. References

- (1) Vizitiu, D.; Lazar, C.; Halden, B. J.; Lemieux, R. P. *J. Am. Chem. Soc.* **1999**, *121*, 8229.
- (2) Boulton, C. J.; Finden, J. G.; Yuh, E.; Sutherland, J. J.; Wand, M. D.; Wu, G.; Lemieux, R. P. *J. Am. Chem. Soc.* **2005**, *127*, 13656.
- (3) Boulton, C. J.; Sutherland, J. J.; Lemieux, R. P. *J. Mater. Chem.* **2003**, *13*, 644.
- (4) Maslak, P.; Varadarajan, S.; Burkey, J. *J. Org. Chem.* **1999**, *64*, 8201.
- (5) Nieman, J. A.; Keay, B. A. *Tetrahedron: Asymmetry* **1995**, *6*, 1575.
- (6) Yuh, E. M.Sc. thesis, Queen's University, 2005.
- (7) Finden, J. G.; Yuh, E.; Huntley, C.; Lemieux, R. P. *Liq. Cryst.* **2007**, *34*, 1095.

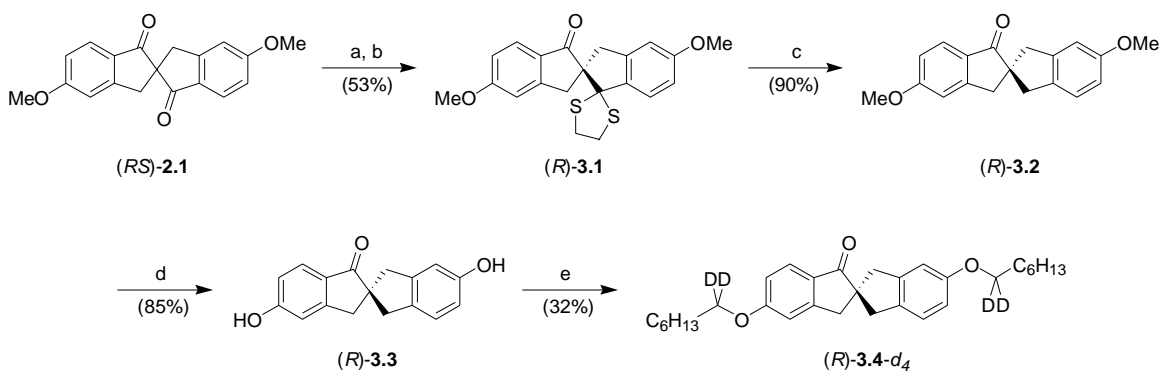
phase HPLC on a Daicel Chiralpak AS column. The first HPLC eluent was assigned the absolute configuration (*R*) based on the elution order of the enantiomers of the 2,2'-spirobiindan-1,1'-dione **1.15a**. The absolute configuration of the latter was established by circular dichroism spectroscopy based on the exciton chirality method.^{3, 4, 5} The dithioketal was then reduced using Raney[®] nickel to give (*R*)-**3.2** in good yield (90%). Deprotection of the methoxy groups was achieved with AlCl₃ to give (*R*)-**3.3** in 85 % yield. Alkylation of the diol with 1,1-*d*₂-heptanol⁶ using a Mitsunobu reaction resulted in the enantiomerically pure (*R*)-**3.4-d**₄ dopant.

Dopant (*R*)-**3.8-d**₄ was synthesized using the same approach to that of (*R*)-**3.4-d**₄ in 33 % yield, as shown in Scheme 3-2. The starting material, 6,6'-dimethoxy-2,2'-spirobiindan-1,1'-dione (*RS*)-**2.4** was synthesized according to Boulton and Finden, as shown in Scheme 2-2 in the previous chapter. Similar yields were obtained for the formation of the dithioketal derivative (*R*)-**3.5** (53%) and mono-reduced compound (*R*)-**3.6** (90%). Deprotection of the methoxy groups to give the corresponding diol (*R*)-**3.7** (99%) followed by alkylation (33%) gave the dopant (*R*)-**3.8-d**₄ (Scheme 3-2).

The diester dopant (*R*)-**3.9-d**₄ was obtained by esterification of the diol (*R*)-**3.7-d**₄ as shown in Scheme 3-3.

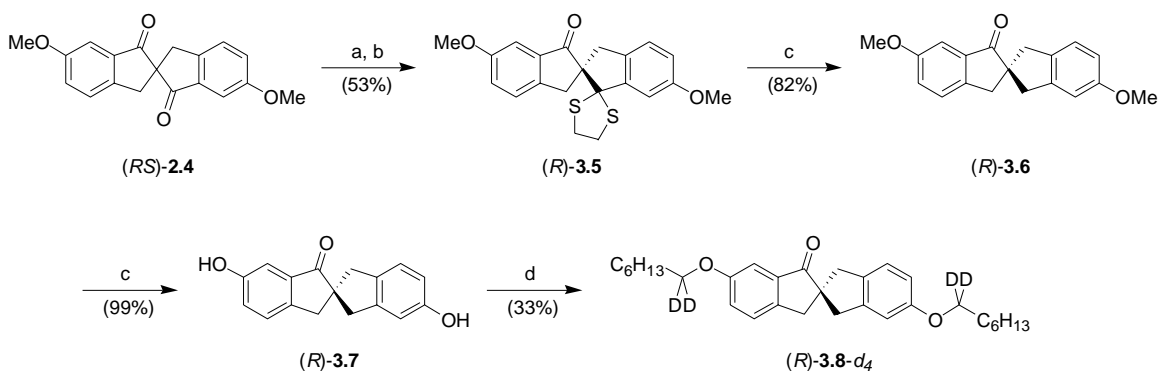
Prior to doping into the liquid crystal hosts, each dopant was recrystallized from hexanes after filtration through a 0.45 μm PTFE membrane.

Scheme 3-1.



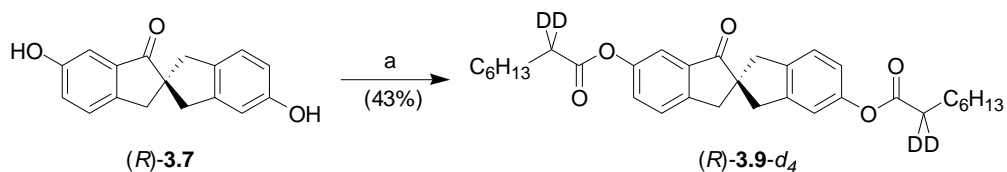
Reagents and Conditions: (a) 1,2-ethanedithiol, $\text{BF}_3 \cdot \text{O}(\text{C}_2\text{H}_5)_2$, acetic acid, rt, (b) chiral HPLC resolution, Daicel Chiralpak AS, 1:1 hexanes/EtOH, (c) Raney[®] Ni, THF, reflux, (d) AlCl_3 , toluene, reflux, (e) 1,1-*d*₂-heptanol, PPh_3 , DIAD, THF, rt.

Scheme 3-2.



Reagents and Conditions: (a) ethane dithiol, $\text{BF}_3 \cdot \text{O}(\text{C}_2\text{H}_5)_2$, acetic acid, rt, (b) chiral HPLC resolution, Daicel Chiralpak AS, 4:1 hexanes/EtOH, (c) Raney[®] Ni, THF, reflux, (d) AlCl_3 , toluene, reflux, (e) 1,1-*d*₂-heptanol, PPh_3 , DIAD, THF, rt.

Scheme 3-3.



Reagents and Conditions: (a) 2,2-*d*₂-octanoic acid, DCC, DMAP, CH_2Cl_2 , rt.

3.2. Results

3.2.1. Dopant-host Compatibility

Solubility limits previously determined by Boulton *et. al.* for the 5,5'- and 6,6'-diheptyloxy-2,2'-spirobiindan-1,1'-dione in **NCB76** provided a basis for determining those limits for the 2,2'-spirobiindan-1-one analogues. The solubility limits of (*R*)-**3.4- d_4** , (*R*)-**3.8- d_4** and (*R*)-**3.9- d_4** were determined based on the appearance of biphasic regions when observed by polarized microscopy. The phase diagram for (*R*)-**3.4- d_4** in **NCB76** (Figure 3-1(a)) suggests that 10 mol % is the solubility limit for this system, although the temperature range of the SmC* phase is less than 10 K, which is not optimal for polarization power measurements. As expected, biphasic regions generally broaden with higher dopant concentration. The phase diagram of (*R*)-**3.8- d_4** in **NCB76** (Figure 3-1(b)) shows an increased stability of the SmC* phase, with temperature ranges of more than 10 K at mole fractions up to 10 mol %. This is inconsistent within the phase diagrams obtained for (*R*)-**1.15a** and (*R*)-**1.16a**, which show increasing destabilization of the SmC phase with x_d , but a more pronounced destabilization for the 6,6'-spirobiindandione. A partial phase diagram of dopant (*R*)-**3.9- d_4** is shown in Figure 3-2.

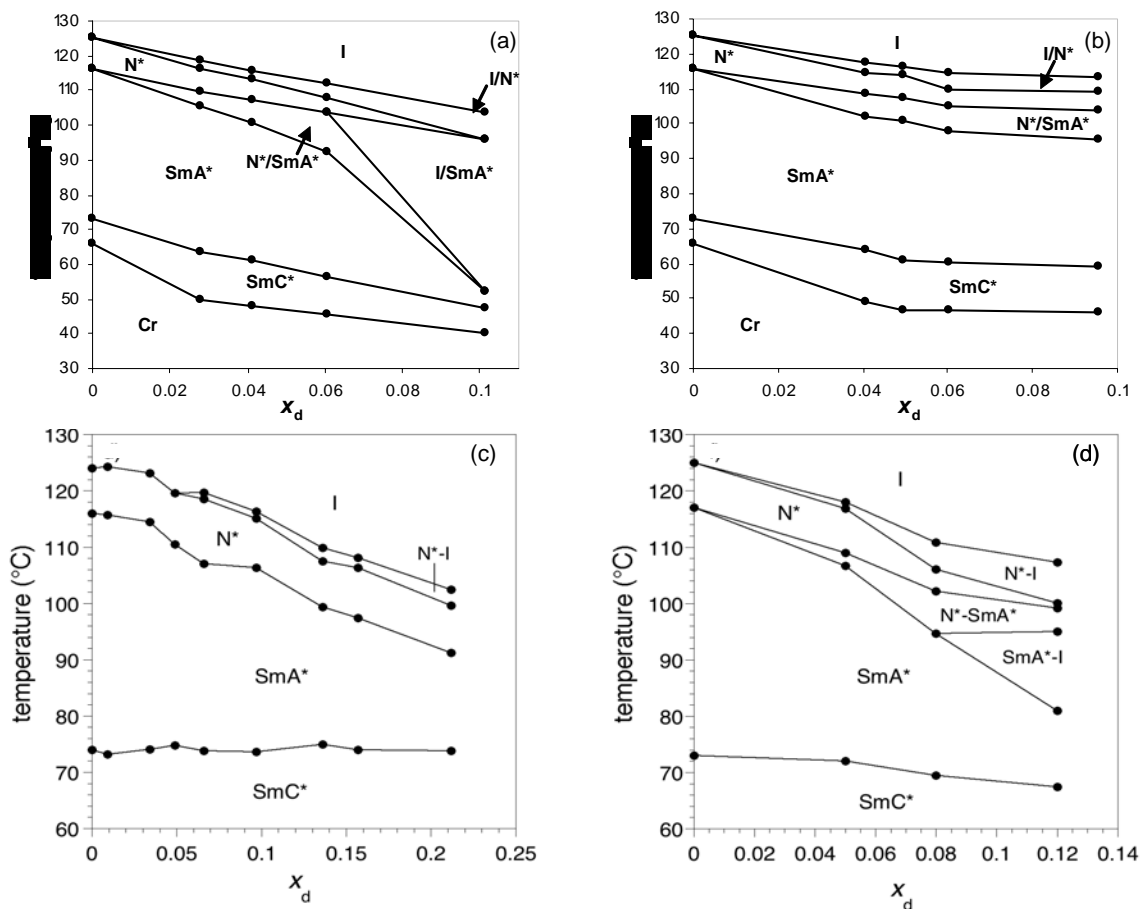


Figure 3-1. Partial phase diagram for mixtures of (a) (R) -3.4- d_4 , (b) (R) -3.8- d_4 , (c) (R) -1.15a and (d) (R) -1.16a in NCB76. The phase transitions were determined by polarized microscopy upon cooling.

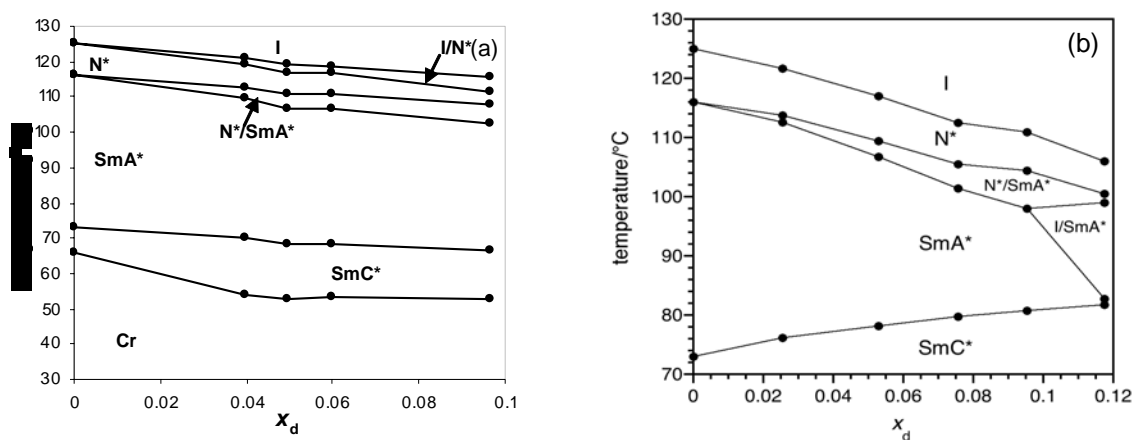


Figure 3-2. Partial phase diagram for mixtures of (a) (R) -3.9- d_4 and (b) (R) -1.16c in NCB76. The phase transitions were determined by polarized microscopy upon cooling.

3.2.2. Polarization Power Measurements

Homogenous mixtures of (R)-3.4- d_4 , (R)-3.8- d_4 and (R)-3.9- d_4 in **NCB76** were aligned in SSFLC films using commercial ITO glass cells with a rubbed polyimide coating. Spontaneous polarization (P_S) and tilt angle (θ) measurements were obtained for dopants in the SmC* phase at $T-T_C = -10$ K using the triangular wave method,⁷ for mole fractions $0.03 > x_d > 0.10$. Corresponding P_o values were calculated according to Equation 1-4. As shown in Figure 3-3, the plots of P_o vs. x_d for all dopants in **NCB76** show a good least-squares fit, with R^2 values greater than 0.97. The polarization power values derived from the P_o vs. x_d plots using Equation 1-3 are listed in Table 3-1. The sign of polarization was assigned from the relative configuration of the electric field and the switching position of the electric field according to the established convention.⁸

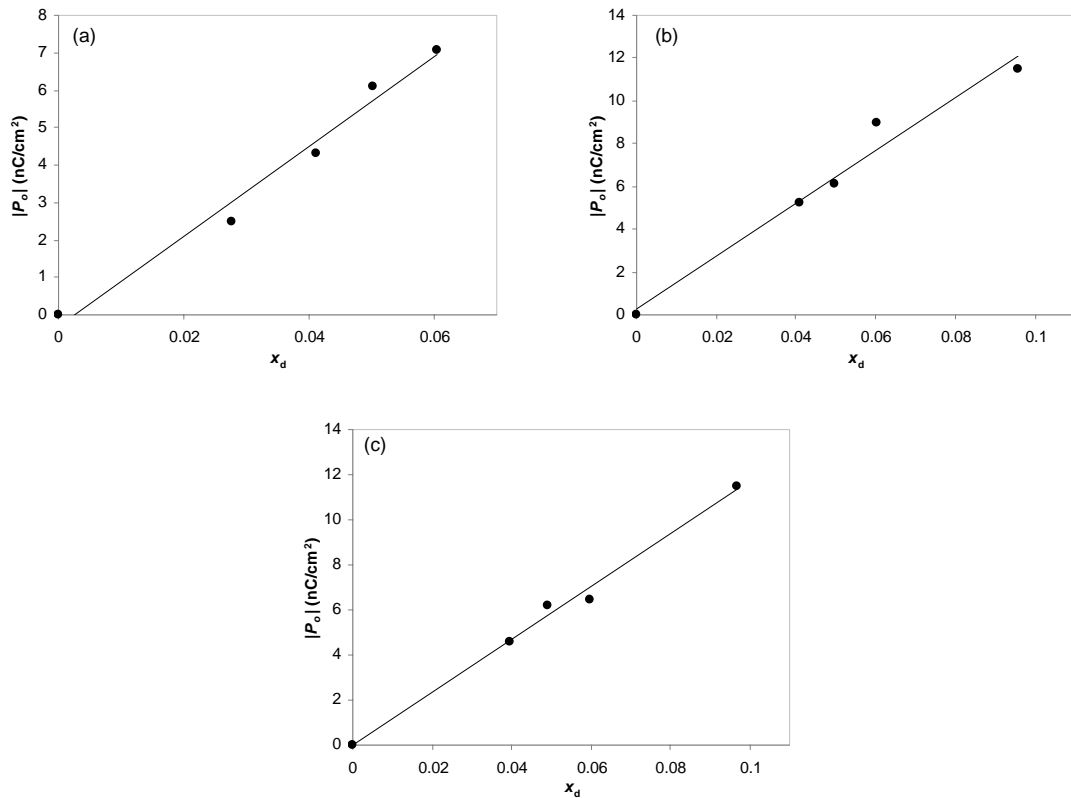


Figure 3-3. Absolute reduced polarization, $|P_o|$, versus mole fraction, x_d , of (a) (R)-3.4- d_4 , (b) (R)-3.8- d_4 and (c) (R)-3.9- d_4 in the SmC host **NCB76** at $T-T_C = -10$ K.

As expected, the mono-carbonyl dopants (*R*)-**3.4-*d*₄, (*R*)-**3.8-*d*₄ and (*R*)-**3.9-*d*₄ have the same sign of polarization as the dicarbonyl analogues, (*R*)-**1.15a**, (*R*)-**1.16a** and (*R*)-**1.16c**. However, it was observed that there is essentially no difference in the absolute values of δ_p between the 5,5'- and 6,6'- isomers (*R*)-**3.4-*d*₄ and (*R*)-**3.8-*d*₄ ($|\delta_p| = 120, 123$ nC/cm² respectively), unlike the corresponding dione dopants (*R*)-**1.15a** and (*R*)-**1.16a** ($|\delta_p| = 363, 1037$ nC/cm² respectively). Furthermore, a change in the side-chain substituent from a 6,6'-diether monocarbonyl system ((*R*)-**3.4-*d*₄) to the corresponding diester system ((*R*)-**3.9-*d*₄) does not have a significant effect on the δ_p , which is also inconsistent with the observations made for the 6,6'-dione dopants. These results are summarized in Figure 3-4, which shows a comparison of the 5,5'- and 6,6'-diether dicarbonyl systems to their mono-carbonyl analogues, as well as the 6,6'-diester dicarbonyl to the corresponding 6,6'-diester mono-carbonyl.**************

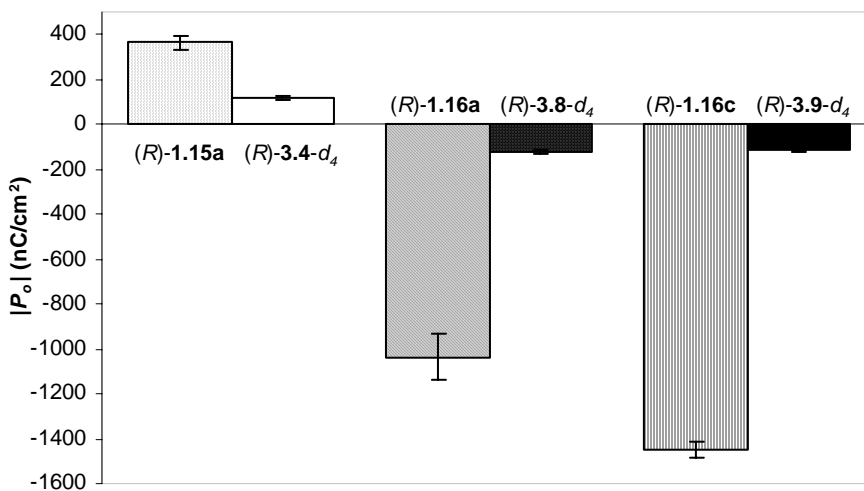
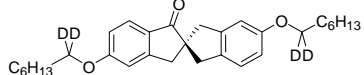
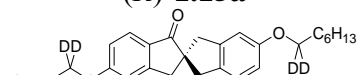
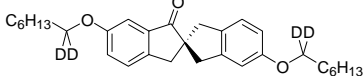
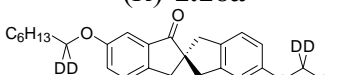
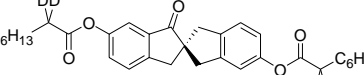
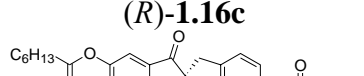


Figure 3-4. Comparison of polarization power values for dopants (*R*)-**1.15a** and (*R*)-**3.4-*d*₄**, (*R*)-**1.16a** and (*R*)-**3.8-*d*₄**, (*R*)-**1.16c** and (*R*)-**3.9-*d*₄**. Note the difference in magnitude between di- and mono-carbonyl systems.

Table 3-1. Polarization powers for dopants (*R*)-**3.4-*d*₄**, (*R*)-**3.8-*d*₄** and (*R*)-**3.9-*d*₄** as compared to the dione analogues (*R*)-**1.15a**, (*R*)-**1.16a** and (*R*)-**1.16c** in NCB76. Polarization power values measured at $T-T_C = -10$ K.

Dopant	δ_p (nC/cm ²) ^{a,b} NCB76
 <p>(<i>R</i>)-3.4-<i>d</i>₄</p>	120 ± 10 (+)
 <p>(<i>R</i>)-1.15a</p>	363 ± 30 (+)
 <p>(<i>R</i>)-3.8-<i>d</i>₄</p>	123 ± 12 (-)
 <p>(<i>R</i>)-1.16a</p>	1037 ± 100 (-)
 <p>(<i>R</i>)-3.9-<i>d</i>₄</p>	117 ± 6 (-)
 <p>(<i>R</i>)-1.16c</p>	1449 ± 36 (-)

^a Sign of polarization in parentheses. ^b Uncertainty is ± standard error of least-squares fit.

According to the conformational analysis of the 5,5'- and 6,6'-disubstituted-2,2'-spirobiindan-1,1'-dione molecules presented in Section 1.7, the **P** conformer is favoured in both cases, resulting in the 5,5'-diether substituted dopants exhibiting positive δ_p , and the 6,6'-diether and diester substituted dopants exhibiting negative δ_p . This is consistent with the results in Table 3-1, which suggest that the **P** conformer is still favoured over the **C**₂ conformer in the cases of the mono-carbonyl derivatives according to the signs of δ_p .

The decrease in δ_p resulting from the reduction of one of the two carbonyl groups is much larger than predicted by our original hypothesis, which states that removal of one of the carbonyl groups should decrease δ_p to ca. half its original value, especially in the

cases of the 6,6'-disubstituted systems (*R*)-**1.16a** and (*R*)-**1.16c**. These results suggest that one must also consider the effect of reducing the chiral topography of the core, in which the only symmetry breaking element is the alkoxy group on the indane segment of the core. Such a reduction in the chiral topography could reduce (or completely eliminate) the contribution of chirality transfer, and perhaps result in a reduction in polar ordering of the polar linking groups in the binding site. Hence, the δ_p induced by any of the mono-carbonyl dopants would result solely from the transverse dipole of the mono-carbonyl core, which would be consistent with the similarity in absolute values of δ_p .

According to Table 3-1, the difference in δ_p between 6,6'-diether (*R*)-**1.16a** and diester (*R*)-**1.16c** systems is 412 nC/cm², which suggests that the polar linking groups contribute to the overall δ_p of the system. However, for the mono-carbonyl analogues, there is essentially no difference in δ_p values, within experimental error. If one considers that the reduction of one of the carbonyl groups makes the chiral topography of the core less pronounced, these results would suggest that, in the absence of a strong chiral perturbation exerted by the core on its local environment, the polar linking groups have no inherent conformational bias to orient along one direction along the polar axis of the SmC* phase, *i.e.* no polar ordering. In other words, influence of the chiral core as a feedback effect would be so weak that it would not extend to the polar linking group, and δ_p values would be expected to be more or less the same.

This interpretation of the results is consistent with the ²H NMR results presented in Section 2.3: the difference in quadrupolar splitting between pairs of doublets $\Delta\Delta\nu_Q$ is ca. 2 kHz for both the 6,6'-diester (*RS*)-**2.3-d₄** (CD₂ at C₂) and the 6,6'-diether (*RS*)-**2.9-d₄** (CD₂ at C₂), which is significantly different than the splitting reported for the 6,6'-

diether (*RS*)-**1.16a-d₄** (CD₂ at C₁, $\Delta\Delta\nu_Q = 30$ kHz). These results suggest that the influence of a chiral perturbation from the core making the deuterons diastereotopic decreases in a dramatic fashion as one moves away from the core, and that a decrease in chiral topography of the core would be expected to have a similar effect on its immediate environment.

The fact that the reduction of one carbonyl group in three dopants (*R*)-**1.15a**, (*R*)-**1.15a** and (*R*)-**1.16c** drastically reduced δ_p values and levels them off as to make them identical, within error, suggests that the contribution of the polar linking groups in the di-carbonyl systems is due to a chiral perturbation exerted by the core on its local environment, which desymmetrizes the conformational distribution of the linking groups. This would be consistent with a *lower* δ_p value (and $\Delta\Delta\nu_Q$ values) for (*R*)-**1.15a** compared to (*R*)-**1.16a** and (*R*)-**1.16c** since the 5,5'-system has a less pronounced chiral topography than the 6,6'-system.

3.3. References

- (1) Nieman, J. A.; Keay, B. A. *Tetrahedron: Asymmetry* **1995**, *6*, 1575.
- (2) Boulton, C. J.; Finden, J. G.; Yuh, E.; Sutherland, J. J.; Wand, M. D.; Wu, G.; Lemieux, R. P. *J. Am. Chem. Soc.* **2005**, *127*, 13656.
- (3) Berova, N.; Nakanishi, K. In *Exciton Chirality Methods: Principles and Applications*; Berova, N., Nakanishi, K., Woody, R., Eds.; Wiley-VCH: New York, 2000.
- (4) Falk, H.; Fröstl, W.; Hofer, O.; Schlögl, K. *Monatsh. Chem.* **1974**, *105*, 598.
- (5) Langer, E.; Lehner, H.; Neudeck, H.; Schlögl, K. *Monatsh. Chem.* **1978**, *109*, 987.

- (6) Finden, J. G. Ph.D. thesis, Queen's University, 2006.
- (7) Miyasato, K.; Abe, S.; Takezoe, H.; Fukuda, A.; Kuze, E. *Jpn. J. Appl. Phys.* **1983**, 22, L661.
- (8) Walba, D. M. In *Advances in the Synthesis and Reactivity of Solids*; Mallouck, T. E., Ed.; JAI Press, Ltd.: Greenwich, CT, 1991; Vol. 1, p 173.

Chapter 4. Conclusions and Future Work

The aim of this project was twofold: first, to further our understanding of chirality transfer feedback in SmC* liquid crystal mixtures consisting of substituted 2,2'-spirobiindan-1,1'-dione dopants and the achiral liquid crystal host **NCB76** using ^2H NMR spectroscopy. Second, we sought to investigate the effect of reducing the chiral topography of a dopant on the magnitude of its polarization power (δ_p).

The magnitude of perturbations exerted by the 5,5'- and 6,6'-diester substituted 2,2'-spirobiindan-1,1'-dione dopants (*RS*)-**2.3- d_4** and (*RS*)-**2.6- d_4** was determined based on the splitting of quadrupolar doublets ($\Delta\nu_Q$) in the ^2H NMR spectra. Quadrupolar splitting values were 82 kHz for the 5,5'-diester, compared to 68 kHz for the 6,6'-diester. As described in Chapter 1, $\Delta\nu_Q$ is proportional to the C-D bond order; thus it can be deduced that a decrease in $\Delta\nu_Q$ in the 6,6'-diester is a reflection of an increased perturbation on the system. In addition, moving the CD_2 deuterons one carbon further away from the stereogenic centre results in a reduction of $\Delta\Delta\nu_Q$ values to ca. 2 kHz (C_2 diester- d_4 (*RS*)-**2.6- d_4** and C_2 diether- d_4 (*RS*)-**2.9- d_4**) in **NCB76**, which is significantly smaller than that reported for dopant (*RS*)-**1.16a- d_4** ($\Delta\Delta\nu_Q = 30$ kHz). These results suggest that the effect of chiral perturbations exerted by the chiral core on the desymmetrization of the CD_2 group is highly sensitive to the distance of the latter from the chiral centre of the dopant.

The 5,5'- and 6,6'- spirobiindandione cores were reduced to the mono-carbonyl analogues (*R*)-**3.4- d_4** , (*R*)-**3.8- d_4** and (*R*)-**3.9- d_4** in order to study the effect of core modification on polarization power. We had hypothesized that a reduction of one

carbonyl group would reduce polarization power values by ca. half those reported for the dione system. It was found that a reduction of one of the carbonyl groups of the spirobiindandione core has profound effects on decreasing the polarization power. These three dopants in **NCB76** have the same sign of polarization as the corresponding dione systems, indicating that the **P** conformer is still favoured in the **P/C₂** conformational equilibrium. The magnitude of absolute polarization power for the 5,5'- and 6,6'-diheptyloxy mono-carbonyl dopants ((*R*)-**3.4-d₄** and (*R*)-**3.8-d₄**) in **NCB76** were essentially identical, matching the value obtained with the 6,6'-dioctanoyloxy mono-carbonyl dopant (*R*)-**3.9-d₄** in the same host. These results suggest that a reduction in the chiral topography of the spiro core may result in a significant decrease of the perturbation exerted by the chiral core on the polar groups linking the side-chains to the core. These results are consistent with ²H NMR results presented in Chapter 2, which suggest that shifting CD₂ deuterons further from the chiral core of the dopant decreases the amount of diastereotopic character exhibited by the deuterons. Thus, decreasing the chiral topography of the core *or* moving the CD₂ deuterons further away from the core of the molecule have the same effect in showing that chiral perturbations from dopant to host is a local effect.

Studies are currently underway in the Lemieux lab to modify the spirobiindanone core, by introducing halogenated substituents to the 6-position on a 5,5'-disubstituted spirobiindandione core. It is hoped that these studies will show that halogenated moieties exert a bias favouring the **P** conformer in the **P/C₂** equilibrium, and thus be reflected in the δ_p . Halogenation at the 6-position will also enhance the chiral topography of the core.

Finally, probe experiments analogous to those described in Section 1.5.2., involving (*R*)- and (*S*)-5,5'-diether as a probe with 6,6'-diester as a dopant are being investigated to determine if the chiral perturbations exerted from dopant (*R*)-**1.16c** to host **NCB76** are due to a short-range (as the ²H NMR suggests) or a long-range effect.

Chapter 5. Experimental

5.1. Synthesis and Characterization

5.1.1. General

^1H , ^{13}C , and ^2H NMR spectra were recorded on Bruker Avance 300, 400, 500 and 600 MHz spectrometers, using deuterated chloroform or deuterated acetone as solvent. The chemical shifts of the spectra are reported in δ (ppm) relative to tetramethylsilane. Low-resolution mass spectra were recorded using an Applied Biosystems/MDS Sciex QSTAR XL QqTOF mass spectrometer. Peaks are reported as m/z , percent intensity relative to the base peak. High resolution mass spectra were recorded using a Waters/Micromass GCT mass spectrometer. Electron impact (EI) was the method of ionization unless otherwise stated. Melting points were acquired using a Fisher-Johns melting point apparatus and are uncorrected. Flash chromatography was performed using 60 Å silica gel (Silicycle Inc., Quebec) as the stationary phase. Preparative chiral stationary phase HPLC separations were performed using a Daicel Chiralpak AS column (50 cm x 5 cm ID) in mixtures of hexanes/EtOH at a flow rate of 55 mL/min unless otherwise stated.

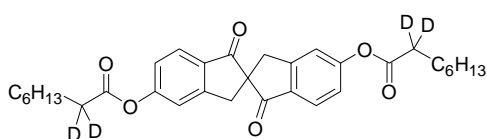
5.1.2. Materials

All solvents and reagents were obtained from commercial sources and used without further purification unless otherwise specified. Anhydrous solvents were obtained from an Innovative Technology Inc. solvent purification system. The liquid crystal hosts 4-(4'-heptyl[1,1'-biphenyl]-4-yl)-1-hexylcyclohexanecarbonitrile (**NCB76**) and 2-(4-butoxyphenyl)-5-(octyloxy) pyrimidine (**PhP1**) were obtained from Clariant.

The liquid crystal hosts 4-[(±)-4-methylhexyl]oxy]-phenyl 4-decyloxybenzoate (**PhB**) and 2',3'-difluoro-4''-heptyl-4-nonyl-[1,1',4,1'']terphenyl (**DFT**) were synthesized according to literature procedures by Lemieux group members and shown to have the expected physical and spectra properties.^{1, 2} 2,2-*d*₂-Octanoic acid was purchased from C/D/N Isotopes Inc (Quebec). The dopants (*R*)-5,5'-diheptyloxy-2,2'-spirobiindan-1,1'-dione ((*R*)-**1.15a**) and (*R*)-5,5'-diheptanoyloxy-2,2'-spirobiindan-1,1'-dione ((*R*)-**1.15b**) were synthesized by Eagranie Yuh.³ The dopants (*R*)-6,6'-diheptyloxy-2,2'-spirobiindan-1,1'-dione ((*R*)-**1.16a**), (*R*)-5,5'-Bis(heptyloxy-1,1-*d*₂)-2,2'-spirobiindan-1,1'-dione ((*RS*)-**1.15a-d₄**), (*RS*)-6,6'-bis(heptyloxy-1,1-*d*₂)-2,2'-spirobiindan-1,1'-dione ((*RS*)-**1.16a-d₄**) and (*R*)-6,6'-diheptanoyloxy-2,2'-spirobiindan-1,1'-dione ((*R*)-**1.16c**) were synthesized by Jeremy Finden. The compound (*RS*)-5,5'-dimethoxy-2,2'-spirobiindan-1'-one-1-ethylenethioketal ((*RS*)-**3.1**) was adapted from a procedure from Langer and Lehner.⁴

5.1.3. Synthetic Procedures

(*RS*)-5,5'-Bis(octanoyloxy-2,2-*d*₂)-2,2'-spirobiindan-1,1'-dione ((*RS*)-2.3-*d*₄). Under



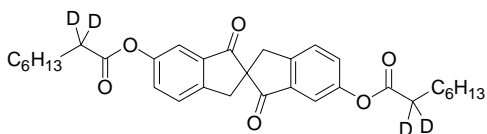
an argon atmosphere, a mixture of (*RS*)-**2.2** (110 mg, 0.38 mmol), 2,2-*d*₂-octanoic acid (0.30 mL, 1.15 mmol), DMAP (0.14 g, 1.15 mmol) and 20 mL anhydrous CH₂Cl₂ was cooled to 0

°C and allowed to stir for 5 minutes. A solution of DCC (0.24 g, 1.15 mmol) in 5 mL anhydrous CH₂Cl₂ was added dropwise to the reaction mixture. The mixture was allowed to warm to room temperature, with continuous stirring over 5 days. The mixture was filtered, concentrated, and then dissolved in EtOAc, washed with 2 % HCl, dried (MgSO₄) and concentrated. The crude product was purified by flash chromatography on

silica gel (2:1 hexanes/EtOAc), and recrystallized from hexanes after passing through a 0.45 μm PTFE filter to give 0.11 g (52 %) of *(RS)*-**2.3- d_4** as a white solid: m.p. 117.5 - 118.5 $^\circ\text{C}$; ^1H NMR (300 MHz, CDCl_3) δ 7.77 (d, $J = 8$ Hz, 2H), 7.30 (s, 2H), 7.12 (d, $J = 8$ Hz, 2H), 3.69 (d, $J = 17$ Hz, 2H), 3.18 (d, $J = 17$ Hz, 2H), 1.75 (m, 4H), 1.31 (m, 16H), 0.89 (m, 6H); ^{13}C NMR (100 MHz, CDCl_3) δ 14.0, 22.6, 24.7, 28.8, 29.0, 31.6, 34.0 (quintet, $J = 17$ Hz), 37.9, 65.6, 119.3, 121.9, 126.1, 132.8, 155.5, 156.5, 171.7, 201.1; MS (TOF-MS) m/z 536 ($[\text{M}]^+$, 2), 409 (48), 282 (100), 281 (55); HRMS (TOF-MS) calc'd for $\text{C}_{33}\text{H}_{36}\text{D}_4\text{O}_6$ 536.3076, found 536.3089.

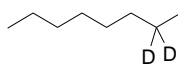
***(RS)*-6,6'-Bis(octanoyloxy-2,2- d_2)-2,2'-spirobiindan-1,1'-dione (*(RS)*-**2.6- d_4**).** Under

an argon atmosphere, 2,2- d_2 -octanoic acid (0.14 mL, 0.54 mmol) was added dropwise to a stirred mixture of *(RS)*-**2.5** (0.05 g, 0.18 mmol), DMAP (0.07 g, 0.54 mmol), DCC (0.11g, 0.54 mmol) and 10 mL anhydrous CH_2Cl_2 . The mixture was allowed to stir at room temperature for 6 days. The mixture was filtered, concentrated, and then dissolved with EtOAc, washed with 2 % HCl (2x), brine, dried (MgSO_4) and concentrated. The crude product was purified by flash chromatography on silica gel (3:1 hexanes/EtOAc), and recrystallized from hexanes after passing through a 0.45 μm PTFE filter to give 0.07 g (70 %) of *(RS)*-**2.6- d_4** as a white solid: m.p. 100 - 101 $^\circ\text{C}$; ^1H NMR (300 MHz, CDCl_3) δ 7.55 (d, $J = 8$ Hz, 2H), 7.44 (d, $J = 2$ Hz, 2H), 7.36 (dd, $J = 2, 8$ Hz, 2H), 3.69 (d, $J = 17$ Hz, 2H), 3.16 (d, $J = 17$ Hz, 2H), 1.74 (m, 4H), 1.30 (m, 16H), 0.88 (m, 6H); ^{13}C NMR (100 MHz, CDCl_3) δ 14.0, 22.6, 24.8, 28.9, 29.0, 31.6, 33.7 (quintet, $J = 18$ Hz), 37.7, 66.5, 117.5, 127.1, 129.2, 136.6, 150.6, 150.8, 201.5; MS (TOF-MS) m/z 536 ($[\text{M}]^+$, 7),



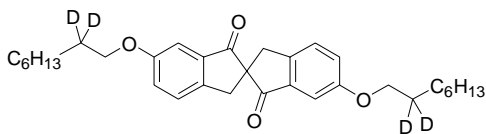
409 (54), 282 (96), 281 (100); HRMS (TOF-MS) calc'd for C₃₃H₃₆D₄O₆ 536.3076, found 536.3093.

2,2-*d*₂-Octanol (2.8). Under an argon atmosphere, 2,2-*d*₂-octanoic acid (0.15 mL, 0.57



mmol) in 16 mL of anhydrous Et₂O was added dropwise to a mixture of LiAlH₄ (110 mg, 2.87 mmol) in 8 mL of anhydrous Et₂O, and the reaction mixture was refluxed for 24 h. Note: 2,2-*d*₂-octanoic acid was stored under an argon atmosphere over 3 Å molecular sieves overnight. After cooling to room temperature, the mixture was quenched (1:2 MeOH/Et₂O), acidified (5 % H₂SO₄), and extracted with Et₂O (3x). The combined organic extracts were washed with water, 5 % NaHCO₃, dried (MgSO₄) and concentrated to yield 45 mg (60 %) as a clear oil; ¹H NMR (400 MHz, CDCl₃) δ 3.62 (s, 2H), 1.28 (m, 10H), 0.87 (m, 3H); ¹³C NMR (125 MHz, CDCl₃) δ 14.1, 22.6, 25.5, 29.3, 29.3, 31.8, 32.0 (quintet, *J* = 19 Hz), 63.0.

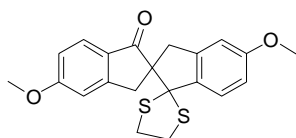
(*RS*)-6,6'-Bis(octyloxy-2,2-*d*₂)-2,2'-spirobiindan-1,1'-dione ((*RS*)-2.9-*d*₄). Under an



argon atmosphere, 2,2-*d*₂-octanol (**2.8-*d*₂**) (77 mg, 0.58 mmol) in 2 mL of THF was added to a stirred solution of (*RS*)-**2.5** (59 mg, 0.21 mmol) and PPh₃ (131 mg, 0.50 mmol) in 5 mL of THF. After 5 minutes, DIAD (101 mg, 0.50 mmol) was added and the solution was stirred at room temperature overnight. The solution was concentrated and purified by flash chromatography on silica gel (4:1 hexanes/EtOAc), then recrystallized from hexanes after passing through a 0.45 μm PTFE filter to give 71 mg (66 %) of product as a white solid: m.p. 105 - 106 °C; ¹H NMR (400 MHz, CDCl₃) δ 7.42 (d, *J* = 9 Hz, 2H), 7.22 (m, 2H), 7.15 (s, 2H), 3.95 (s, 4H), 3.61 (d, *J* = 16 Hz, 2H), 3.09 (d, *J* = 16 Hz, 2H), 1.41 (m, 4H), 1.28 (m, 16H), 0.88 (m, 6H); ¹³C NMR (125 MHz, CDCl₃) δ 14.1, 22.6, 25.8, 28.3

(quintet, $J = 18$ Hz), 29.2, 29.2, 31.8, 37.5, 66.7, 68.4, 106.6, 125.1, 126.9, 136.6, 146.5, 159.2, 202.8; MS (TOF-MS) m/z 508 ($[M^+]$, 100); HRMS (TOF-MS) calc'd for $C_{33}H_{40}D_4O_4$ 508.3491, found 508.3470.

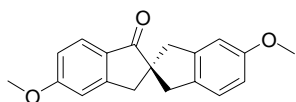
(R)- and (S)-5,5'-Dimethoxy-2,2'-spirobiindan-1'-one-1-ethylenedithioketal ((R)- and



(S)-3.1). Under an argon atmosphere, 5 mL (60 mmol) of 1,2-ethanedithiol and 5 mL (41 mmol) of $BF_3 \cdot O(C_2H_5)_2$ were added

to a solution of 0.5 g (1.7 mmol) (*RS*)-**2.1** in 25 mL of acetic acid, and was allowed to stir at room temperature overnight. The reaction mixture was neutralized with 10 % aq. KOH. The aqueous layer was extracted with CH_2Cl_2 (3x), washed with water, dried ($MgSO_4$) and concentrated. The crude product was purified by flash chromatography on silica gel (4:1 hexanes/EtOAc), to give 0.33 g (53 %) of (*RS*)-**3.1** as a beige solid: m.p. 161 - 163 °C; 1H NMR (400 MHz, $CDCl_3$) δ 7.65 (d, $J = 9$ Hz, 1H), 7.41 (d, $J = 9$ Hz, 1H), 6.87 (m, 3H), 6.64 (d, $J = 3$ Hz, 1H), 3.88 (s, 3H), 3.77 (s, 3H), 3.67 (d, $J = 17$ Hz, 1H), 3.45 (m, 2H), 3.19 (m, 3H), 3.12 (d, $J = 4$ Hz, 2 H); ^{13}C NMR (100 MHz, $CDCl_3$) δ 38.0, 40.8, 41.0, 42.2, 55.4, 55.6, 67.2, 78.5, 109.3, 109.3, 114.0, 115.4, 124.7, 126.2, 129.3, 139.5, 140.1, 155.3, 159.9, 165.5, 203.2; MS (TOF-MS) m/z 384 ($[M^+]$, 2), 308 (47), 291 (100), 280 (21); HRMS (TOF-MS) calc'd for $C_{21}H_{20}O_3S_2$ 384.0854, found 384.0860. The enantiomers were resolved by chiral phase HPLC using a Daicel Chiralpak AS column and a mobile phase of 1:1 hexanes/EtOH to give (*R*)- and (*S*)-**3.1** in optically pure form.

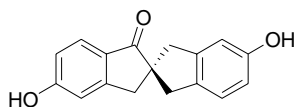
(R)-5,5'-Dimethoxy-2,2'-spirobiindan-1-one ((R)-3.2). A solution of (*R*)-**3.1** (144 mg,



0.38 mmol) in 5 mL of THF was added slowly to a suspension of 1.5 g Raney[®] nickel 2800 slurry (washed 3x with distilled water,

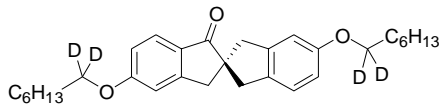
CAUTION: pyrophoric) in 2 mL of THF. The mixture was heated to reflux for 3 h, then carefully filtered to remove the Raney[®] nickel. The filtrate was extracted with Et₂O (3x), dried (MgSO₄) and concentrated to yield 100 mg (90 %) of (*R*)-**3.2** as a white solid: m.p. 90 – 92 °C; ¹H NMR (300 MHz, CDCl₃) δ 7.75 (d, *J* = 8 Hz, 1H), 7.10 (d, *J* = 8 Hz, 1H), 6.93 (d, *J* = 8 Hz, 1H), 6.85 (s, 1H), 6.77 (s, 1H), 6.74 (d, *J* = 8 Hz, 1H), 3.88 (s, 3H), 3.79 (s, 3H), 3.47 (d, *J* = 16 Hz, 1H), 3.40 (d, *J* = 15 Hz, 1H), 3.12 (s, 2H), 2.77 (d, *J* = 16 Hz, 1H), 2.74 (d, *J* = 15 Hz, 1H); ¹³C NMR (125 MHz, CDCl₃) δ 44.2, 44.9, 55.3, 55.6, 58.2, 109.7, 110.0, 112.5, 115.5, 124.8, 125.9, 129.4, 133.5, 143.2, 155.5, 159.1, 165.6, 207.0; MS (TOF-MS) *m/z* 294 ([M]⁺, 100), 277 (28), 145 (17); HRMS (TOF-MS) calc'd for C₁₉H₁₈O₃ 294.1256, found 294.1267.

(*R*)-5,5'-Dihydroxy-2,2'-spirobiindan-1-one ((*R*)-3.3). Under an argon atmosphere, a



mixture of (*R*)-**3.2** (39 mg, 0.13 mmol), AlCl₃ (62 mg, 0.46 mmol) and toluene (5 mL) was heated to reflux for 2 h. The mixture was quenched slowly with water, taken up in EtOAc, and extracted further with EtOAc (3x). The combined organic extracts were dried (MgSO₄) and concentrated to yield 30 mg (85 %) (*R*)-**3.3** as a white solid. The crude material was used without further purification: m.p. 238 °C (dec.); ¹H NMR (300 MHz, (CD₃)₂CO) δ 9.41 (s, 1H), 8.12 (s, 1H), 7.59 (d, *J* = 8 Hz, 1H), 7.00 (d, *J* = 8 Hz, 1H), 6.90 (m, 2H), 6.70 (s, 1H), 6.66 (d, *J* = 8 Hz, 1H), 3.25 (t, *J* = 16 Hz, 2H), 3.07 (s, 2H), 2.75 (d, *J* = 16 Hz, 1H), 2.72 (d, *J* = 15, 1H). ¹³C NMR (125 MHz, (CD₃)₂CO) δ 44.9, 45.1, 45.7, 59.1, 112.7, 113.5, 115.0, 117.3, 126.1, 127.0, 129.8, 133.5, 144.6, 157.1, 158.0, 165.3, 207.2. MS (TOF-MS) *m/z* 266 ([M]⁺, 100), 265 (34), 249 (38); HRMS (TOF-MS) calc'd for C₁₇H₁₄O₃ 266.0943, found 266.0942.

(R)-5,5'-Bis(heptyloxy-1,1-*d*₂)-2,2'-spirobiindan-1-one ((R)-3.4-*d*₄). Under an argon



atmosphere, 1,1-*d*₂-heptanol (110 mg, 0.91 mmol) in 2 mL of THF was added to a stirred solution of (*R*-

3.3 (87 mg, 0.33 mmol) and PPh₃ (210 mg, 0.79 mmol) in 5 mL of THF. After 5

minutes, DIAD (0.16 mL, 0.79 mmol) was added and the solution was stirred at room

temperature overnight. Initial purification by flash chromatography (4:1 hexanes/EtOAc)

on silica gel yielded the mono-substituted product exclusively as a white solid (61 %).

The reaction was repeated using the same reaction conditions to obtain the dialkylated

product. The product was purified by flash chromatography (4:1 hexanes/EtOAc) and

recrystallized from hexanes after passing through a 0.45 μm PTFE filter to give 50 mg

(overall yield 32 %) of product as a white solid: m.p. 54 - 58 °C; ¹H NMR (300 MHz,

CDCl₃) δ 7.73 (d, *J* = 8 Hz, 1H), 7.07 (d, *J* = 8 Hz, 1H), 6.91 (d, *J* = 8 Hz, 1H), 6.82 (s,

1H), 6.78 (s, 1H), 6.76 (d, *J* = 8 Hz, 1H), 3.45 (d, *J* = 16 Hz, 1H), 3.40 (d, *J* = 15 Hz,

1H), 3.10 (s, 2H), 2.74 (d, *J* = 16 Hz, 1H), 2.71 (d, *J* = 15 Hz, 1H), 1.76 (m, 4H), 1.31

(m, 14 H), 0.89 (m, 6H); ¹³C NMR (125 MHz, CDCl₃) δ 14.0, 22.6, 22.6, 25.9, 26.0,

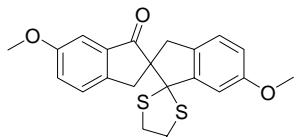
28.8, 29.0, 29.1, 29.1, 31.7, 31.8, 44.2, 44.9, 58.2, 67.6 (quintet, *J* = 21 Hz), 110.3, 110.7,

113.1, 115.8, 124.8, 125.9, 129.2, 133.3, 143.1, 155.5, 158.6, 165.2, 207.0; MS (TOF-

MS) *m/z* 466 ([M]⁺, 100), 59 (14); HRMS (TOF-MS) calc'd for C₃₁H₃₈D₄O₃ 466.3385,

found 466.3399.

(R)- and (S)-6,6'-Dimethoxy-2,2'-spirobiindan-1'-one-1-ethylenedithioacetal ((R)-



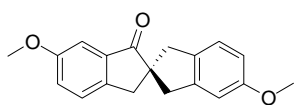
and (S)-3.5). Under an argon atmosphere, 1 mL of 1,2-

dithioethane (12 mmol) and 1 mL (8 mmol) BF₃·O(C₂H₅)₂ were

added to a solution of 0.158 g (0.51 mmol) (*RS*)-**2.4** in 5 mL acetic acid, and was allowed

to stir at room temperature overnight. The reaction mixture was neutralized with 10 % aq. KOH. The aqueous layer was extracted with CH₂Cl₂ (3x), washed with water, dried (MgSO₄) and concentrated. The crude product was purified by flash chromatography on silica gel (4:1 hexanes/EtOAc), to give 0.11 g (53 %) of (*R*)-**3.5** as a white solid: m.p. 145 - 147 °C; ¹H NMR (400 MHz, CDCl₃) δ 7.36 (d, *J* = 8 Hz, 1H), 7.20 (dd, *J* = 2, 8 Hz, 1H), 7.13 (s, 1H), 7.03 (m, 2H), 6.77 (dd, *J* = 2, 8 Hz, 1H), 3.83 (s, 3H), 3.80 (s, 3H), 3.63 (d, *J* = 17 Hz, 1H), 3.46 (m, 2H), 3.24 (m, 3H), 3.10 (s, 2H); ¹³C NMR (125 MHz, CDCl₃) δ 37.1, 40.8, 41.0, 41.3, 55.4, 55.6, 68.2, 78.6, 105.7, 108.7, 114.6, 124.2, 125.0, 126.8, 130.3, 137.2, 145.2, 148.9, 159.5, 159.6, 205.0; MS (TOF-MS) *m/z* 384 ([M⁺], 2), 323 (27), 291 (100), 290 (27); HRMS (TOF-MS) calc'd for C₂₁H₂₀O₃S₂ 384.0854, found 384.0866. The enantiomers were resolved by chiral phase HPLC using a Daicel Chiralpak AS column and a mobile phase of 4:1 hexanes/EtOH to give (*R*)- and (*S*)-**3.5** in optically pure form.

(*R*)-6,6'-Dimethoxy-2,2'-spirobiindan-1-one ((*R*)-3.6). THF (2 mL) was added to 1.0

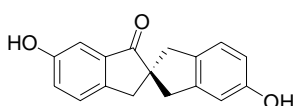


g of Raney[®] nickel 2800 slurry (washed 3x with distilled water,

CAUTION: pyrophoric) in the reaction flask. A solution of (*R*)-**3.5** (78 mg, 0.20 mmol) in 5 mL of THF was added slowly to the suspension. The mixture was heated to reflux for 3 h, then carefully filtered to remove Raney[®] nickel. The filtrate was extracted with Et₂O (3x), dried (MgSO₄), and concentrated to yield 52 mg (90 %) (*R*)-**3.6** as a beige solid: m.p. 96 – 98°C; ¹H NMR (400 MHz, CDCl₃) δ 7.31 (d, *J* = 8 Hz, 1H), 7.23 (dd, *J* = 2, 8 Hz, 1H), 7.09 (d, *J* = 8 Hz, 1H), 6.77 (s, 1H), 6.74 (d, *J* = 8 Hz, 1H), 3.85 (s, 3H), 3.79 (s, 3H), 3.46 (d, *J* = 15 Hz, 1H), 3.40 (d, *J* = 15 Hz, 1H), 3.09 (s, 2H), 2.79 (d, *J* = 15 Hz, 1H), 2.76 (d, *J* = 15 Hz, 1H); ¹³C NMR (125 MHz,

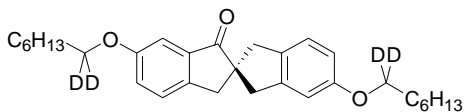
CDCl₃) δ 43.5, 44.2, 44.9, 55.4, 55.6, 58.9, 105.5, 110.0, 112.6, 124.3, 124.9, 127.3, 133.5, 137.4, 143.1, 145.5, 159.1, 159.6, 209.0; MS (TOF-MS) m/z 294 ([M]⁺, 100), 279 (30), 277 (34), 120 (26); HRMS (TOF-MS) calc'd for C₁₉H₁₈O₃ 294.1256, found 294.1242.

(R)-6,6'-Dihydroxy-2,2'-spirobiindan-1-one ((R)-3.7). Under an argon atmosphere, a



mixture of (R)-3.6 (80 mg, 0.27 mmol), AlCl₃ (130 mg, 0.95 mmol) and toluene (10 mL) was heated to reflux for 3 h. The mixture was quenched slowly with water and extracted with EtOAc (3x). The combined organic extracts were dried (MgSO₄) and concentrated to yield 71 mg (99 %) of (R)-3.7 as a beige solid. The crude material was used without further purification: m.p. 172 °C (dec); ¹H NMR (400 MHz, (CD₃)₂CO) δ 8.72 (s, 1H), 8.08 (s, 1H), 7.34 (d, J = 8 Hz, 1H), 7.19 (dd, J = 2, 8 Hz, 1H), 7.12 (d, J = 2 Hz, 1H), 7.00 (d, J = 8 Hz, 1H), 6.71 (s, 1H), 6.65 (dd, J = 2, 8 Hz, 1H), 3.28 (d, J = 16 Hz, 1H), 3.23 (d, J = 15 Hz, 1H), 3.06 (s, 2H), 2.78 (d, J = 16 Hz, 1H), 2.74 (d, J = 15 Hz, 1H). ¹³C NMR (125 MHz, (CD₃)₂CO) δ 43.8, 44.7, 45.2, 59.3, 109.1, 112.2, 114.5, 124.3, 125.6, 128.5, 133.0, 138.3, 144.0, 144.8, 157.5, 158.1, 208.8. MS (TOF-MS) m/z 266 ([M]⁺, 100), 251 (23), 249 (43); HRMS (TOF-MS) calc'd for C₁₇H₁₄O₃ 266.0943, found 266.0939.

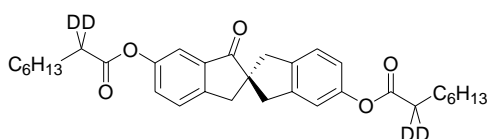
(R)-6,6'-Bis(heptyloxy-1,1-d₂)-2,2'-spirobiindan-1-one ((R)-3.8-d₄). Under an argon



atmosphere, 1,1-d₂-heptanol (60 mg, 0.46 mmol) in 4 mL of THF was added to a stirred solution of (R)-3.7 (44 mg, 0.16 mmol) and PPh₃ (100 mg, 0.39 mmol) in 3 mL of THF. After 5 minutes, DIAD (0.08 mL, 0.39 mmol) was added and the solution was stirred at room temperature overnight. Initial purification by flash chromatography (3:1 hexanes/EtOAc)

on silica gel yielded the mono-substituted product exclusively as a yellow oil (38 %). The reaction was repeated using the same reaction conditions to obtain the dialkylated product. The product was purified by flash chromatography (3:1 hexanes/EtOAc) and recrystallized from hexanes after passing through a 0.45 μm PTFE filter to give 25 mg (overall yield 33 %) of (*R*)-**3.8- d_4** as a sticky white solid: m.p. 65 - 67 $^\circ\text{C}$; ^1H NMR (400 MHz, CDCl_3) δ 7.22 (m, 3H), 7.07 (d, $J = 8$ Hz, 1H), 6.75 (s, 1H), 6.73 (d, $J = 8$ Hz, 1H), 3.45 (d, $J = 16$ Hz, 1H), 3.39 (d, $J = 15$ Hz, 1H), 3.08 (s, 2H), 2.77 (d, $J = 16$ Hz, 1H), 2.74 (d, $J = 15$ Hz, 1H), 1.76 (m, 4H), 1.30 (m, 14H), 0.89 (m, 6H); ^{13}C NMR (125 MHz, CDCl_3) δ 209.1, 159.1, 158.7, 145.2, 143.1, 137.4, 133.2, 127.3, 124.8, 124.7, 113.2, 110.7, 106.2, 74.4, 58.9, 44.9, 44.3, 43.5, 31.8, 31.8, 29.1, 29.1, 29.0, 28.9, 26.0, 25.9, 22.6, 21.6, 14.1; MS (TOF-MS) m/z 466 ($[\text{M}]^+$, 100), 366 (23); HRMS (TOF-MS) calc'd for $\text{C}_{31}\text{H}_{38}\text{D}_4\text{O}_3$ 466.3385, found 466.3397.

(*R*)-6,6'-Bis(octanoyloxy-2,2- d_2)-2,2'-spirobiindan-1-one ((*R*)-3.9- d_4**).** Under an



argon atmosphere, a mixture of (*R*)-**3.7** (29 mg,

0.11 mmol), 2,2- d_2 -octanoic acid (0.09 mL, 0.33 mmol), DMAP (40 g, 0.33 mmol), DCC (70 mg, 0.33 mmol) and 10 mL of anhydrous CH_2Cl_2 was allowed stir at room temperature for 3 days. The mixture was filtered, concentrated, and then dissolved in EtOAc, washed with 2 % HCl, dried (MgSO_4) and concentrated. The crude product was purified by flash chromatography on silica gel (4:1 hexanes/EtOAc), and passed through a 0.45 μm PTFE filter to give 25 mg (43 %) of (*R*)-**3.9- d_4** as a yellow oil; ^1H NMR (400 MHz, CDCl_3) δ 7.49 (d, $J = 2$ Hz, 1H), 7.43 (d, $J = 8$ Hz, 1H), 7.32 (dd, $J = 2, 8$ Hz, 1H), 7.18 (d, $J = 8$ Hz, 1H), 6.92 (s, 1H), 6.88 (d, $J = 8$ Hz), 3.46 (t, $J = 14$ Hz, 2H), 3.16 (s, 2H), 2.83 (d, $J = 16$ Hz, 2H), 2.81 (d, $J = 15$ Hz),

1.74 (m, 4H), 1.30 (m, 16H), 0.89 (m, 6H); ^{13}C NMR (125 MHz, CDCl_3) δ 14.0, 22.6, 24.8, 24.9, 28.9, 28.9, 29.0, 29.0, 31.6, 31.6, 34.0 (quintet, $J = 20$ Hz), 43.6, 44.3, 44.7, 58.8, 117.0, 117.8, 120.0, 125.0, 127.4, 128.8, 137.4, 138.7, 142.9, 149.7, 150.4, 172.7, 202.5; MS (TOF-MS) m/z 522 ($[\text{M}]^+$, 11), 396 (74), 395 (100), 394 (71), 268 (94), 267 (54); HRMS (TOF-MS) calc'd for $\text{C}_{33}\text{H}_{38}\text{D}_4\text{O}_5$ 522.3283, found 522.3268.

5.2. ^2H NMR Spectroscopy

A Bruker 600 MHz spectrometer (^2H frequency = 92.13 MHz) was used to record the ^2H NMR spectra. The samples were prepared in conical glass vials by weighing or by stock solution, stirred in the isotropic phase to ensure complete mixing, cooled to the crystalline phase, and transferred to a standard 5 mm NMR tube. Inside the spectrometer, samples were heated to the isotropic phase and then cooled to $T - T_C = -10$ K and allowed to equilibrate for 30 minutes. Calibration of the temperature control unit of the spectrometer was accomplished using a sample of 80 % ethylene glycol (by volume) in $\text{DMSO}-d_6$ according to a known procedure.⁵ The temperatures are considered accurate to within ± 1 K and could be controlled to within ± 0.1 K. The spectra were recorded for stationary samples using a solid echo pulse sequence, collecting 4096 points per scan over a 250 kHz spectral width. For each spectrum in the liquid crystal phase, approximately 17,000-20,000 scans were collected. Line broadening (250 Hz), exponential multiplication, and iterative left-shifting of the data (to ensure that the first data point of the FID coincides with the beginning of the echo delay) were carried out prior to Fourier transformation and phasing.

5.3. Determination of Transition Temperatures by Polarized Microscopy

Phase transitions of liquid crystal mixtures were determined upon cooling by viewing thin films of the samples on untreated glass slides with a cover slip using a Nikon Eclipse E600 POL microscope and a Linkam LTS 350 hot stage. The phase transitions I-N*, N*-SmA*, and SmC*-Cr were determined based on changes in texture as observed between crossed polarizers. The SmA*-SmC* phase transition temperature was determined to be the temperature at which a P_S peak appeared.

5.4. Ferroelectric Polarization Measurements

5.4.1. Sample Preparation

Mixtures for ferroelectric polarization measurements were prepared by weighing appropriate amounts of dopant and host into conical glass vials and stirring in the isotropic phase to ensure complete mixing. Capillary action was used to load each sample into a polyimide-coated ITO glass cell; 4 μm thickness and 0.160 cm^2 addressed area (E.H.C. Co., Japan). Cell thicknesses were determined by the nulling of the empty cell using a Liquid Crystal Analytical System (LCAS, LC Vision, LLC, Boulder, CO). Ferroelectric polarization power measurements were carried out using the LCAS in conjunction with a Nikon Eclipse E600 POL and a Linkam LTS 350 hot stage. Each cell was heated to the isotropic phase under an AC triangular wave (100 Hz, 6 V/ μm), and held until any air bubbles in the addressed area disappeared. Alignment was optimized by slow cooling of the filled cells from the isotropic phase through the N* and SmA* phase, before holding at $T-T_C = -5$ K and $T-T_C = -10$ K in the SmC* phase.

5.4.2. Polarization Measurements

Spontaneous polarization (P_S) values were measured as a function of temperature using the triangular wave method (100 Hz, 6 V/ μm).⁶ Tilt angles, θ , were measured as a function of temperature between crossed polarizers as half the rotation between two extinction positions corresponding to opposite polarization orientations. The sign of P_S along the polar axis was assigned from the relative configuration of a previously determined known sample, 10 mol % **MDW 950** (Displaytech Inc., Longmont, CO) in the liquid crystal host **PhP1** ($-P_S$).⁷ The reduced polarization, P_o , was calculated for each mixture at $T-T_C = -10$ K, according to Equation 1-4.

5.5. References

- (1) Keller, P. *Ferroelectrics* **1984**, 58, 3.
- (2) Gray, G. W.; Hird, M.; Lacey, D.; Toyne, K. J. *J. Chem. Soc., Perkin Trans. II* **1989**, 2041.
- (3) Boulton, C. J.; Finden, J. G.; Yuh, E.; Sutherland, J. J.; Wand, M. D.; Wu, G.; Lemeieux, R. P. *J. Am. Chem. Soc.* **2005**, 127, 13656.
- (4) Langer, E.; Lehner, H. *Tetrahedron* **1973**, 29, 375.
- (5) Braun, S.; Kalinowski, H.-O.; Berger, S. *150 and More Basic NMR Experiments*; Wiley-VCH: Weinheim, 1998.
- (6) Miyasato, K.; Abe, S.; Takezoe, H.; Fukuda, A.; Kuze, E. *Jpn. J. Appl. Phys.* **1983**, 22, L661.
- (7) Thompson, M. P.; Hegmann, T.; Wand, M. D.; Lemeieux, R. P. *Liq. Cryst.* **2007**, 34, 987.

Appendix 1. ^1H NMR Spectra of Novel Compounds

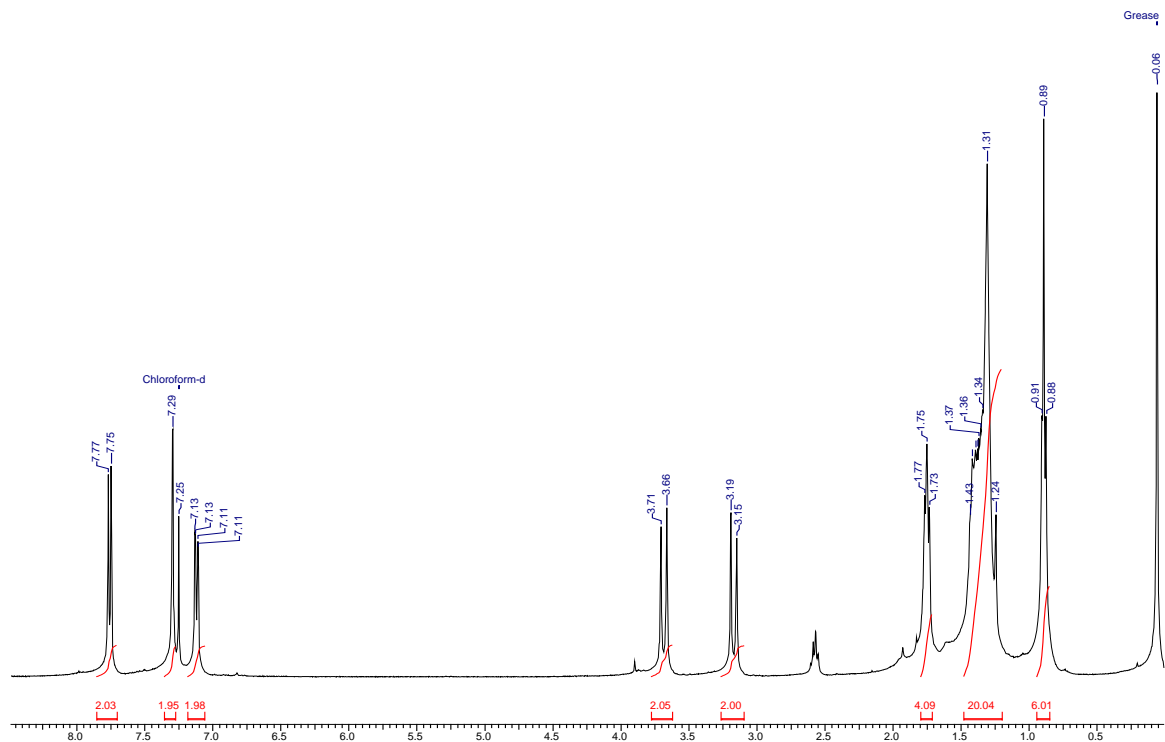


Figure A1-1. 400 MHz ^1H NMR spectrum of (RS) -2.3- d_4 .

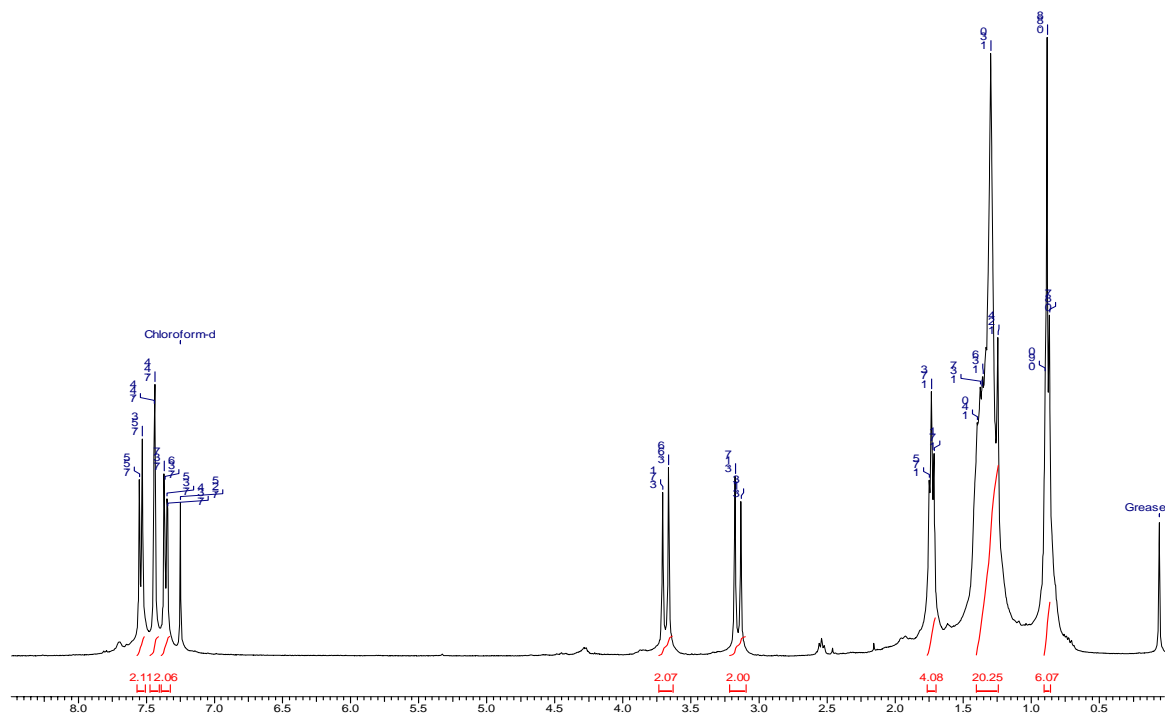


Figure A1-2. 400 MHz ^1H NMR spectrum of (RS) -2.6- d_4 .

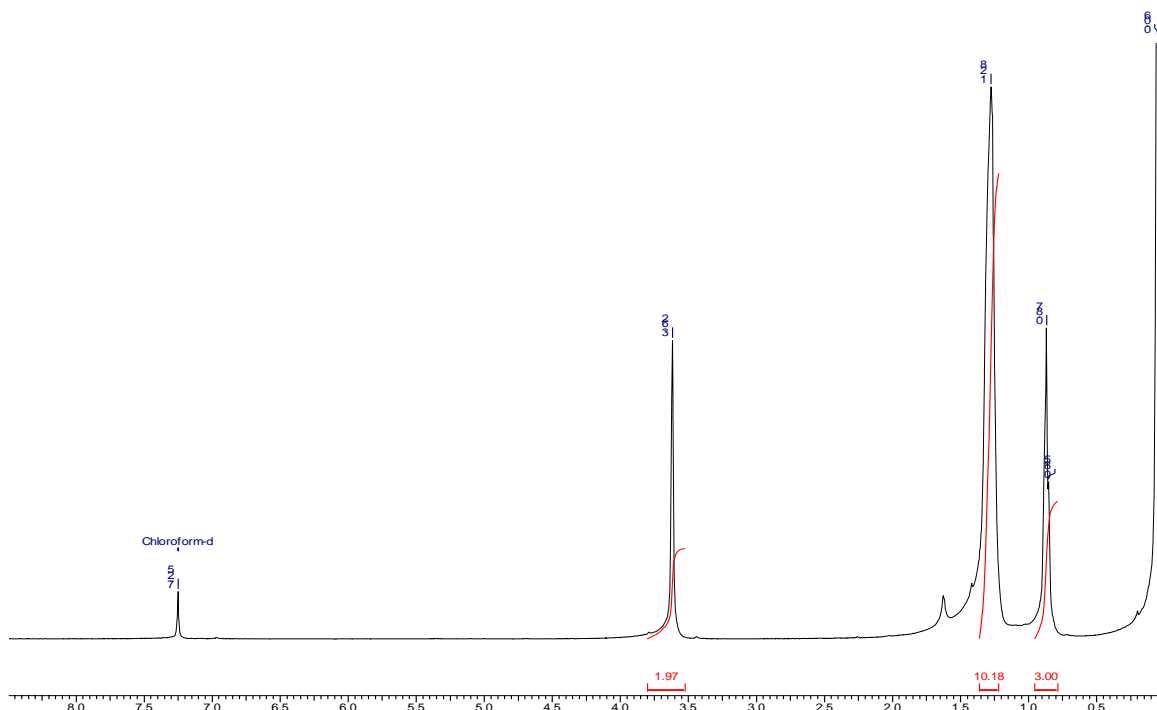


Figure A1-4. 400 MHz ^1H NMR spectrum of **2.8**.

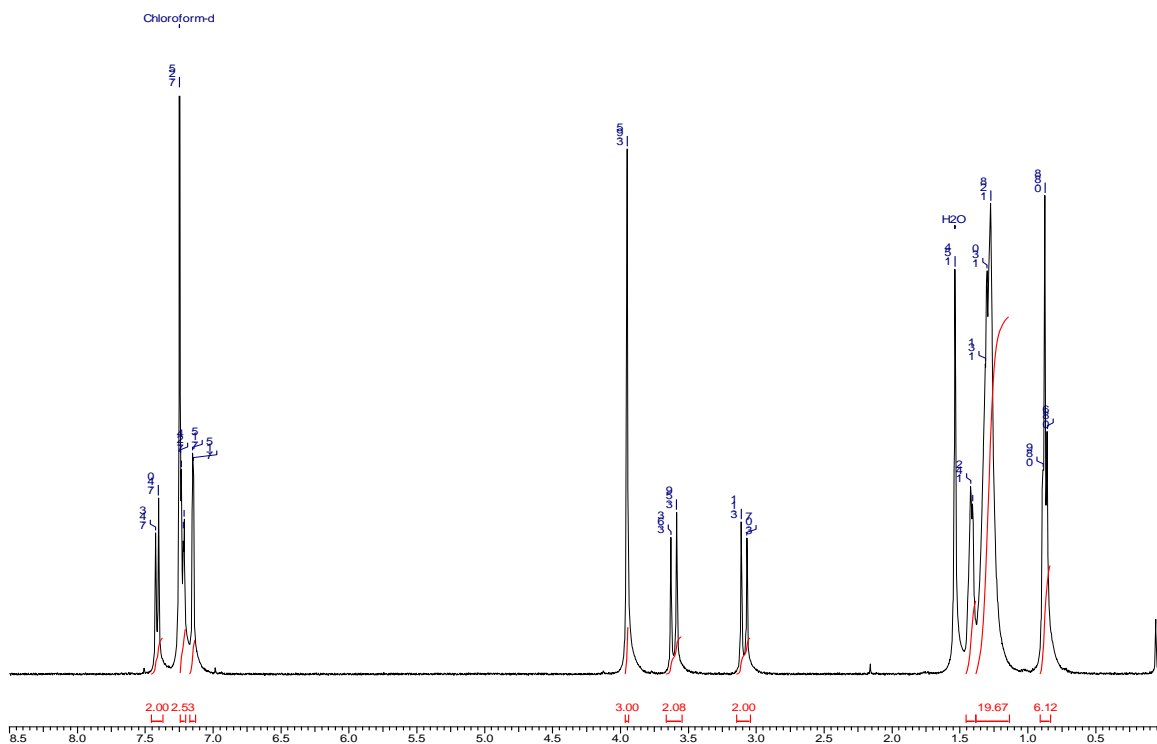


Figure A1-3. 400 MHz ^1H NMR spectrum of *(RS)*-**2.9- d_4** .

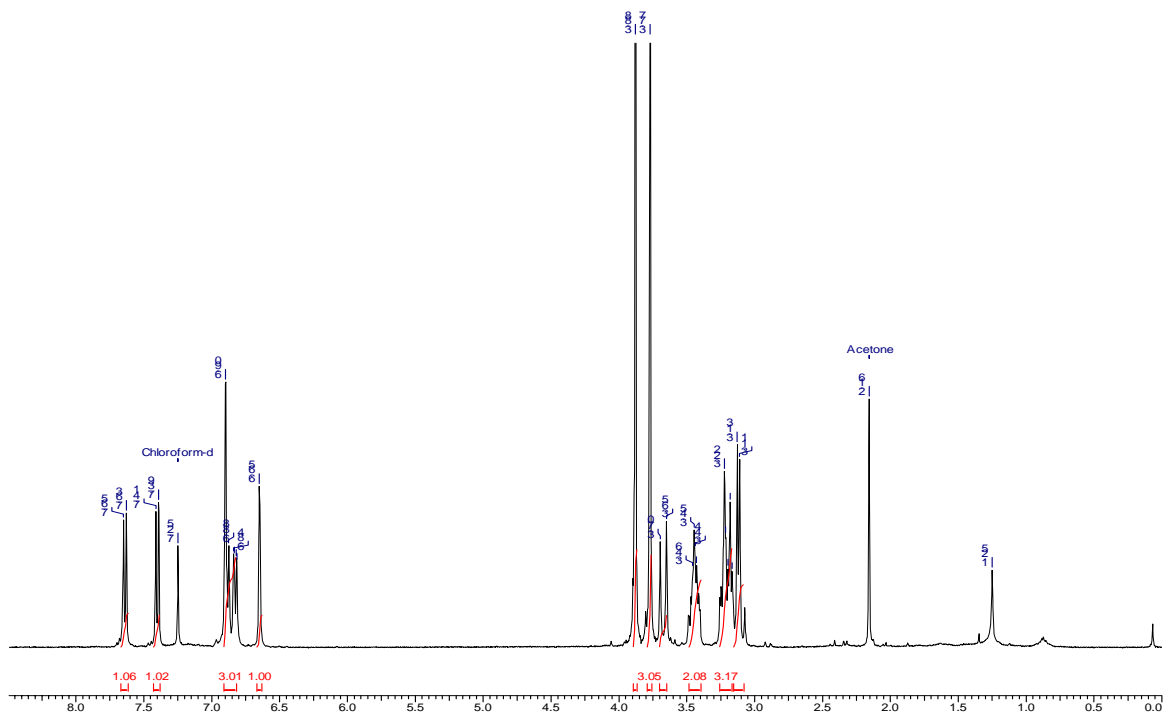


Figure A1-5. 400 MHz ^1H NMR spectrum of (RS)-3.1.

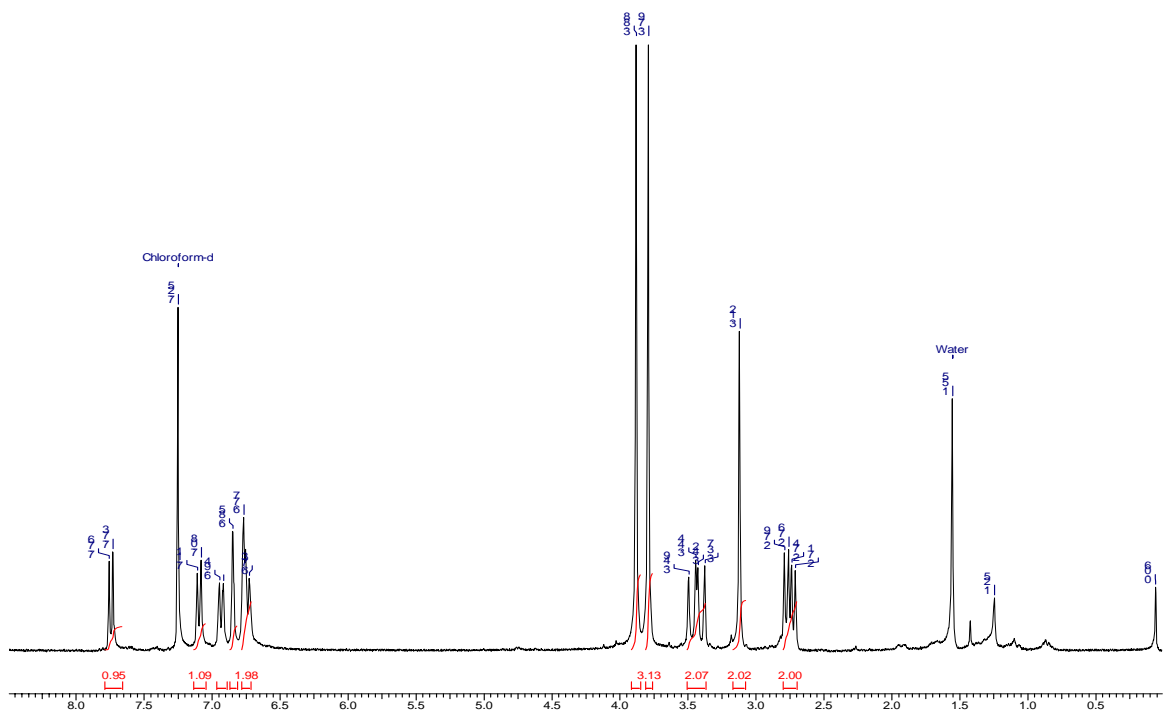


Figure A1-6. 400 MHz ^1H NMR spectrum of (R)-3.2.

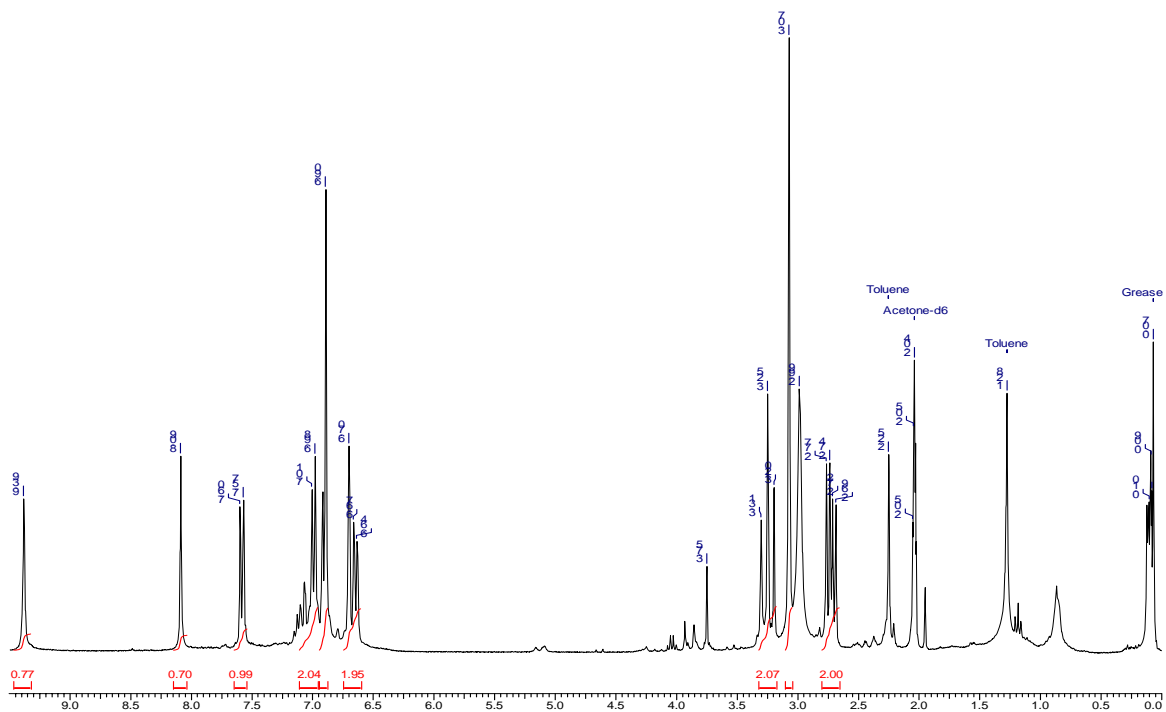


Figure A1-7. 400 MHz ^1H NMR spectrum of (*R*)-3.3.

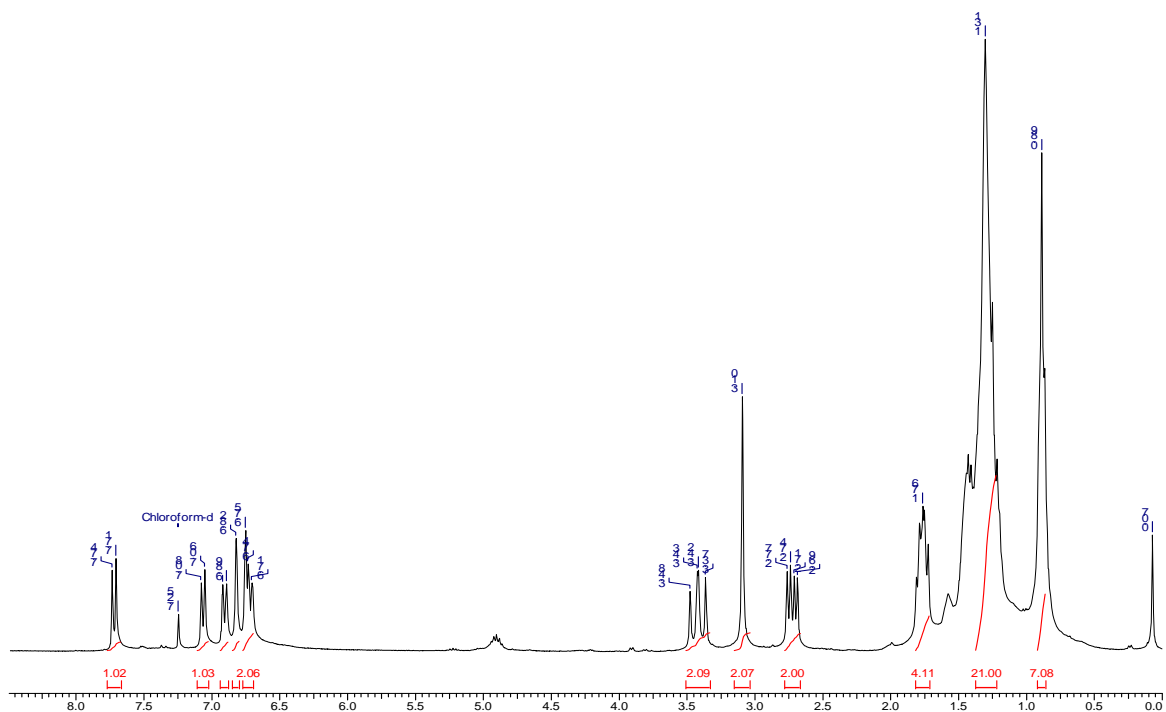


Figure A1-8. 400 MHz ^1H NMR spectrum of (*R*)-3.4- d_4 .

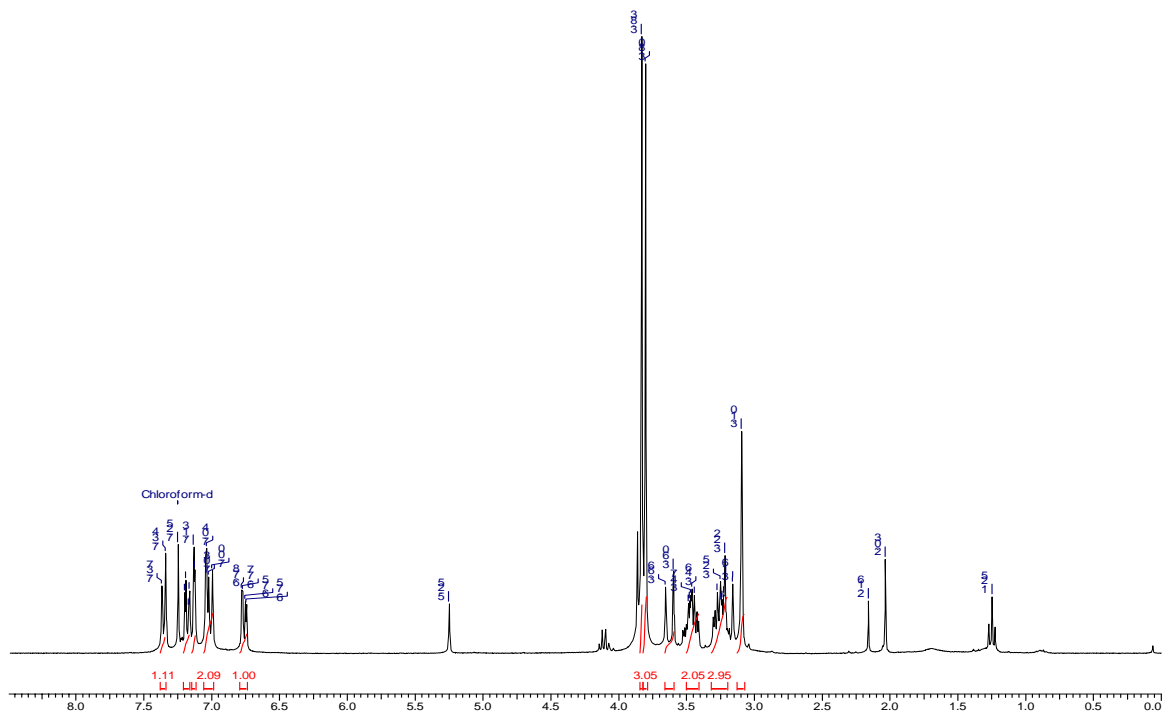


Figure A1-9. 400 MHz ^1H NMR spectrum of (*R*)-3.5.

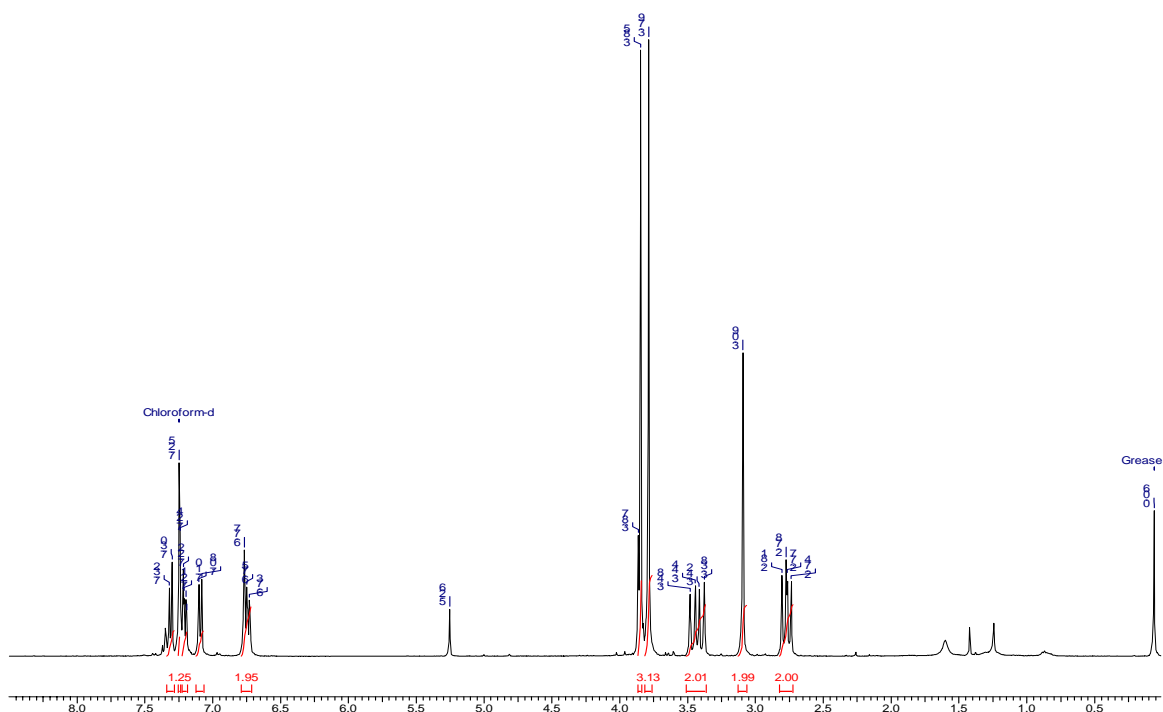


Figure A1-10. 400 MHz ^1H NMR spectrum of (*R*)-3.6.

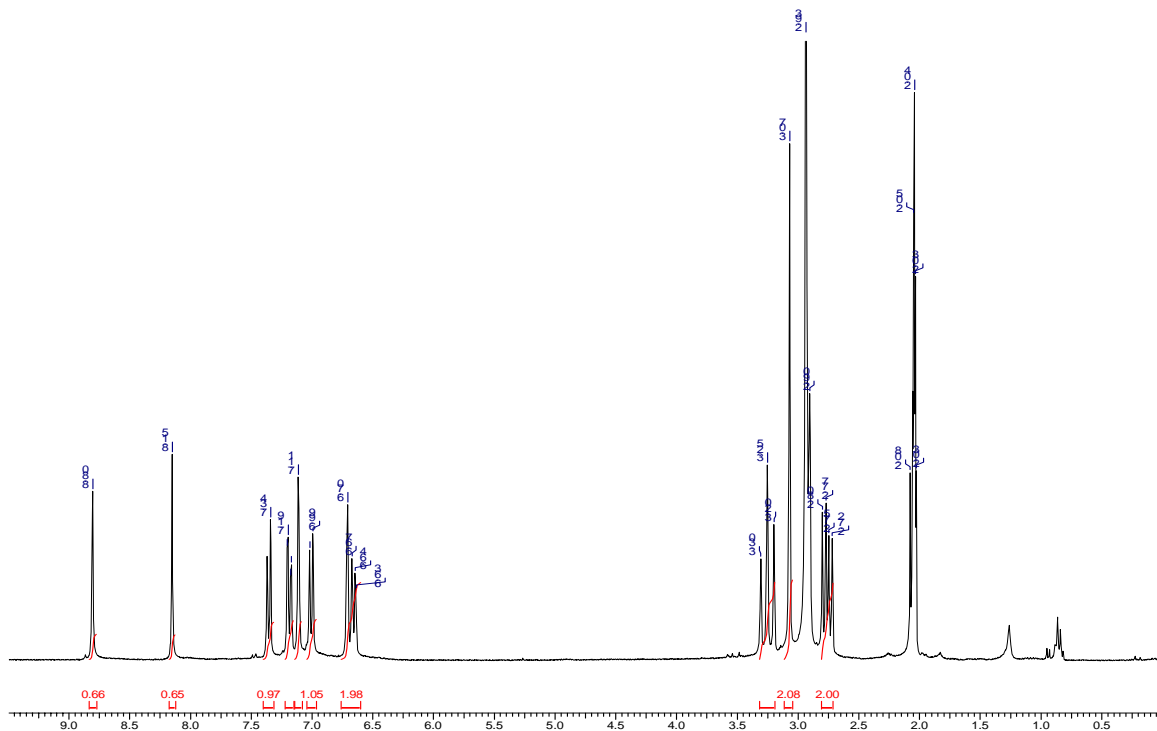


Figure A1-11. 400 MHz ^1H NMR spectrum of (*R*)-3.7.

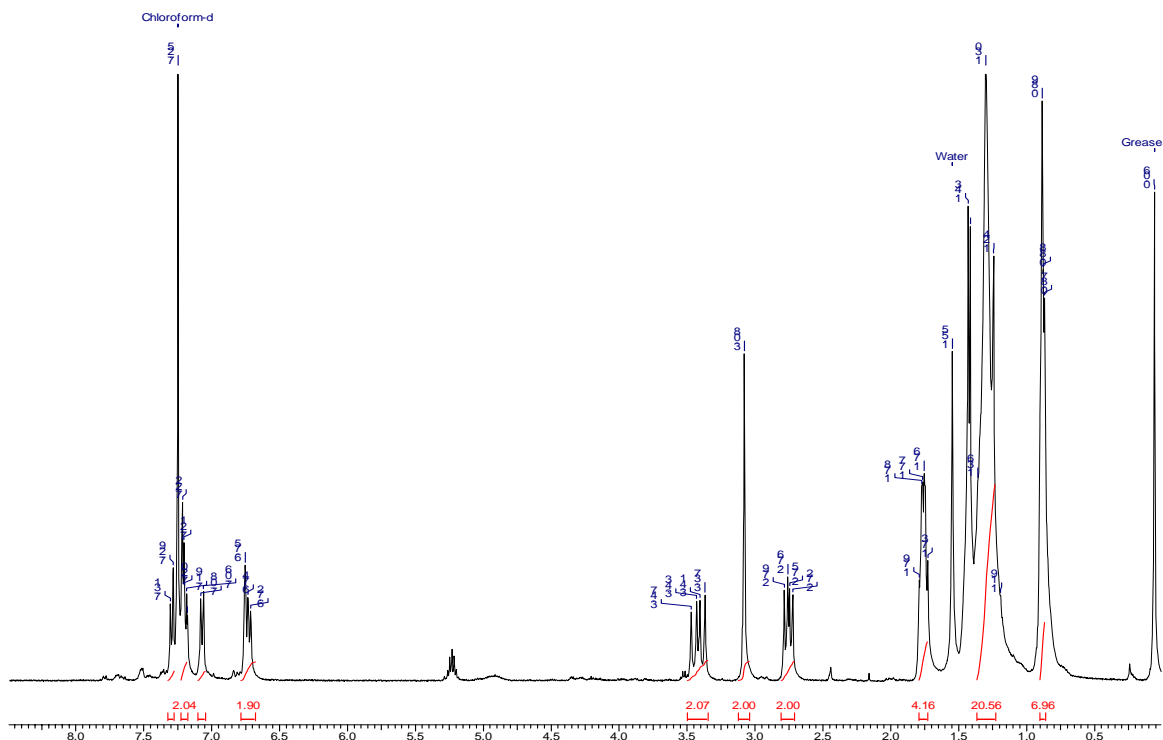


Figure A1-12. 400 MHz ^1H NMR spectrum of (*R*)-3.8- d_4 .

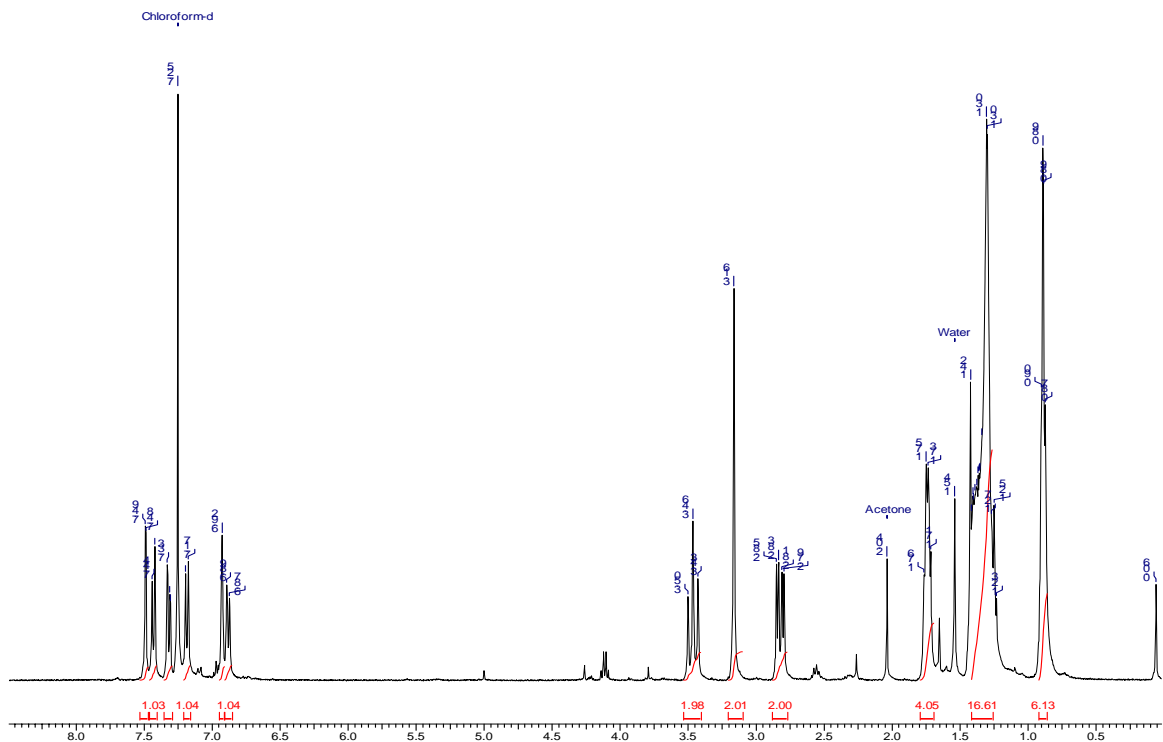


Figure A1-13. 400 MHz ¹H NMR spectrum of (R)-3.9-d₄.

Appendix 2. Polarization Power Data

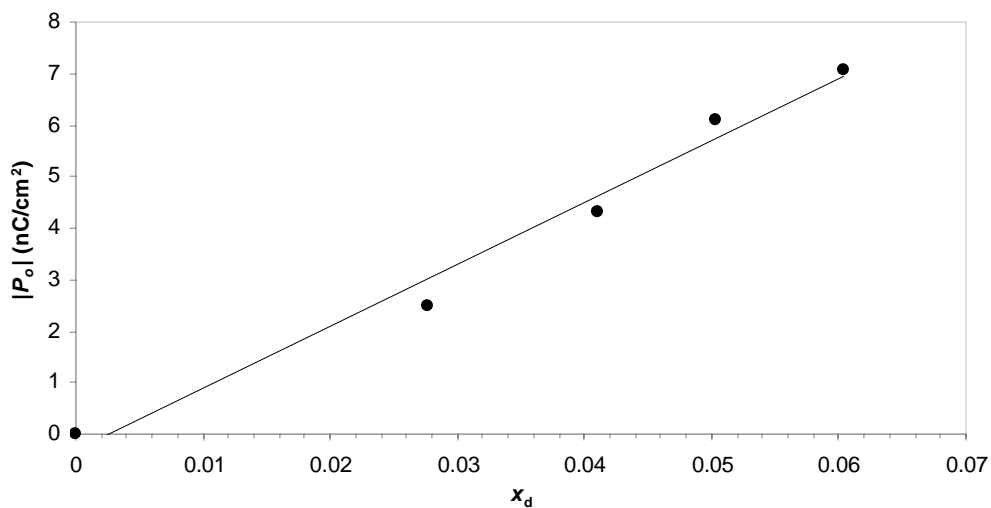


Figure 3-3(a). Absolute reduced polarization, $|P_o|$, versus mole fraction, x_d , of (R)-3.4- d_4 in the SmC host NCB76 at $T-T_C = -10$ K.

(R)-3.4- d_4 in NCB76

x (R)-3.4- d_4	P_S (nC/cm ²)	θ (°)	P_o (nC/cm ²)
0			0
0.0277	+ 1.28	30.7	+ 2.5
0.0411	+ 2.22	31.0	+ 4.3
0.0503	+ 3.13	30.8	+ 6.1
0.0604	+ 3.70	31.6	+ 7.1

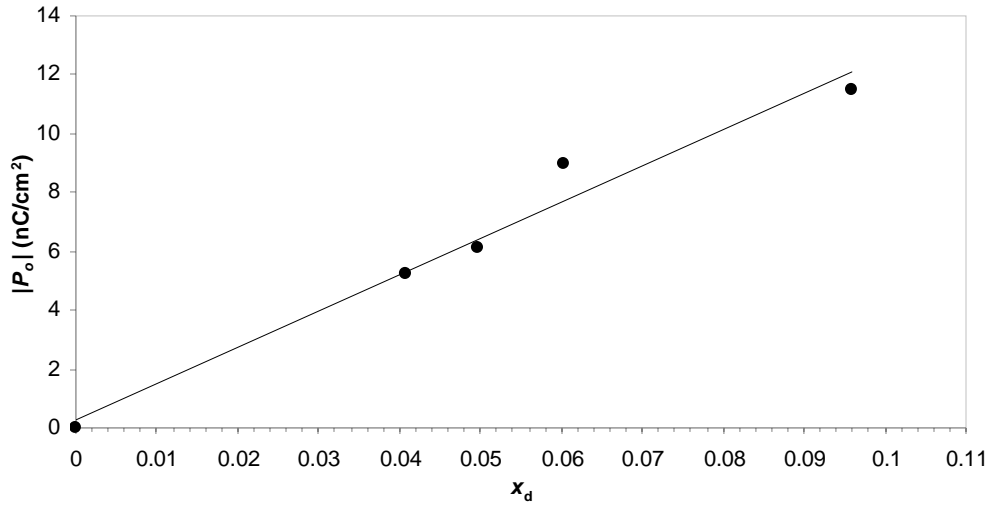


Figure 3-3(b). Absolute reduced polarization, $|P_o|$, versus mole fraction, x_d , of (R) -3.8- d_4 in the SmC host NCB76 at $T-T_C = -10$ K.

(R) -3.8- d_4 in NCB76

x (R) -3.8- d_4	P_S (nC/cm ²)	θ (°)	P_o (nC/cm ²)
0			0
0.0409	- 2.54	28.9	- 5.2
0.0496	- 3.08	30.1	- 6.1
0.0604	- 4.62	30.9	- 9.0
0.0958	- 5.79	30.3	- 11.5

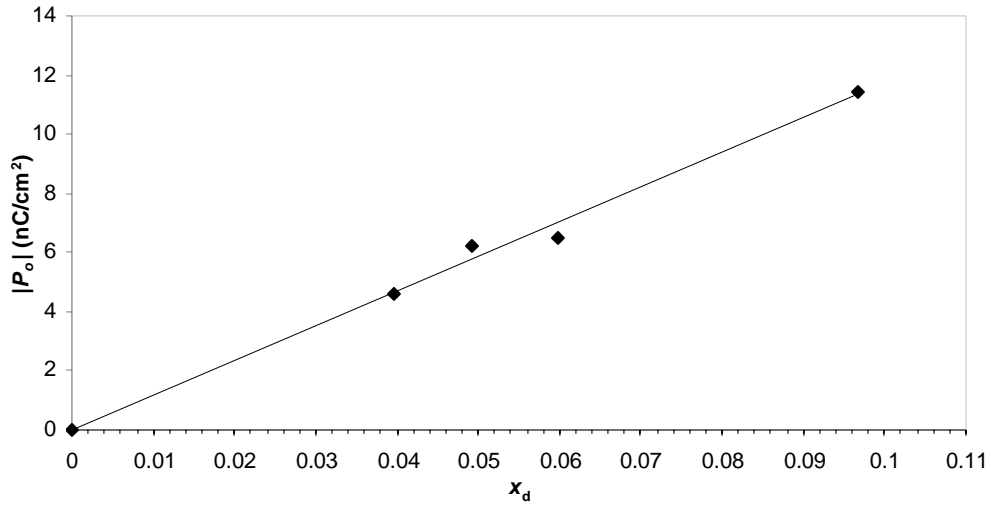


Figure 3-3(c). Absolute reduced polarization, $|P_o|$, versus mole fraction, x_d , of (R) -3.9- d_4 in the SmC host NCB76 at $T-T_C = -10$ K.

(R) -3.9- d_4 in NCB76

x (R) -3.9- d_4	P_S (nC/cm ²)	θ (°)	P_o (nC/cm ²)
0			0
0.0397	- 2.37	30.9	- 4.6
0.0493	- 3.20	31.0	- 6.2
0.0598	- 3.35	31.2	- 6.5
0.0968	- 5.90	31.0	- 11.5